arXiv:2203.07040v1 [cond-mat.dis-nn] 14 Mar 2022

Soft-margin classification of object manifolds

Uri Cohen[1] and Haim Sompolinsky[1,2,*]

[1] *Edmond and Lily Safra Center for Brain Sciences, Hebrew University of Jerusalem, Israel*
[2] *Center for Brain Science, Harvard University, Cambridge, MA, USA*

(Dated: March 15, 2022)

A neural population responding to multiple appearances of a single object defines a manifold in the neural response space. The ability to classify such manifolds is of interest, as object recognition and other computational tasks require a response that is insensitive to variability within a manifold. Linear classification of object manifolds was previously studied for max-margin classifiers. Soft-margin classifiers are a larger class of algorithms and provide an additional regularization parameter used in applications to optimize performance outside the training set by balancing between making fewer training errors and learning more robust classifiers. Here we develop a mean-field theory describing the behavior of soft-margin classifiers applied to object manifolds. Analyzing manifolds with increasing complexity, from points through spheres to general manifolds, a mean-field theory describes the expected value of the linear classifier's norm, as well as the distribution of fields and slack variables. By analyzing the robustness of the learned classification to noise, we can predict the probability of classification errors and their dependence on regularization, demonstrating a finite optimal choice. The theory describes a previously unknown phase transition, corresponding to the disappearance of a non-trivial solution, thus providing a soft version of the well-known classification capacity of max-margin classifiers.

Keywords: linear classification, soft classification, object manifolds, SVM, replica theory, mean-field theory

I. INTRODUCTION

Max-margin and soft-margin classification When performing linear classification, the naive approach would aim for classifying all the training samples correctly with the largest possible margin, an approach known as max-margin classification [1, 2]. An alternative approach, known as soft-margin classification [3, 4], is to allow for misclassification of some of the samples, in order to increase the classification margin of most samples. Soft-margin classification is common in applications, where the data is not necessarily linearly separable. Furthermore, it allows for minimizing generalization error by optimizing a regularization parameter that balances between classification errors on the training set and achieving a larger margin. Both max-margin and soft-margin classification problems are solved by Support Vector Machine algorithms (hereafter, SVM).

Previous works on manifold classification The problem of manifold classification arises in neuroscience and machine learning when a population of biological or artificial neurons represents an object, and variability in object appearance would define a manifold in the neural response space. In invariant object recognition tasks, the response of output neurons is determined by object identity alone, which is naturally defined as performing manifold classification, i.e., using target labels that are constant within manifolds. The ability to perform max-margin classification on manifolds of increased complexity was analyzed in recent years. Building on the seminal work of Gardner [5] which considered the classification of points, recent works have extended theory to describe manifolds of any shape [6, 7] and to allow for certain correlations between manifolds [8]. Those theoretical advances described only max-margin classifiers, which are not common in applications. Here we close this gap by analyzing soft classification of manifolds of increasing complexity, going from points, through spheres, to general manifolds.

Previous works on soft classification theory Previous theoretical works on soft-margin classifiers have analyzed the classification of points. Statistical learning tools were used to provide bounds on generalization error when using different kernels and different regularization schemes [9, 10]. A statistical physics analysis of soft-margin classification in a teacher-student setup described the learning curve, i.e., the dependence of training and generalization error on the number of samples [11], thus extending the max-margin analysis [12]. Here we avoid making specific assumptions on the teacher and instead consider soft classification performance when averaging over random choice of labels.

The role of noise When a soft-margin classifier is learned on a training set and then evaluated on a held-out test set, the classification errors achieved are called the training error and the test error, respectively. In general we expect the training error to be minimized for the max-margin classifier while the test error may be minimized at a finite value of the soft classification regularization parameter, which needs to be found empirically. Here we aim to analyze this setting by con-

* Corresponding author: haim@fiz.huji.ac.il

sidering a test set that is a noisy version of the training set. This corresponds to noise-resistance of the classifier, and not to the notion of generalization error in machine-learning where it is assumed that the training and test set are sampled from the same distribution.

II. RESULTS

A. Soft classification of points

Max-margin classification of points is discussed by [5]; here we extend this seminal work to soft classification. Given P pairs $\{(\boldsymbol{x}^\mu, y^\mu)\}_{\mu=1}^P$ of points $\boldsymbol{x}^\mu \in \mathbb{R}^N$ and labels $y^\mu \in \{\pm 1\}$, soft classification is defined by a set of weights $\boldsymbol{w} \in \mathbb{R}^N$ and slack variables $\vec{s} \in \mathbb{R}^P$ such that the fields at the solution obey for all $\mu \in [1..P]$

$$h^\mu = y^\mu \boldsymbol{w} \cdot \boldsymbol{x}^\mu \geq 1 - s^\mu \tag{1}$$

The bold notation for $\boldsymbol{x}^\mu$ and $\boldsymbol{w}$ indicates that they are vectors in $\mathbb{R}^N$, whereas the arrow notation is used for other vectors, such as $\vec{s}$. Given a regularization parameter $c \geq 0$ the optimal classifier and slack variables are defined $\boldsymbol{w}^*, \vec{s}^* = \arg\min_{\boldsymbol{w},\vec{s}} L(\boldsymbol{w}, \vec{s})$ for a Lagrangian

$$L = \|\boldsymbol{w}\|^2/N + c\|\vec{s}\|^2/N \ s.t. \ \forall \mu \ h^\mu \geq 1 - s^\mu \tag{2}$$

and L^* denotes the minimal value of L.

Replica theory From the Lagrangian the volume of solutions $V(L, c)$ for a given value of the loss L and a choice of regularization c is given by:

$$V(L,c) = \int d^N \boldsymbol{w} \int d^P \vec{s} \delta\left(\|\boldsymbol{w}\|^2 + c\|\vec{s}\|^2 - NL\right) \tag{3}$$

$$\cdots \prod_\mu^P \delta\left(y^\mu \boldsymbol{w} \cdot \boldsymbol{x}^\mu - h^\mu\right) \Theta\left(h^\mu - 1 + s^\mu\right) \tag{4}$$

The volume is defined for any positive L, c but we are interested in the problem parameters where it vanishes, which is expected to happen only at the minimal value L^*. Thus by analyzing the conditions where $V \to 0$ we characterize the optimal solution achieved by the optimization procedure, without introducing an additional temperature variable as is usually done [12–16]. This allows us to describe not only L^* but also the expected norms of the weights $\|\boldsymbol{w}\|$ and slack variables $\|\vec{s}\|$, and the relation between N and P where the solution is achieved. For random labels $\vec{y} \in \{\pm 1\}^P$ and points $\boldsymbol{x}_i^\mu \sim \mathcal{N}(0, 1/N)$ we calculate the volume through replica identity:

$$[\log V]_{x,y} = \lim_{n \to 0} \left[\frac{V^n - 1}{n}\right]_{x,y} \tag{5}$$

We solve this problem using a (replica symmetric) mean-field theory, which is expected to be exact in the thermodynamic limit $N, P \to \infty$ with a finite ratio $\alpha = P/N$. Analyzing the case where $V \to 0$ we obtain an expression for the loss L in terms of two order parameters q and k (see details in section C 1):

$$L/q = \frac{k-1}{k} + \frac{c}{1+ck}\alpha\alpha_0^{-1}\left(1/\sqrt{q}\right) \tag{6}$$

where $\alpha_0^{-1}(\kappa) = \int_{-\infty}^{\kappa} Dt\,(\kappa - t)^2$ is Gardner's points capacity [5], $q = \|\boldsymbol{w}\|^2/N$ is the norm of the weight vector, and the interpretation of k is discussed below. Note we assumed here $\|\boldsymbol{x}^\mu\| = 1$; if instead $\|\boldsymbol{x}^\mu\| = a$, then q, c need to be scaled by $1/a^2$.

Self-consistent equations We expect the solution to satisfy saddle-point equations $0 = \frac{\partial L}{\partial q} = \frac{\partial L}{\partial k}$, yielding 2 self-consistent equations for q, k (see section C 2):

$$1 = \frac{(ck)^2}{(1+ck)^2}\alpha\alpha_0^{-1}\left(1/\sqrt{q}\right) \tag{7}$$

$$1 - k = \frac{ck}{(1+ck)}\alpha H\left(-1/\sqrt{q}\right) \tag{8}$$

for $H(x) = \int_x^\infty \frac{dt}{\sqrt{2\pi}} e^{-x^2/2}$ the Gaussian tail function.

The mean-field equations can be solved numerically for any load α (see algorithm at section B 1); figure 1a-b shows the resulting values of q and k, respectively. We observe that $k(\alpha)$ decreases monotonically from 1 at 0 (figure 1b), and similarly $\|\vec{s}\|$ increases monotonically from 0 to 1 (figure 1c). Those are tightly related as from equations 2,6,7 we have that $q/(ck)^2 = \alpha\langle s^2\rangle$, so that ck describes the ratio between the weights' norm and the slack norm at the optimization target (equation 2). Furthermore, the first moment of the slack is related to the optimal cost through $L^* = \alpha c \langle s\rangle$ (see section C 4).

In contrast, $q(\alpha)$ is non-monotonic, increasing from 0 to a peak at a finite value, then decreasing (figure 1a). This is an indication of the trade-off between achieving a larger margin (small q) and making only small errors (small $\|\vec{s}\|$). Figure S1 compares simulation results for q with the results of solving the self-consistent equations.

We now consider some interesting limits (see details in section C 2). When $\alpha \to 0$ we have $k \to 1$ and $q \to 0$ so that $\alpha_0^{-1}\left(1/\sqrt{q}\right) \approx 1/q$ and thus $k \approx 1 - \alpha c/(1+c)$ and $q \approx \alpha c^2/(1+c)^2$. When $\alpha \to \infty$ we have $k \to 0$ and $q \to 0$ with scaling $k \approx 1/c\alpha$, $q \approx 1/\alpha$. Both limits are marked in figure S1.

Infinite c limit When $c \to \infty$ and $\alpha < 2$ there is a solution for $\boldsymbol{w}$ (of unconstrained norm) where $\vec{s} = \vec{0}$, so the Lagrangian becomes that of max-margin classifiers:

$$L = \min \|\boldsymbol{w}\|^2 \ s.t. \ \forall \mu \ h^\mu \geq 1 \tag{9}$$

In this regime k is finite while ck diverges, so equation 7 recovers the max-margin theory [5] and q diverges for α near 2. On the other hand, for $c \to \infty$ and $\alpha > 2$

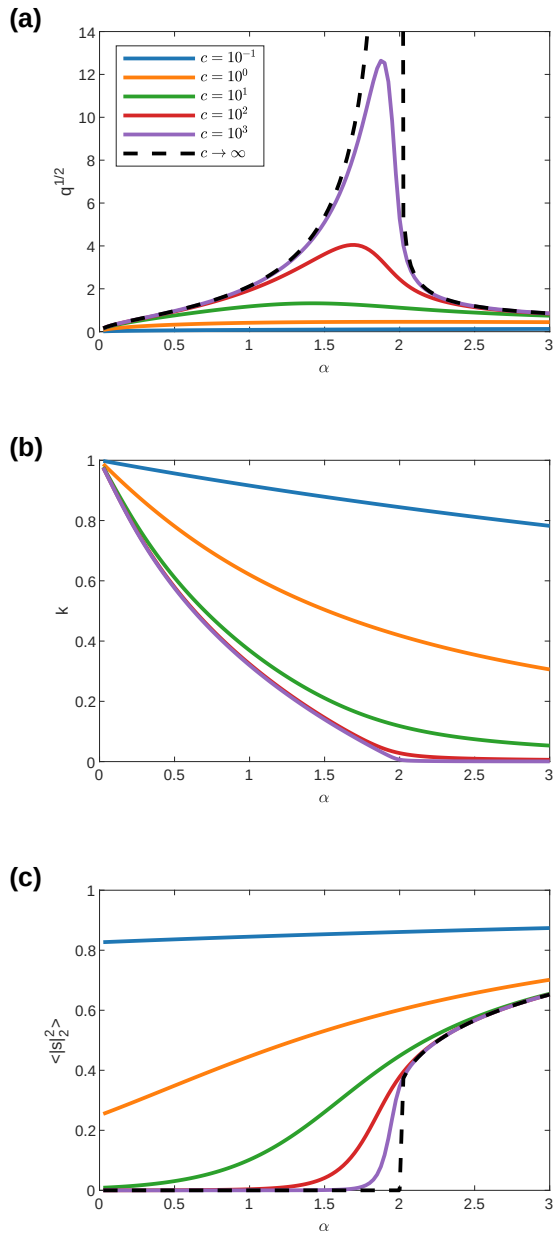


FIG. 1: Order parameters in soft classification of points. (a) The optimal weights' norm $q^{1/2}$ (y-axis) for different values of α (x-axis) and choices of the regularization variable c (color coded), including the $c \to \infty$ limit (dashed line). (b) The order parameter k (y-axis) for different values of α (x-axis) and choices of c (color coded). (c) The mean slack norm $\|\vec{s}\|^2$ (y-axis) for different values of α (x-axis) and choices of c (color coded), including the $c \to \infty$ limit (dashed line).

there is no solution with $\vec{s} = \vec{0}$ so this term dominates the loss and the Lagrangian becomes:

$$L = \min \|\vec{s}\|^2 \ s.t. \ \forall \mu \ h^\mu \geq 1 - s^\mu \tag{10}$$

A mean-field solution of this Lagrangian involves two order parameters $q = \|\boldsymbol{w}\|^2/N$ and $K = \lim_{c\to\infty} ck$, which follow the self-consistent equations 7-8 (where k on the left-hand-side of equation 8 approaches 0, see section C 2). Thus in the limit of $c \to \infty$ the mean-field theory reduces to a simple relation between q and α (dashed line in figure 1a):

$$\alpha = \begin{cases} \alpha_0 \left(1/\sqrt{q}\right) & \alpha < 2 \\ \alpha_0^{-1} \left(1/\sqrt{q}\right) / H^2 \left(-1/\sqrt{q}\right) & \alpha > 2 \end{cases} \tag{11}$$

Field distribution The theory also provides the joint distribution of h, s; their variance is due to the quenched variability in the choice of the classification labels and the arrangement of points (see details in section C 3). The field distribution is a concatenation of two truncated Gaussian variables, each representing a different solution regime:

$$h \sim \begin{cases} \mathcal{N}\left(\frac{ck}{1+ck}, \frac{q}{(1+ck)^2}\right) & h < 1 \\ \mathcal{N}\left(0, q\right) & h \geq 1 \end{cases} \tag{12}$$

Fields $h \geq 1$ are the "interior" regime (i.e., of points beyond the separating hyper-plane), where $s = 0$, while fields $h < 1$ are the "touching" regime (i.e., of points touching the separating hyper-plane), where $s > 0$. This distribution is shown for several choices of c and α in figure 2a-b, and figure S2 compares theory to the empirical histogram from simulations. The distribution of slack variables then follows from $s = \max\{1 - h, 0\}$.

Classification errors We now turn our focus to the classification errors achieved when performing soft classification. The classification error on the training set is defined $\varepsilon_{tr} = P(h < 0) = P(s > 1)$ and from the field distribution we have:

$$\varepsilon_{tr} = H\left(ck/\sqrt{q}\right) = H\left(1/\sqrt{\alpha \langle s^2 \rangle}\right) \tag{13}$$

A comparison of the training error observed in simulations with the theoretical predictions is given in figure S3. As demonstrated in figure 2c, the training error is monotonically increasing with α and monotonically decreasing with c throughout (a proof for this is provided in section C 6). For $\alpha < 2$ where max-margin classifiers achieve no errors this is to be expected, but surprisingly this is also the case for $\alpha \geq 2$ (see classification error for $\alpha \geq 2$ and $c \to \infty$ in figure 2c).

Thus we turn to analyze classification error in the presence of noise, where a finite c may be optimal. When Gaussian noise $\mathcal{N}\left(0, \sigma^2/N\right)$ is applied at each component of the input vectors, a noise $\mathcal{N}\left(0, \sigma^2 q\right)$ is

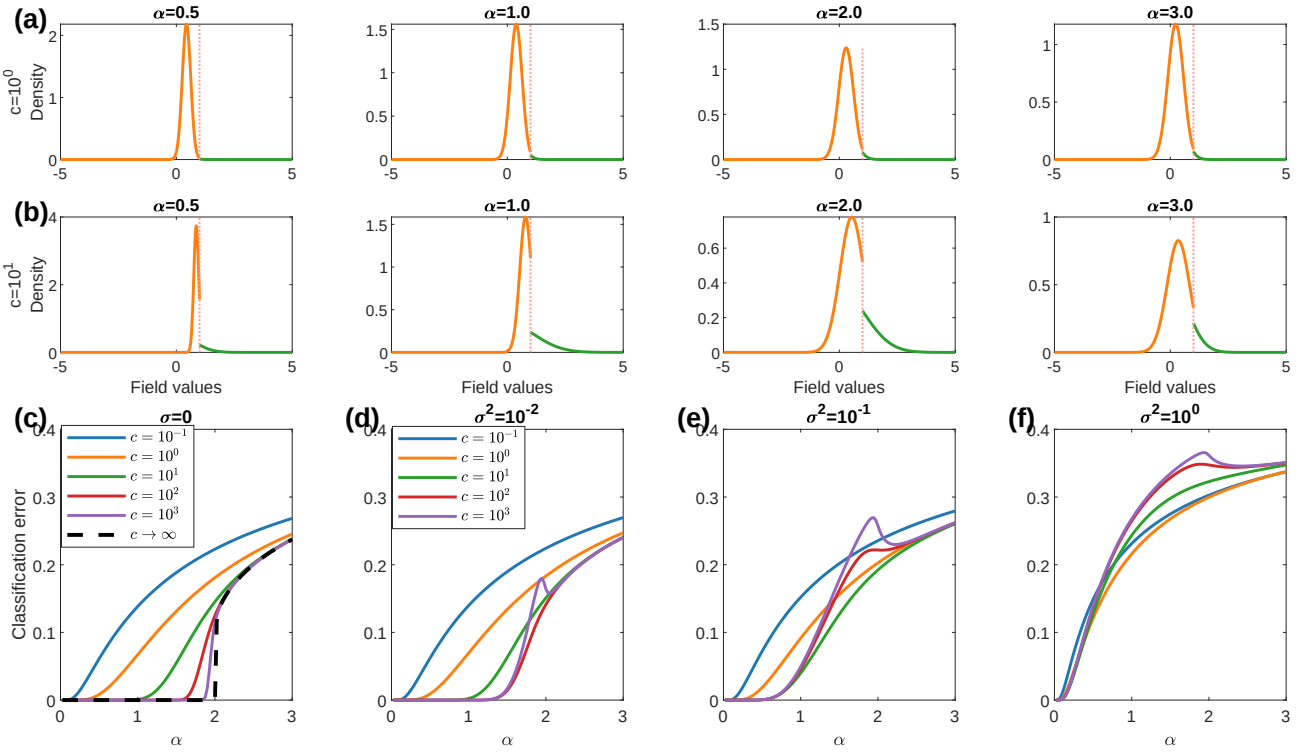


FIG. 2: Field distribution and errors in soft classification of points. (a-b) Field distributions at different values of α (panels), with color coded regime (orange: "touching" regime; green: "interior" regime; a dashed line at $h = 1$ indicates regime boundary), using $c = 1$ (a) and $c = 10$ (b). (c-f) Classification error (y-axis) for different values of α (x-axis) and choices of c (color coded), including the $c \to \infty$ limit (dashed line in (c)). Each panel (c-f) shows the error at a different noise level σ^2 (indicated in title).

added to the fields, so test error with respect to such noise is give by $\varepsilon_g = P\left(h + \eta\sigma\sqrt{q} < 0\right)$, where η is a standard Gaussian, or equivalently:

$$\varepsilon_g = \langle H\left(h/\sigma\sqrt{q}\right)\rangle_h \tag{14}$$

Equation 14 can be evaluated using the field distribution (equation 12). The resulting theoretical predictions are shown in figure 2d-f, exhibiting non-monotonic dependence on both c and α. A comparison of the theoretical predictions with simulation results for different choices of c and levels of noise is provided in figure S4.

Classification errors for small noise While an explicit expression for the error is complicated, when the noise is small relative to the margin from the optimal hyper-plane $\sigma \ll 1/\sqrt{q}$, we provide a simple approximation for the test error which can be written as a signal-to-noise ratio $\varepsilon_g \approx H(\mathcal{S})$ (hereafter: SNR; see details in section C 5):

$$\mathcal{S} = ck/\sqrt{q\left(1 + (1+ck)^2\sigma^2\right)} \tag{15}$$

From the scaling of q, k for large and small α-s we have:

$$\mathcal{S} \approx \begin{cases} 1/\sqrt{\alpha\left(1/(1+c)^2 + \sigma^2\right)} & \alpha \ll 1 \\ 1/\sqrt{\alpha\left(1+\sigma^2\right)} & \alpha \gg 1 \end{cases} \tag{16}$$

In this regime the optimal choice of c can be found by maximizing $\mathcal{S}$ (equation 15) with respect to c, that is solving $0 = \frac{\partial \mathcal{S}^{-2}}{\partial c}$ for c, which yields (see section C 6):

$$c^* = \frac{\sigma^{-2}}{1-k} - \frac{1}{k} \tag{17}$$

which is positive in the regime where the SNR is a valid approximation, and needs to be solved self-consistently as k depends on c. Due to the dependence on k we have that c^* depends on α, but this analysis also suggests a "canonical choice" of c which is independent of α:

$$c \approx \sigma^{-2} \tag{18}$$

This choice is expected to capture the order of magnitude of c^*, except when α is very small or very large (as equation 17 diverges for both $k \to 0$ and $k \to 1$).

Figure 3a demonstrates the optimal choice of c calculated by solving equation 17 and compares it to equation 18, showing this approximation is within the correct scale for a large range of α values. The resulting norm of the optimal solution changes smoothly with α (figure 3b) and the canonical choice of c achieves classification error which differs from the optimal one only when the error is much smaller than 1 (figure 3c), and is superior to other sub-optimal choices of c (figure S5).

B. Methods for soft classification of manifolds

A manifold $M^\mu \subseteq \mathbb{R}^N$ for index $\mu \in [1..P]$ is parameterized by its axes $\left\{\boldsymbol{u}_l^\mu \in \mathbb{R}^N\right\}_{l=0..D}^{\mu=1..P}$ and the manifold's intrinsic coordinates $\vec{S} \in \mathcal{M}^\mu \subseteq \mathbb{R}^{D+1}$. Each point in the manifold is a vector $\boldsymbol{x}^\mu(\vec{S}) \in M^\mu$ such that:

$$\boldsymbol{x}^\mu(\vec{S}) = \sum_{l=0}^{D} \boldsymbol{u}_l^\mu S_l \tag{19}$$

As above, the bold notation for $\boldsymbol{x}^\mu$ and $\boldsymbol{u}_l^\mu$ indicates that they are vectors in $\mathbb{R}^N$, whereas the arrow notation is used for other vectors, such as the coordinates $\vec{S}$ (not to be confused with the slack $\vec{s}$). By convention $\boldsymbol{u}_0^\mu$ is the manifold center and we take $S_0 = 1$, so that distances are measured in units of the center norm. When classifying P manifolds with weights $\boldsymbol{w} \in \mathbb{R}^N$, denoting axes projections $v_l^\mu = y^\mu \boldsymbol{u}_l^\mu \cdot \boldsymbol{w}$ the fields become:

$$h^\mu(\vec{S}) = y^\mu \boldsymbol{w} \cdot \boldsymbol{x}^\mu(\vec{S}) = v_0^\mu + \vec{S} \cdot \vec{v}^\mu \tag{20}$$

The classic soft classification formalism [3], called here point-slack SVM, uses one slack variable per sample. It is usually inapplicable for manifold classification as the number of samples may be infinite. Thus we consider two simple alternatives which allow for soft classification of manifolds, both require only a single slack variable per manifold. In several specific cases where the point-slack formalism can be used, it will be compared to those formalisms.

Center-slack method A naive approach for the classification of manifolds is to assume the soft classifier is learned using only the manifolds' centers and then evaluated on the entire manifolds. Formally, soft classification using center-slacks is defined by weights $\boldsymbol{w} \in \mathbb{R}^N$ and slack variables $\vec{s} \in \mathbb{R}^P$ such that the central fields obey for all $\mu \in [1..P]$:

$$v_0^\mu = y^\mu \boldsymbol{w} \cdot \boldsymbol{u}_0^\mu \geq 1 - s^\mu \tag{21}$$

Given a regularization parameter $c \geq 0$ the optimal classifier is defined by Lagrangian:

$$L = \|\boldsymbol{w}\|^2/N + c\|\vec{s}\|^2/N \ s.t.\ \forall \mu \ v_0^\mu \geq 1 - s^\mu \tag{22}$$

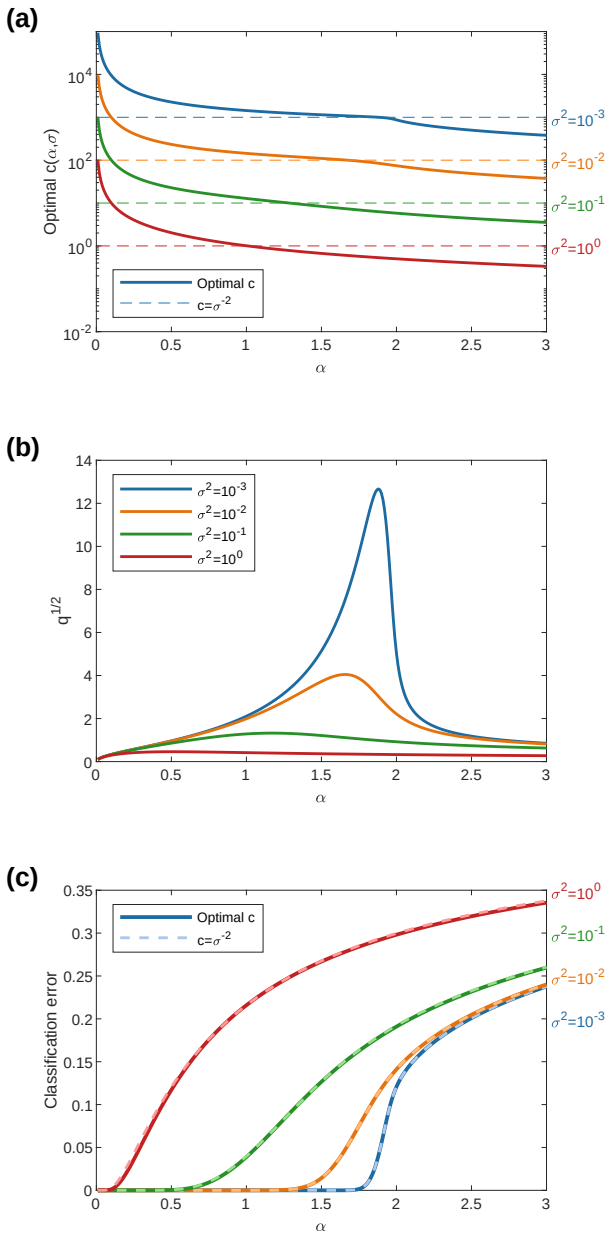


FIG. 3: The optimal choice of c in soft classification of points. (a) The optimal choice of c (y-axis, log scale) for different values of α (x-axis) and levels of noise σ^2 (color coded). Compares the optimal choice c^* (solid lines) and the canonical choice $c = \sigma^{-2}$ (dashed lines). (b) The weights' norm $q^{1/2}$ (y-axis) for different values of α (x-axis) and levels of noise σ^2 (color coded) when using the optimal value of c. (c) Classification error (y-axis) for different values of α (x-axis) and levels of noise σ^2 (color coded). Compares the optimal choice c^* (solid lines) and the canonical choice $c = \sigma^{-2}$ (dashed lines).

Using this method the manifold structure is not used during training, so the weights' norm and field distribution (with respect to the centers) are given by points classification theory from previous section. However, an evaluation of classification errors on the manifold would require additional assumptions on the manifold.

Manifold-slack method The previous method uses a slack variable to constrain the mean of the fields on the manifold. A natural alternative would be to constrain the minimal field on the manifold. Using the fields definition $h^\mu(\vec{S})$, soft classification using manifold-slacks is defined by weights $\boldsymbol{w} \in \mathbb{R}^N$ and slack variables $\vec{s} \in \mathbb{R}^P$ where the minimal fields obey for all $\mu \in [1..P]$:

$$h^\mu_{min} \doteq \min_{\vec{S} \in \mathcal{M}^\mu} h^\mu(\vec{S}) \geq 1 - s^\mu \tag{23}$$

That is, given a regularization parameter $c \geq 0$ the optimal classifier is defined by Lagrangian:

$$L = \|\boldsymbol{w}\|^2/N + c\|\vec{s}\|^2/N \ s.t. \ \forall \mu \ h^\mu_{min} \geq 1 - s^\mu \tag{24}$$

Figure 4 illustrates soft classification of points (or manifold centers, as noted above), spheres and general manifolds. In what follows we first discuss spheres, then extend the discussion to general manifolds.

C. Soft classification of spheres

A D-dimensional sphere of radius R in $\mathbb{R}^N$ is defined:

$$\boldsymbol{x}^\mu(\vec{S}) = \boldsymbol{u}^\mu_0 + R\sum_{l=1}^{D} S_l \boldsymbol{u}^\mu_l \ s.t. \ \|\vec{S}\| \leq 1 \tag{25}$$

As in the case of points we would analyze the classification problem for random labels $\vec{y} \in \{\pm 1\}^P$ and random axes $\boldsymbol{u}^\mu_{li} \sim \mathcal{N}(0, 1/N)$, i.e., again scaling $\|\boldsymbol{u}^\mu_l\| \approx 1$.

1. Center-slack

Using center-slacks the classifier properties are given by the theory of soft classification of points, self-consistent equations 7-8, and the distribution of the fields on the centers follows equation 12.

The classification error on the sphere is defined $\varepsilon = P(v_0 + R\sum_l v_l S_l \leq 0)$ but as $v_l = y\boldsymbol{w} \cdot \boldsymbol{u}_l$ where $\boldsymbol{w}$ is independent of $\boldsymbol{u}_l$ in this case, we have that $v_l \sim \mathcal{N}(0, q)$, and as $\|\vec{S}\| = 1$ on the sphere $R\sum_l v_l S_l \sim \mathcal{N}\left(0, qR^2\right)$. If we assume Gaussian noise $\mathcal{N}\left(0, \sigma^2/N\right)$ is added independently for each sample component, as we have done for points, we have noise of $\mathcal{N}\left(0, q\left(\sigma^2 + R^2\right)\right)$ at the fields. Thus the error is given by $\varepsilon = P\left(v_0 + \sqrt{(\sigma^2 + R^2)\, q}\eta \leq 0\right)$ where η is a standard Gaussian, or equivalently:

$$\varepsilon = \left\langle H\left(v_0/\sqrt{(\sigma^2 + R^2)\, q}\right)\right\rangle_{v_0} \tag{26}$$

where surprisingly, the dimensionality D of the spheres plays no role in this setting.

We conclude that soft classification of spheres of radius R using center-slacks with noise level of σ^2 is equivalent to soft classification of points with effective noise $\sigma^2_{eff} = \sigma^2 + R^2$. Several corollaries can be made from the analysis of points, by using the effective noise σ^2_{eff} instead of σ^2. First, when $\left(\sigma^2 + R^2\right) q \ll 1$ we expect a good SNR approximation $\varepsilon \approx H(\mathcal{S})$ using:

$$\mathcal{S} = ck/\sqrt{q\left(1 + (\sigma^2 + R^2)\,(1 + ck)^2\right)} \tag{27}$$

Figure 5a show the resulting error when sampling from the sphere (i.e., $\sigma = 0$) for different values of R, and figure S6 compares the theory to the error measured empirically. Second, the optimal choice of c is then given by equation 17, as well as the "canonical choice"

$$c \approx 1/\left(\sigma^2 + R^2\right) \tag{28}$$

Contrary to the result from classification of points, due to the contribution of R, here the optimal choice for c is finite even for $\sigma = 0$, as illustrated in figure 5b.

2. Manifold-slack

We now consider soft classification of the entire manifold, that is $h^\mu_{min} \geq 1 - s^\mu$, thus generalizing the analysis of max-margin classifiers for spheres [6]. For spheres the point with the "worst" field, or minimal overlap with $\boldsymbol{w}$, is given by $\vec{S} = -\hat{v}$ (where $\hat{v} = \vec{v}/\|\vec{v}\|$), and hence a necessary and sufficient condition for the soft classification of the entire sphere is given by $v^\mu_0 - R\|\vec{v}^\mu\| \geq 1 - s^\mu$.

Replica theory This observation allows us to write an expression for the volume $V(L, c)$ of solutions achieving a target value of the loss L:

$$V(L, c) = \int d^N\boldsymbol{w} \int d^P\vec{s}\,\delta\left(\|\boldsymbol{w}\|^2 + c\|\vec{s}\|^2 - NL\right) \tag{29}$$

$$\cdots \prod_\mu^P \delta\left(v^\mu_0 - R\|\vec{v}^\mu\| - h^\mu\right)\Theta\left(h^\mu - 1 + s^\mu\right) \tag{30}$$

A replica analysis yields the following relation between L, α and the two order parameters q, k when the volume of solutions vanishes (see details in section C 7):

$$L/q = \frac{k-1}{k} + \frac{\alpha}{k}\int D^D\vec{t} \int Dt_0 F\left(\vec{t}, t_0\right) \tag{31}$$

$$F\left(\vec{t}, t_0\right) = \min_{v_0 - R\|\vec{v}\| \geq 1/\sqrt{q}} \left\{\|\vec{v} - \vec{t}\|^2 + \frac{ck}{1 + ck}\left(v_0 - t_0\right)^2\right\} \tag{32}$$

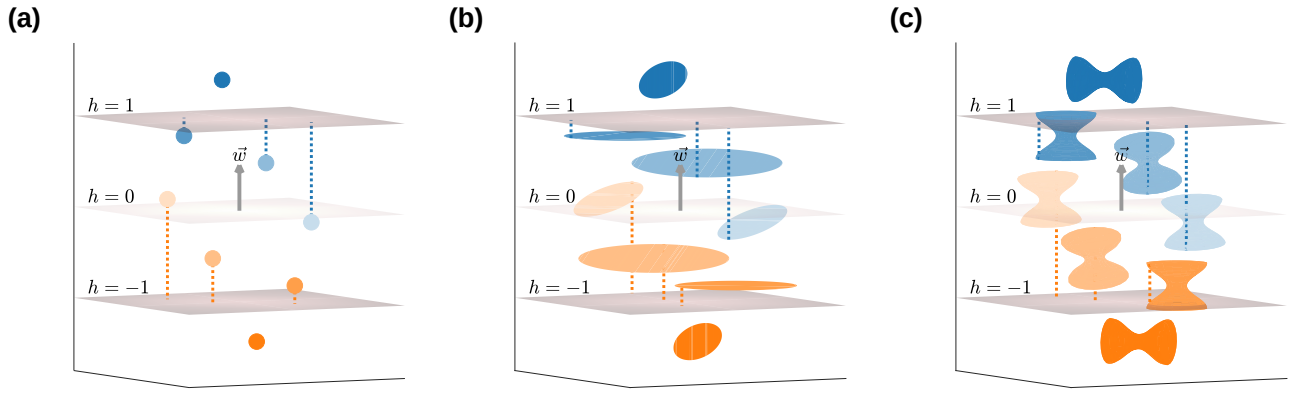


FIG. 4: Illustration of soft classification of points, spheres and general manifolds. A weight vector $\boldsymbol{w}$ (gray arrow) defines the signed fields $h = \boldsymbol{w} \cdot \boldsymbol{x}$ on the manifolds being classified, satisfies $y\boldsymbol{w} \cdot \boldsymbol{x} \geq 1 - s$. The light gray hyper-plane depicts the decision boundary $h = 0$; points above it are labeled $+1$ and below it -1. The dark gray hyper-planes depicts the boundaries $h = \pm 1$. The length of each manifold's slack is indicated by a dashed line from the manifold point with the minimal field $y\boldsymbol{w} \cdot \boldsymbol{x}$ to the hyper-plane $h = y$. Each panel depicts the classification of 4 blue manifolds (target label is $+1$) against 4 orange manifolds (target label is -1). The blue and orange manifolds are symmetrically positioned for illustration purposes only. Manifolds are numbered from darkest to lightest. (a) Classification of points: the 1st point is in the interior $y\boldsymbol{w} \cdot \boldsymbol{x} > 1$, has $s = 0$; the 2nd and 3rd points have non-zero slack $0 < s < 1$, are classified correctly; the 4th point is below the decision boundary $y\boldsymbol{w} \cdot \boldsymbol{x} < 0$, corresponds to an error, has $s > 1$. (b) Classification of spheres: the 1st sphere is in the interior $y\boldsymbol{w} \cdot \boldsymbol{x} > 1$, the 2nd sphere is fully embedded within the hyper-plane $y\boldsymbol{w} \cdot \boldsymbol{x} = 1 - s$, the 3rd and 4th spheres touching the hyper-plane $y\boldsymbol{w} \cdot \boldsymbol{x} \geq 1 - s$ with the minimal field above 0 for the 3rd, below 0 for the 4th. (c) Classification of general manifolds: the 1st manifold is in the interior $y\boldsymbol{w} \cdot \boldsymbol{x} > 1$, the 2nd manifold has a face embedded within the hyper-plane $y\boldsymbol{w} \cdot \boldsymbol{x} = 1 - s$, the 3rd and 4th manifolds touching the hyper-plane $y\boldsymbol{w} \cdot \boldsymbol{x} \geq 1 - s$ with the minimal field above 0 for the 3rd, below 0 for the 4th.

where $q = \|\boldsymbol{w}\|^2/N$ and $Dt_0 = dt_0 e^{-t_0^2/2}/\sqrt{2\pi}$ so $\vec{t}, t_0$ are $D+1$ Gaussian variables representing the quenched noise in the solution, due to the variability of the labels $\{y^\mu\}$ and the manifolds' axes $\{\boldsymbol{u}_l^\mu\}$.

Solving the inner problem (equation 32) using Karush-Kuhn-Tucker conditions [17] (hereafter: KKT), allows us to describe the joint distribution of v_0, $v = \|\vec{v}\|$, and s conditioned on $t_0, t = \|\vec{t}\|$ at different solution regimes (see details in section C 8):

1. "Interior" regime: the entire sphere is classified correctly with $h > 1$ and a margin larger than $1/\sqrt{q}$ from the hyper-plane $h = 0$; in this regime the slack is not utilized $s = 0$ and the solution satisfies $v_0 = t_0$, $v_l = t_l$ so that $F = 0$. This regime is in effect for $1/\sqrt{q} + Rt \leq t_0 \leq \infty$.

2. "Touching" regime: the tip of the sphere touches the hyper-plane $h = 1 - s$; in this regime v_0, v, s have non-trivial values. This regime is in effect for $1/\sqrt{q} - \frac{1+ck}{ck} t/R \leq t_0 \leq 1/\sqrt{q} + Rt$.

3. "Embedded" regime: the entire sphere is within the hyper-plane $h = 1 - s$; in this regime $v = 0$ but v_0, s have non-trivial values. This regime is in effect for $-\infty < t_0 \leq 1/\sqrt{q} - \frac{1+ck}{ck} t/R$.

The KKT analysis also provides the minimization value $F(t_0, t)$ achieved at each regime, so that denoting $f(R, D, ck, q) = \int D^D \vec{t} \int Dt_0 F\left(\vec{t}, t_0\right)$ we have (see details in section C 8):

$$f(R, D, ck, q) = \int \chi_D(t) \int_{-\infty}^{1/\sqrt{q} - \frac{1+ck}{ck} t/R} Dt_0 \left[\frac{ck}{1+ck} \left(1/\sqrt{q} - t_0\right)^2 + t^2 \right] \tag{33}$$

$$+ \int \chi_D(t) \int_{1/\sqrt{q} - \frac{1+ck}{ck} t/R}^{1/\sqrt{q} + Rt} Dt_0 \frac{ck}{1 + ck\left(1 + R^2\right)} \left(1/\sqrt{q} + Rt - t_0\right)^2 \tag{34}$$

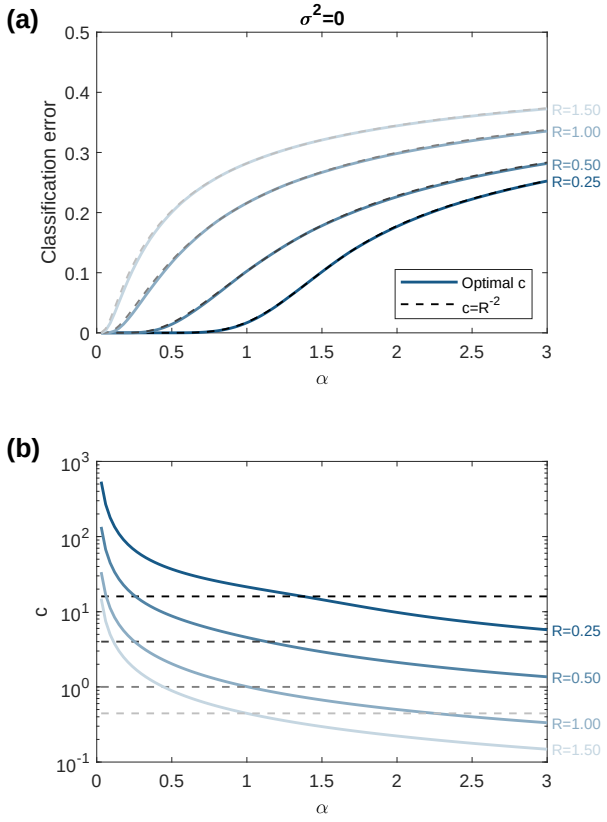


FIG. 5: Soft classification of spheres using center-slacks. (a) Classification error (y-axis) for different values of α (x-axis) and R (color coded), without noise $\sigma^2 = 0$, using the optimal choice of c (solid lines) and the canonical choice $c = R^{-2}$ (dashed lines). (b) The optimal choice of c (y-axis, log scale) for different values of α (x-axis) and R (color coded), without noise $\sigma^2 = 0$. The canonical choice $c = R^{-2}$ is indicated by the dashed horizontal lines.
Those results are independent of D, see main text.

where $\chi_D(t)$ is the Chi distribution with D degrees of freedom, $\chi_D(t) = \frac{2^{1-D/2}}{\Gamma(D/2)} t^{D-1} e^{-t^2/2} dt$, and the mean-field equation becomes:

$$L/q = \frac{k-1}{k} + \frac{1}{k}\alpha f(R, D, ck, q) \tag{35}$$

Self-consistent equations Assuming the optimal loss L^* satisfies saddle-point conditions $0 = \frac{\partial L}{\partial q} = \frac{\partial L}{\partial k}$, we have 2 self-consistent equations for k, q, similar to those found in the case of points:

$$1 = \alpha f - \alpha k \frac{\partial}{\partial k} f \tag{36}$$

$$1 - k = \alpha f + \alpha q \frac{\partial}{\partial q} f \tag{37}$$

See the concrete form, equations C277,C279, in section C 9. Those equations can be solved numerically to predict the weights' norm; the algorithm is formally described in section B 2. This prediction is compared to the norm observed in simulations (i.e., by finding the optimal weights for classification of spheres, using an algorithm described in section B 3). Figure 6 shows the resulting q, k for specific values of R, D (and additional ones are presented in figure S8); $k(\alpha)$ decrease monotonically from 1 to 0 while $q(\alpha)$ has a single peak, increasing from 0 to a finite value at the peak, then decreasing monotonically.

As in the case of points, in the limit $c \to \infty$, we find a different behavior below and above α_C^{Hard}, the max-margin capacity. For $\alpha < \alpha_C^{Hard}$ we have that k is finite while ck diverges, with equation 36 becoming the mean-field equation from max-margin classification [6], and the underlying Lagrangian is given by

$$L = \|\boldsymbol{w}\|^2/N \quad s.t.\ \forall \mu\ h_{min}^{\mu} \geq 1 \tag{38}$$

On the other hand, for $\alpha > \alpha_C^{Hard}$ we have that k approaches 0 while q and $K = \lim_{c\to\infty} ck$ are finite (see details in section C 10), with the underlying Lagrangian

$$L = \|\vec{s}\|^2/N \quad s.t.\ \forall \mu\ h_{min}^{\mu} \geq 1 - s^{\mu} \tag{39}$$

A second interesting limit is $\alpha \to 0$. In this limit we expect the order parameters to behave as in the case of points, $q \to 0$ and $k \to 1$. We find that for small α the self-consistent equations are simplified and for $\alpha \ll 1$ we have the approximations $k \approx 1 - \alpha(1 + D)$ and $q \approx \alpha (ck)^2 / (1 + ck)^2$ (see figures 6, S8 where those approximations are marked; see details in section C 10).

Phase-transition An analysis of the mean-field equations reveals that for spheres (unlike points) there is a finite value of α where $q \to 0$, and above which there is no solution with $q > 0$ (visible also in figures 6, S8). The corresponding simulation results indicate that when the theory equations cannot be solved the optimal classifier is $\boldsymbol{w} = \boldsymbol{0}$, that is $q = 0$, with all the slack variable saturating at $\vec{s} \equiv 1$. Thus, soft-margin classification problems always have a solution, unlike max-margin classification problem; but when there is no solution with loss below $L = c\alpha$, the optimal choice uses zero weights and unit slack variables.

The critical value for α can be found by assuming that both $k, \sqrt{q} \ll 1$; using a scaling of $x = ck/\sqrt{q}$ we get that $\alpha = \alpha_C$ would satisfy:

$$\alpha_C^{-1} = \int_0^{xR} \chi_D(t)\, t^2 + xR \int_{xR}^{\infty} \chi_D(t)\, t \tag{40}$$

$$x = \left(1 + R^2 \int_{xR}^{\infty} \chi_D(t)\right)^{-1} R \int_{xR}^{\infty} \chi_D(t)\, t \tag{41}$$

where x is the self-consistent solution of equation 41. Above this value of α there is no solution for k, q (see details in section C 11).

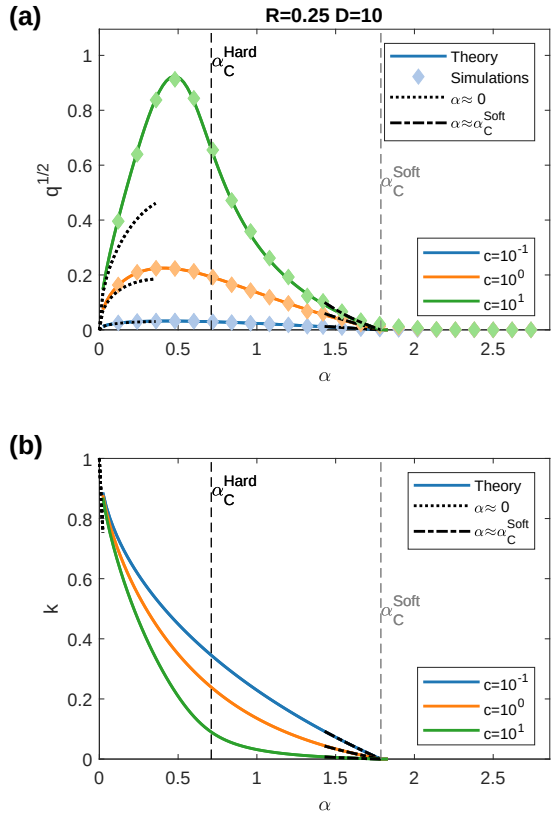


FIG. 6: Order parameters in soft classification of spheres using manifold-slacks. (a) The weights' norm $q^{1/2}$ (y-axis) for different values of α (x-axis), and choices of c (color coded), for radius $R = 0.25$ and dimension $D = 10$. Compares theory results (solid lines) to simulation results (diamonds).
(b) The order parameter k (y-axis) for different values of α (x-axis), and choices of c (color coded).
(a-b) Theory for the limits of $\alpha \to 0$, $\alpha \to \alpha_C^{Soft}$ is marked as black dotted, dash-dot lines, respectively.

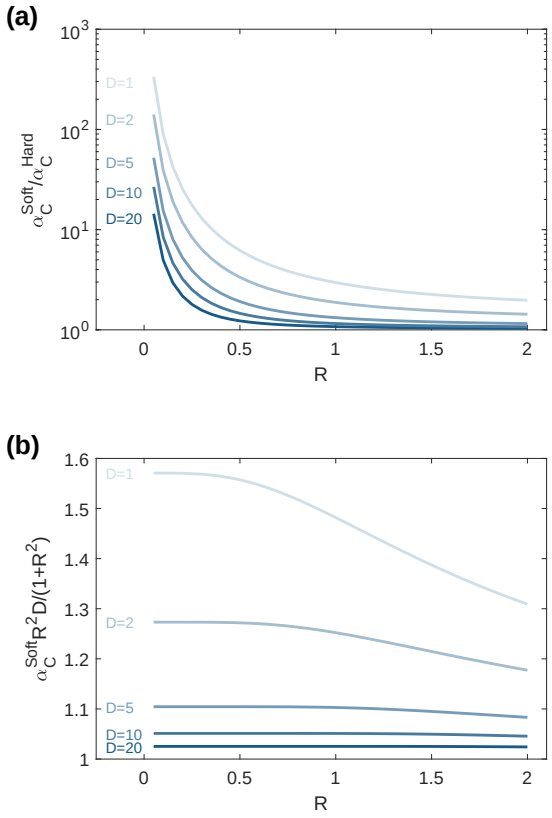


FIG. 7: Capacity in manifold-slack classification of spheres. (a) The ratio between α_C^{Soft} and α_C^{Hard} (y-axis, log scale) for different values of R (x-axis) and D (color coded). (b) The ratio between α_C^{Soft} and equation 42 approximation (y-axis) for different values of R (x-axis) and D (color coded).

Surprisingly, the critical value is independent of c and we denote it α_C^{Soft}, as a soft analog of the max-margin capacity α_C^{Hard} [6]. Notably, the former is always larger $\alpha_C^{Soft} \geq \alpha_C^{Hard}$, as shown in figure 7a.

For $R \to 0$ we have that $x = R\int_0^\infty \chi_D(t)\, t = R\sqrt{2}\Gamma\left(\frac{D}{2}+\frac{1}{2}\right)/\Gamma\left(\frac{D}{2}\right)$ and $\alpha_C^{-1} = x^2$. Thus, for small R, the critical value α_C^{Soft} diverges as R^{-2} (and in the limit of points there is no phase transition). Conversely, for $R \to \infty$ we have $x \approx 0$ and $\alpha_C^{Soft} = D^{-1}$, whereas in this limit $\alpha_C^{Hard} = (D+1/2)^{-1}$ [6]. Intuitively, in both cases $\boldsymbol{w}$ must be perpendicular to the PD manifold axes; for soft classification this implies just $N > PD$ or $\alpha < D^{-1}$, while for max-margin classification due to the finite capacity when classifying the centers this means $P/(N-PD) < 2$ or $\alpha < (D+1/2)^{-1}$.

The existence of a sharp transition in the manifold-slack problem is the result of the thermodynamic limit. For small N, the existence of a solution at any given α depends on the particular labels realization. As N increases, the probability of having a solution approaches 1 for $\alpha < \alpha_C$ and zero for $\alpha > \alpha_C$ (figure S7).

Phase-transition for large D regime When $D \gg 1$ the phase-transition equations 40-41 implies a simple expression for capacity:

$$\alpha_C^{Soft} \approx \left(1+R^2\right)/R^2 D \tag{42}$$

Figure 7b compares this approximation to the full expression for different values of R, D; as observed, this approximation is reasonable for large D independently of the value of R (see details in section C 11). In this regime the max-margin capacity is given by [6]:

$$\alpha_C^{Hard} \approx \left(1+R^2\right)\alpha_0(R\sqrt{D}) \tag{43}$$

Classification errors As for points, the mean-field theory also provides the full distribution of the fields and slack variables (see details in section C 12). Figure S9 compares the theoretical slack distribution to the histogram of the values observed in simulations. In what follows we use these distributions to calculate different kinds of classification errors.

In the framework of manifold-slacks it is natural to consider the probability of error anywhere on the manifold, or equivalently the fraction of manifolds where the worst point is misclassified. This is the fraction of slack variables that are larger than 1, i.e., $\varepsilon_{tr}^{manifold} = P(s \geq 1)$, which can be evaluated from the slack distribution (equation C357 in section C 12). This entire-manifold classification error is given by $\varepsilon_{tr}^{manifold} = H(\mathcal{S})$ for $\mathcal{S}$ from equation C363 in section C 13.

A different kind of error is the probability of classification error on uniformly sampled points from the sphere, that is $\varepsilon_{tr}^{sample} = P(h < 0)$, similar to the error considered above for center-slacks. These fields can be written as $h = v_0 + Rvz$, where $z = \cos(\theta)$ for θ the angle between the weight vector and the point on the sphere, v_0 and $v = \|\vec{v}\|$ are the projections of the weight vector on the center and the sphere subspace. Thus, $\varepsilon_{tr}^{sample} = P(v_0 + Rvz < 0)$, where the joint distribution of v_0, v is given by theory (equations C355,C356 in section C 12), and for a uniform sampling from a sphere $z \in [-1, 1]$ has a bell-shaped distribution:

$$P(z) = \frac{1}{\sqrt{\pi}} \left(1 - z^2\right)^{\frac{D-3}{2}} \Gamma\left(\frac{D}{2}\right) / \Gamma\left(\frac{D-1}{2}\right) \quad (44)$$

with moments $\langle z \rangle = 0$ and $\langle \delta z^2 \rangle = 1/D$ (see details in section C 13). In this setting classification error monotonically decreases with c so the optimal value of $\varepsilon_{tr}^{sample}$ is achieved for $c = \infty$.

We now consider the classification error of points on the sphere in the presence of noise, where the classifier is trained on the entire manifold (i.e., with no noise), and tested on noisy samples from the manifold. Assuming Gaussian noise $\mathcal{N}\left(0, \sigma^2/N\right)$ is added to each component of manifold samples, the fields are affected by noise $\mathcal{N}\left(0, \sigma^2 q\right)$, so the probability of error in a sample is given by $P\left(h + \sigma\sqrt{q}\eta < 0\right)$ where η is standard Gaussian, and equivalently:

$$\varepsilon_g^{sample} = \left\langle H\left(\frac{v_0 + Rzv}{\sigma\sqrt{q}}\right)\right\rangle_{v_0,v,z} \quad (45)$$

Large D regime The regime of spheres with $D \gg 1$ is important as real-world manifolds are expected to be high-dimensional, and in this regime it is possible to derive an SNR approximation of equation 45.

When $R \sim O(1)$, α_C^{Soft} is close to α_C^{Hard} (see figure 7). Thus in this regime the benefit of soft classification, in terms of the range of valid solutions, is small. On the other hand, when $R\sqrt{D} \sim O(1)$, α_C^{Soft} can be much larger than α_C^{Hard} (figure 7a), and thus we focus on this regime in our analysis of classification errors.

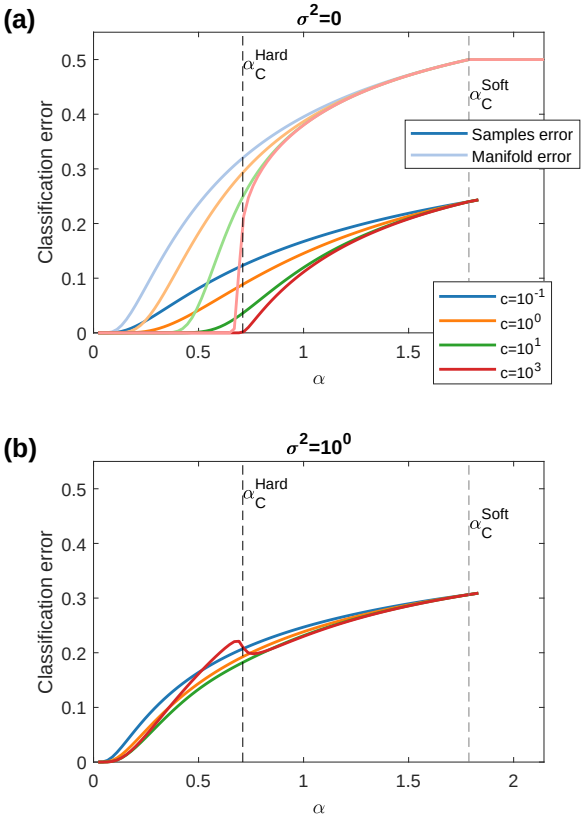


FIG. 8: Errors in soft classification of spheres. Results for spheres of radius $R = 0.25$ and dimension $D = 10$. (a) Classification error without noise (y-axis) for different values of α (x-axis) and choices of c (color coded). Compares samples' classification error (dark lines) and entire-manifold classification error (light lines). (b) Classification error at noise level $\sigma^2 = 1$ (y-axis) for different values of α (x-axis) and choices of c (color coded).

To derive an SNR approximation we assume that in this regime $v_0 + Rzv$ is approximately Gaussian, and that only the "touching" regime contributes to the error, thus substituting the values of v_0, v derived from the mean-field theory in that regime (equations C355,C356 in section C 12). The resulting SNR is provided in equations C380, C381 in section C 13.

Importantly, from this analysis we can calculate the limiting behavior of the SNR. In the $\alpha \to 0$ limit the error anywhere on the manifold (equation C363 in section C 13) scales as $\lim_{\alpha\to 0} \varepsilon_{tr}^{manifold} = H\left(ck/\sqrt{q}\right)$, and

using the order parameters in this limit leads to:

$$\lim_{\alpha\to 0}\varepsilon_{tr}^{manifold}=H\left(\left(1+c\right)/\sqrt{\alpha}\right) \tag{46}$$

which is exactly the scaling for classification of the center points alone ($\varepsilon_{tr}^{centers}$, equation 16 with $\sigma^2=0$). Thus in this regime (i.e., $N\to\infty$) the manifold structure does not affect the classification error and furthermore the error in classification of the entire sphere is the same as the error in classification of samples $\varepsilon_{tr}^{sample}$, as the former is bounded between the two classification errors $\varepsilon_{tr}^{centers}\leq\varepsilon_{tr}^{sample}\leq\varepsilon_{tr}^{manifold}$.

On the other hand, in the $\alpha\to\alpha_C^{Soft}$ limit, from the scaling of k,q in this limit (see section C 10) the error in classifying the entire manifold saturates (using equation C363 in section C 13), but not the error classifying samples (see section C 13):

$$\lim_{\alpha\to\alpha_C^{Soft}}\varepsilon_{tr}^{manifold}=H\left(0\right)=1/2 \tag{47}$$

$$\lim_{\alpha\to\alpha_C^{Soft}}\varepsilon_{g}^{sample}=H\left(\frac{R\sqrt{D}}{1+R^2}\frac{1}{\sqrt{1+\sigma^2}}\right) \tag{48}$$

Figure 8a presents both types of training errors and their dependence on α and c at specific values of R,D, demonstrating that they are monotonically decreasing with c and monotonically increasing with α. Figure 8b presents the test error at a specific noise level; unlike the training error, the test error is not monotonic in c and thus is minimized for a finite value of c. Theory's agreement with empirical simulations is presented for different parameter values and choices of c in figure S10 for the training error, and similarly in figure S11 for the test error. Thus the theory predicts that errors at the phase transition are independent of c (as seen in figure 8) and jump from this finite value to 0.5 (and for a finite N this transition is smoothed, as already discussed above).

The described theory can be used to choose the optimal value of c. Figure S12 compares, for different values of R,D and noise levels, the optimal error achieved in simulations and by optimizing the theoretical value. Figure S13 presents the optimal value of c for different values of α and levels of noise, demonstrating a non-trivial behavior for manifold-slacks, unlike the monotonic behavior predicted by theory for center-slacks.

Comparison with other methods Comparing the performance of the manifold-slack method with other methods requires optimization of the regularization value c independently for each method. When there is no noise, below max-margin capacity $\alpha<\alpha_C^{Hard}$, the optimal choice of c is infinite such that manifold-slack classification converges to max-margin classification. However, in the presence of noise the optimal value of c is finite and using manifold-slacks reduces

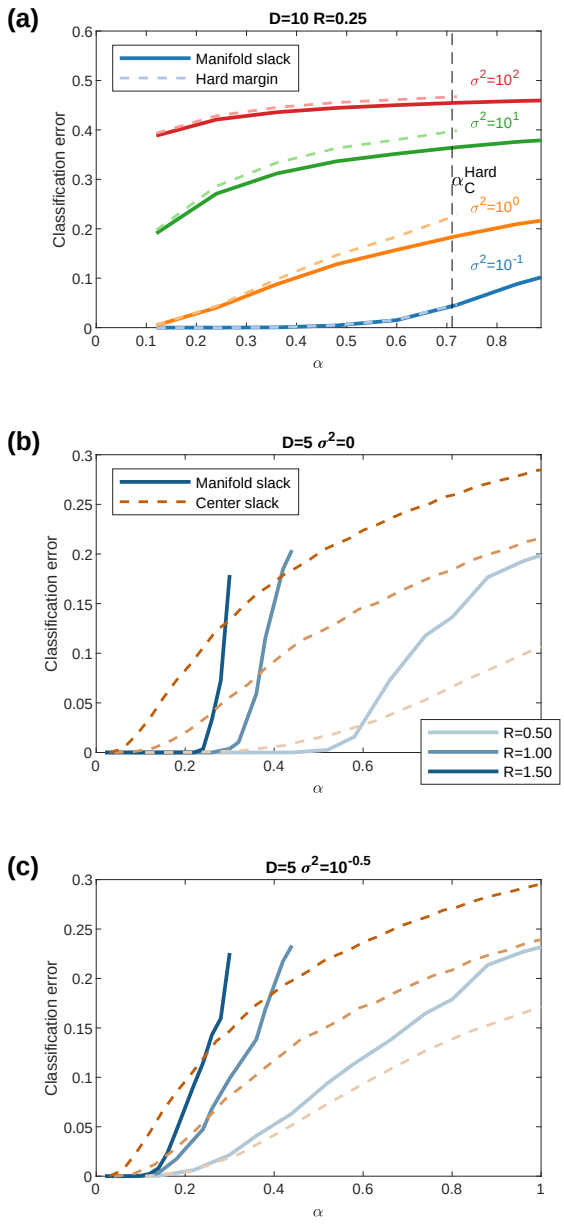


FIG. 9: Comparison of classification errors for spheres using different methods. (a) Classification error (y-axis) using manifold-slacks (at the optimal choice of c, solid lines) or max-margin classification (dashed lines) at different values of α (x-axis) for radius $R=0.25$ and dimension $D=10$. Compares simulation results at different noise levels (color coded). (b-c) Classification error using the optimal choice of c (y-axis) for different values of α (x-axis) and values of R (color coded), for dimension $D=5$. Compares simulation results of manifold-slack classifiers (solid lines) and center-slack classifiers (dashed lines), without noise (b) and with noise (c).

classification error relative to max-margin classification (figure 9a). While the manifold-slack method is strictly better than the max-margin method due to choosing from a larger pool of classifiers, the improvement is usually small and is achieved toward α_C^{Hard} (see figure S14).

A systematic comparison of the manifold-slack and center-slack methods finds that manifold-slacks are better for small α values, with notable benefits at larger R and smaller σ values (see figure 9b-c). Intuitively, when the noise is small, manifold-slacks may achieve near-zero error at a range of α values, while center-slacks performance depends on R as a noise term and thus may be order 1 when R is order 1. For larger α values the performance of center-slacks surpasses that of manifold-slacks, and finally above α_C^{Soft} only the center-slack method is a viable option. Figure S15 presents the field distribution (at the manifold center) when using either center-slack or manifold-slack methods. The differences between those distributions provide intuition for the observed difference in the behavior of errors: at α_C^{Hard} the central fields using manifold-slacks are much larger than using center-slacks, but at α_C^{Soft} the central field distribution using manifold-slacks becomes $\delta(x)$.

As noted above, the point-slack method cannot in general be used for classification of manifolds with an infinite number of points. However, for classification of line segments (i.e., spheres with $D = 1$), a correct classification of the $2P$ end-points is enough to classify the entire line. Figure S16 compares manifold-slack with point-slack classification of the $2P$ end-points, both using the optimal choice of c for a given level of noise. The performance of point-slack SVM is usually close to that of the manifold-slack method, but provides a significant improvement toward α_C^{Soft}. It is interesting to observe that while using the manifold-slack method (with P slack variables) there is a phase transition where the non-trivial classifier vanishes at a finite α, there is no such transition using the point-slack method (with $2P$ slack variables), as expected from the point-slack theory (compare the weights' norms in figure S16a,b).

D. Soft classification of general manifolds

1. Center-slack

The center-slack method is straightforward to generalize to general manifolds, with the centers defined per our definition of a general manifold ($\boldsymbol{u}_0$ in equation 19). A classifier trained on the centers would have a norm per points theory (equations 7-8), and central field distribution per equation 12.

The probability of classification error for a point on the manifold $\boldsymbol{x}(\vec{S})$ would be $\varepsilon(\vec{S}) = P\left(v_0 + \vec{S}\cdot\vec{v} \le 0\right)$ with $\vec{S}\cdot\vec{v} \sim \mathcal{N}\left(0, q\|\boldsymbol{x}(\vec{S}) - \boldsymbol{u}_0\|^2\right)$. A calculation of classification error on a general manifold requires to make further assumptions on the sampling of $\vec{S} \in \mathcal{M}$ (see discussion). However, for the simple case of uniform sampling from a point-cloud manifold where $\boldsymbol{x}_m = \boldsymbol{u}_0 + \delta\boldsymbol{x}_m$ for $m = 1..M$ we have that:

$$\varepsilon = \frac{1}{M}\sum_{m=1}^{M}\left\langle H\left(v_0/\sqrt{(\sigma^2 + \|\delta\boldsymbol{x}_m\|^2)\,q}\right)\right\rangle_{v_0} \tag{49}$$

where σ^2/N is the variance of Gaussian noise added to each component, which generalize equation 26 from spheres, with the empirical $\|\delta\boldsymbol{x}_m\|^2$ taking the role of R^2. Furthermore, when the number of samples is large we expect self-averaging:

$$\varepsilon = \left\langle H\left(v_0/\sqrt{\left(\sigma^2 + \hat{R}^2\right)q}\right)\right\rangle_{v_0} \tag{50}$$

for $\hat{R}^2 = \frac{1}{M}\sum_{m=1}^{M}\|\delta\boldsymbol{x}_m\|^2$ the total variance of the manifold points. Figure S17 compares the full theory (equation 49) and the approximation (equation 50) to empirical measurement of the error using center-slacks.

2. Manifold-slack

Replica theory Generalizing the mean-field equations of spheres (equations 31-32) to the case of general manifolds, following the approach used by [7] for max-margin classifiers, the theory implies:

$$L/q = \frac{k-1}{k} + \frac{\alpha}{k}\int D^D\vec{t}\int Dt_0 F\left(\vec{t}, t_0\right) \tag{51}$$

$$F\left(\vec{t}, t_0\right) = \min_{\min_{S\in\mathcal{M}}\vec{v}\cdot\vec{S}\ge 1/\sqrt{q}}\left\{\|\vec{v} - \vec{t}\|^2 + \frac{ck}{1+ck}\left(v_0 - t_0\right)^2\right\} \tag{52}$$

Generalizing the notion of anchor points from [7], we define them formally as the subgradient $\frac{\partial}{\partial v}$ of the support function $\min_{S\in\mathcal{M}}\vec{v}\cdot\vec{S}$:

$$\tilde{S}\left(\vec{v}\right) = \frac{\partial}{\partial v}\min_{S\in\mathcal{M}}\vec{v}\cdot\vec{S} \tag{53}$$

When the support function is differentiable, the subgradient is unique and is equivalent to the gradient [7]:

$$\tilde{S}\left(\vec{v}\right) = \arg\min_{\vec{S}\in\mathcal{M}}\vec{S}\cdot\vec{v} \tag{54}$$

For a given data manifold $\mathcal{M}^\mu$ and known values of q, k, one can sample from the anchor point distribution using the mean-field theory (see details in section C 14):

$$\tilde{S}\left(\vec{t}, t_0\right) = \frac{\vec{v}^* - \vec{t}}{\frac{ck}{1+ck}\left(v_0^* - t_0\right)} \tag{55}$$

where $\vec{v}^*, v_0^*$ are the values which minimize $F\left(\vec{t}, t_0\right)$, which can be found using least-squares optimization methods. This algorithm for sampling from the anchor point distribution is formally described in section B 4.

Large D regime For large D we may define manifold properties R_M, D_M through the statistics of anchor points, as in max-margin classifiers [7]:

$$R_M^2 = \left\langle \|\delta\tilde{S}\|^2 \right\rangle_{\vec{t},t_0} \tag{56}$$

$$D_M = \left\langle \left(\vec{t}\cdot\delta\tilde{S}\right)^2 / \|\delta\tilde{S}\|^2 \right\rangle_{\vec{t},t_0} \tag{57}$$

Now we may use R_M, D_M to solve for q, k using the self-consistent equations from the theory of spheres. Thus for each value of α, c we can iteratively calculate R_M, D_M by sampling anchor points using the current values of q, k, then update the estimation of q, k, until convergence. This algorithm is formally described in section B 6.

As was the case for spheres, when D is large we expect only the "touching" regime to contribute, and from KKT condition applied to the minimization problem $F\left(\vec{t}, t_0\right)$ we get a self-consistent relation:

$$\vec{v} = \vec{t} + \frac{ck}{1+ck}\left(1/\sqrt{q} - \vec{v}\cdot\tilde{S} - t_0\right)\tilde{S} \tag{58}$$

Thus equations 54,58 can be used to iteratively update $\vec{v}$ and $\tilde{S}$ (see section C 14). This iterative approach allows for finding the anchor points without solving a least-squares optimization problem for each value of $\vec{t}, t_0$ (as the least-squares algorithm, section B 4). This algorithm is formally described in section B 5.

To use a concrete example, for simulations of general manifolds we have used point-cloud manifolds created by sampling M points from a D-dimensional ellipsoid with radii $r_l \sim l^{-\gamma}$. Denoting $R^2 = \sum_{l=1}^{D} r_l^2$ the ellipsoid shape is defined by parameters R, D, γ. Figures 10a-b, S18a-b demonstrate the existence of finite capacity when using manifold-slacks also for those manifolds. The predicted values of q matches the empirically observed values, which vanish at a finite α value (figures 10a, S18a). The dependence of the measured D_M on c and α is quite small (see figures 10c, S18c) and similarly for the measured R_M (see figures 10d, S18d).

Figure S19 presents the weights' norm for the classification of point-cloud manifolds and the theoretical values predicted for q, k, R_M, D_M, using either the iterative or the least-squares algorithm. The two algorithms give very similar results, with a notable difference at large R where the assumption that only the "touching" regime contributes to the solution no longer holds.

As it is favorable to have manifold properties D_M and R_M which do not depend on α, figure S20 shows that using a single choice of D_M, R_M, calculated for α near α_C^{Soft} (i.e., at the largest solvable values) to predict q provides a good approximation for the entire range of α (but not using a single choice of D_M, R_M calculated from a small α value).

Classification errors For general manifolds, the classification error is defined assuming manifold points are sampled according to some measure on the manifold (see discussion); for the simpler case of point-cloud manifolds, we assume this is a uniform distribution.

Figure 11a presents the predictions for the training error using the theory of spheres (equations C363, C380, C381 in section C 13) where the theoretical values of q, k, R_M, D_M, calculated using the least-squares algorithm, are plugged-in. Figure S21 compares the training error predicted using the theory of spheres classification with the error measured in simulations, finding good match. Similarly, figure 11b presents the predicted test error for specific noise level and different choices of c, and figure S22 compares the predicted test error for several noise levels and choices of c with simulation results, demonstrating again the applicability of measuring the manifolds' R_M, D_M and plugging them into the equations from the theory of spheres classification to make predictions regarding non-spherical manifolds.

Comparison with other methods Comparing the performance of different classification methods on point-cloud manifolds reveals a similar behavior to that observed for spheres. Figure S23 compares the manifold-slack method with both center-slack and max-margin methods, using the optimal choice of c for each method. Below α_C^{Hard} manifold-slack classification exhibits improved performance compared to max-margin classification, but this improvement is usually small (figure S23a-b). Figures 11c-d shows that as in the case of spheres, for small α values manifold-slacks are superior to center-slacks, with large qualitative difference at low noise level when R is order 1, while for larger α values the performance of the center-slack method is better (see additional noise levels in figure S23c).

For point-cloud manifolds, when the number of samples per manifold is not too large, the point-slack method can also be used for manifold classification. Figure S24a-d shows that using the point-slack method, there is no phase-transition to zero weights as for the manifold-slack method. Despite this marked difference, the classification error achieved by the point-slack method is only slightly better than that achieved by the manifold-slack method (both using the optimal choice of c, figure S24e-f). This improvement is significant only at small levels of noise and towards α_C^{Soft}. Thus point-slack SVM uses the additional degrees of freedom (and additional computational costs) from assigning a separate slack variable per sample to slightly outperform the manifold-slack method.

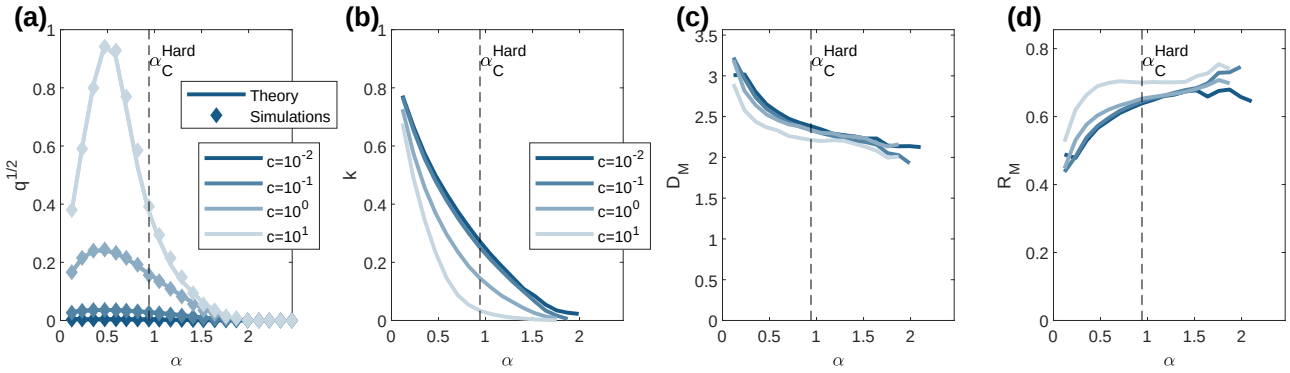


FIG. 10: Order parameters and manifold properties for point-cloud manifolds. Sampling $M = 100$ points from an ellipsoid with $\gamma = 1.5$, $R = 0.25, D = 20$. (a) The weights' norm $q^{1/2}$ (y-axis) for different values of α (x-axis) and choices of c (color coded). Compares theory (solid lines) and simulation results (diamonds). (b-d) The corresponding values of the order parameter k (b), manifold dimension D_M (c) and manifold radius R_M (d) (y-axis) for different values of α (x-axis) and choices of c (color coded).

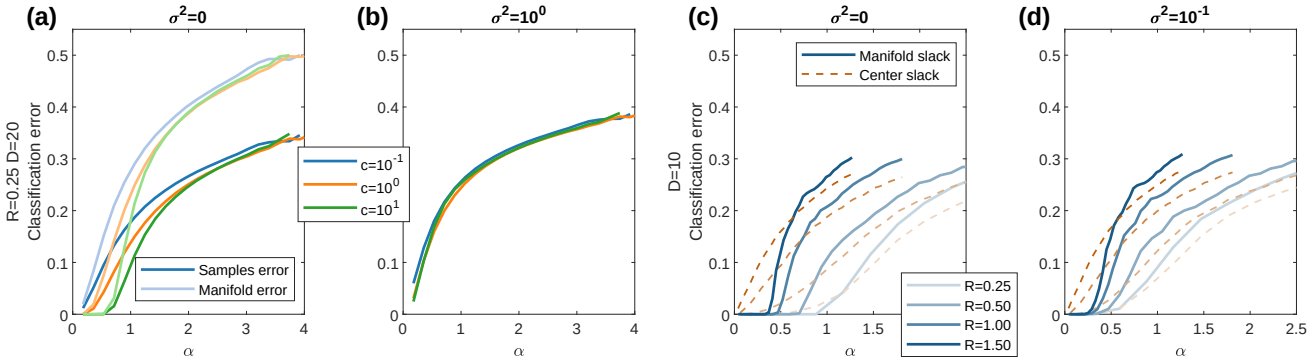


FIG. 11: Errors in soft classification of point-cloud manifolds. (a-b) Results for manifolds of $M = 100$ points from an ellipsoid with $\gamma = 1.5$, radius $R = 0.25$ and dimension $D = 20$. (a) Classification error when using manifold-slacks without noise (y-axis) for different values of α (x-axis) and choices of c (color coded). Compares samples' classification error (dark lines) and entire-manifold classification error (light lines). (b) Classification error when using manifold-slacks (y-axis) for different values of α (x-axis) and choices of c (color coded), at noise level of $\sigma^2 = 1$. (c-d) Results for manifolds of $M = 100$ points from an ellipsoid with $\gamma = 1.5$, radius R and dimension $D = 10$. Classification error using the optimal choice of c (y-axis) for different values of α (x-axis) and values of R (color coded). Compares simulation results of manifold-slack classifiers (solid lines) and center-slack classifiers (dashed lines), without noise (c) and at noise level $\sigma^2 = 0.1$ (d).

III. DISCUSSION

The introduction of slack variables to SVMs allows linear classification of data which is not linearly separable, and for optimizing performance by choosing the right balance between making training errors and increasing classification margin (using the regularization parameter c, equations 2,22,24). Here we analyze the noise resilience of such classification by considering test performance with respect to input noise (with variance σ^2/N applied to each input component).

Point-slack We first study the statistical mechanics of a point-slack model where a set of P random points in N dimensions are independently labeled, and each is assigned a slack variable. We show that the problem has a well defined solution for all load values $\alpha = P/N$ (figure 1). In the absence of input noise, the optimal choice of c is infinite for all α; however, in the presence of noise in the test data, the optimal c is finite (figure 2). Furthermore, the optimal choice of c can be calculated

from theory (equation 17), and is roughly given by the "canonical choice" $c = \sigma^{-2}$ (figure 3).

Manifold classification Our main interest is the case of points arranged in P randomly labeled manifolds, such that all points within a manifold have the same target label. Assuming the number of points per manifold is large (and possibly infinite) assigning a slack variable to each point is not feasible. We introduced and analyzed two schemes of slack algorithms for classification of manifolds, which differ in the manner in which slack variables are attached to manifolds. In the center-slack method, each manifold center is associated with a slack variable, reducing the learning to point-slack SVM of the centers. In the manifold-slack method, a slack variable is associated with the "worst" point in each manifold, relative to the separating hyper-plane. The relation between slack variables and errors is different in the two methods (figure 4); when using center-slacks, if the center is misclassified, most of the manifold may follow, but using manifold-slacks most of it may be classified correctly even if the "worst" point is not.

Center-slack The relatively simple center-slack scheme has several attractive features. First, it has a well defined, non-zero, solution for the weights for all values of α. Second, the associated optimal c is provided by theory (figure 5) and is approximately given by the simple "canonical choice" $c = (R^2+\sigma^2)^{-1}$, where R is the manifold radius, expressing the intuition that the variability of the manifold data relative to the center (quantified by R^2) is an intrinsic noise on top of the extrinsic noise σ^2. Finally, for large α values its performance is superior to the more sophisticated manifold-slack method (figures 9b-c, 11c-d), as discussed below. The disadvantages of the center-slack method are its performance for small α values and that it does not generalize max-margin manifold classification.

Manifold-slack The manifold-slack scheme is a natural extension of max-margin manifold classification [6, 7] in which the optimal weight vector is a sum of anchor points, one per manifold, which are the closest points in each manifold to the separating hyperplane. Here each such point is assigned a slack variable. For α below the error-less classification capacity α_C^{Hard}, when c approaches ∞, manifold-slack classification approaches max-margin classification. However, the optimal c may not be infinite even in this α regime in the presence of noise (figure 8). As for larger values of α, a surprising result of our mean-field theory is that the manifold-slack method possesses a solution with non-zero weight vector only below a second critical value, α_C^{Soft} (figure 6). Thus, this method allows for extending the range of linear classification above the error-less capacity, but for a limited range (figure 7).

The classification-error performance of manifold-slacks is always better than max-margin and may be superior to center-slacks, depending on parameters. The main improvement over max-margin is the extended range of α values (figure 7), as the reduction of the classification error (below max-margin capacity) is usually small (figures 9a, S14, S23a-b). The improved performance compared to center-slacks is substantial for small α values when the noise is small and R is order 1, where manifold-slacks achieves near-zero error while center-slacks error is order 1 (figures 9b-c, 11c-d, S23c).

While many of the results for manifolds were derived in the context of spheres, the theory extends well to general manifolds by recovering their effective radius and dimension (equations 56, 57, figures 10, S18). Importantly, their classification performance is well predicted by plugging those values into the theory of spheres (figures S21, S22), thus demonstrating they capture the classification-relevant aspects of manifolds' geometry.

Measure on manifolds The use of manifold-slacks benefits from being insensitive to the exact measure assumed on the manifolds (as long as it is non-zero). In the case of center-slacks, the center of mass of the manifolds depends in general on the measure. Nevertheless, in some cases, there is a natural choice for the center, as in spheres or ellipsoids (due to symmetry), or in a points-cloud, where using the points' average corresponds to a uniform measure on the points. Furthermore, one can use the measure-independent Steiner point [18] as the manifold center. Regardless of the employed classification method, the evaluation of the errors depends in general on the measure.

Future work Extending the theory of max-margin classification of manifolds to soft classification is an important step in connecting the theory to applications, where soft-margin classifiers are more commonly used. We believe the theory of general manifolds is relevant for the analysis of real-world data. To properly do so, the theory needs to be extended to allow for center correlations, as was done for max-margin classifiers [8]; we expect this to be straightforward as the methods from [8] involve mostly preprocessing of the manifolds, independently of the analysis of the manifolds' geometry.

The issue of robustness to noise would naturally come up when aiming to apply the theory to neural data analysis where noise is a common attribute of the problem, unlike the artificial networks analyzed in [8]. It would be interesting to apply the methods described here to analyze object representations with non-Gaussian noise, such as neural noise with Poisson-like characteristics.

On a broader scope, the discussion of robustness to noise is a limited form of generalization. In general, we would like to be able to discuss generalization with respect to a finite number of samples from a manifold, where the scaling behavior of the classification error with the number of samples is an open question. Recent work on the few-shot learning setup, where the number of samples is very small, has revealed relatively simple behavior of the classification error [19].

ACKNOWLEDGEMENTS

HS is partially supported by the Gatsby Charitable Foundation, the Swartz Foundation, the National Institutes of Health (Grant No. 1U19NS104653) and the MAFAT Center for Deep Learning.

[1] V. Vapnik and A. Y. Lerner, Recognition of patterns with help of generalized portraits, Avtomat. i Telemekh **24**, 774 (1963).

[2] B. E. Boser, I. M. Guyon, and V. N. Vapnik, A training algorithm for optimal margin classifiers, in *Proceedings of the fifth annual workshop on Computational learning theory* (1992) pp. 144–152.

[3] C. Cortes and V. Vapnik, Support-vector networks, Machine learning **20**, 273 (1995).

[4] B. Schölkopf, A. J. Smola, R. C. Williamson, and P. L. Bartlett, New support vector algorithms, Neural computation **12**, 1207 (2000).

[5] E. Gardner, The space of interactions in neural network models, Journal of physics A: Mathematical and general **21**, 257 (1988).

[6] S. Chung, D. D. Lee, and H. Sompolinsky, Linear readout of object manifolds, Physical Review E **93**, 060301 (2016).

[7] S. Chung, D. D. Lee, and H. Sompolinsky, Classification and geometry of general perceptual manifolds, Physical Review X **8**, 031003 (2018).

[8] U. Cohen, S. Chung, D. D. Lee, and H. Sompolinsky, Separability and geometry of object manifolds in deep neural networks, Nature communications **11**, 1 (2020).

[9] J. Shawe-Taylor and N. Cristianini, On the generalization of soft margin algorithms, IEEE Transactions on Information Theory **48**, 2721 (2002).

[10] D.-R. Chen, Q. Wu, Y. Ying, and D.-X. Zhou, Support vector machine soft margin classifiers: error analysis, The Journal of Machine Learning Research **5**, 1143 (2004).

[11] S. Risau-Gusman and M. B. Gordon, Statistical mechanics of learning with soft margin classifiers, Physical Review E **64**, 031907 (2001).

[12] R. Dietrich, M. Opper, and H. Sompolinsky, Statistical mechanics of support vector networks, Physical review letters **82**, 2975 (1999).

[13] M. Mézard, G. Parisi, and R. Zecchina, Analytic and algorithmic solution of random satisfiability problems, Science **297**, 812 (2002).

[14] L. Zdeborová and F. Krząkała, Phase transitions in the coloring of random graphs, Physical Review E **76**, 031131 (2007).

[15] S. Ganguli and H. Sompolinsky, Statistical mechanics of compressed sensing, Physical review letters **104**, 188701 (2010).

[16] M. Advani and S. Ganguli, Statistical mechanics of optimal convex inference in high dimensions, Physical Review X **6**, 031034 (2016).

[17] H. Kuhn and A. Tucker, Nonlinear programming. berkeley, University of California Press **13**, 54 (1951).

[18] G. C. Shephard, The steiner point of a convex polytope, Canadian Journal of Mathematics **18**, 1294 (1966).

[19] B. Sorscher, S. Ganguli, and H. Sompolinsky, The geometry of concept learning, bioRxiv (2021).

[20] D. B. Owen, A table of normal integrals: A table, Communications in Statistics-Simulation and Computation **9**, 389 (1980).

Appendix A: Supplementary Figures

1. Points

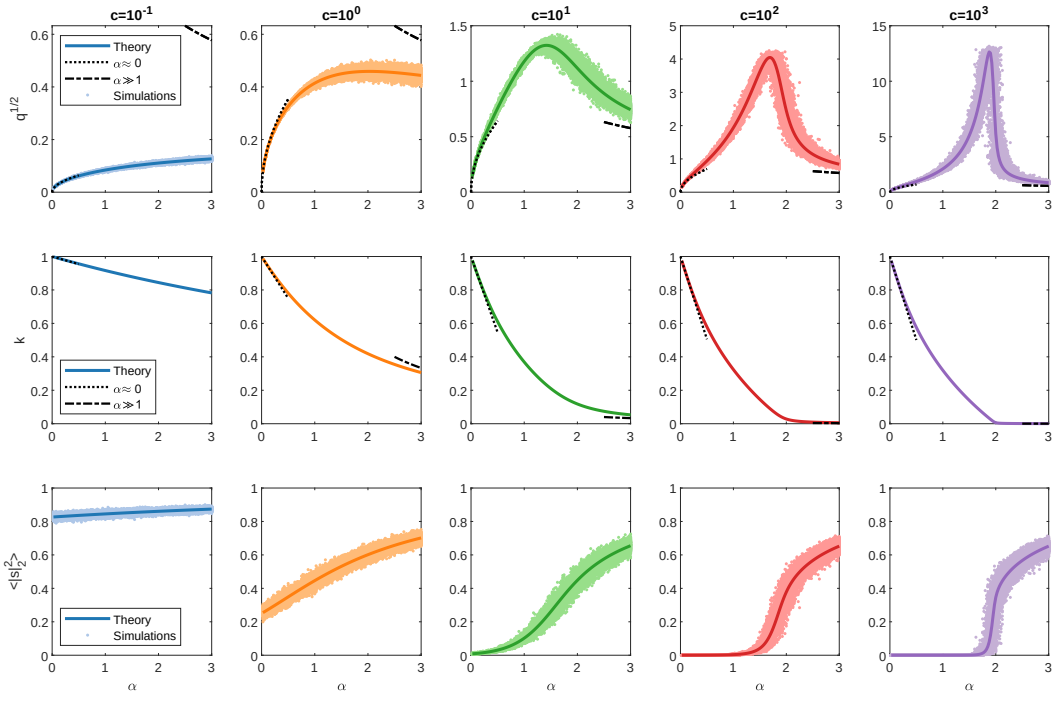


FIG. S1: Order parameters in soft classification of points. Top row: weights' norm $q^{1/2}$ (y-axis) at different values of α (x-axis) and choices of c (panels). Compares theoretical predictions (solid dark lines), simulation results (light dots), and the theoretical prediction in the limits of $\alpha \to 0$ and $\alpha \to \infty$ (dotted and dash-dot lines, respectively). Middle row: the order parameter k (y-axis) at different values of α (x-axis) and choices of c (panels). Compares theoretical predictions (solid dark lines) and the theoretical prediction in the limits of $\alpha \to 0$ and $\alpha \to \infty$ (dotted and dash-dot lines, respectively). Bottom row: slack norm $\|\vec{s}\|^2$ (y-axis) at different values of α (x-axis) and choices of c (panels). Compares theoretical predictions (solid dark lines) and simulation results (light dots).

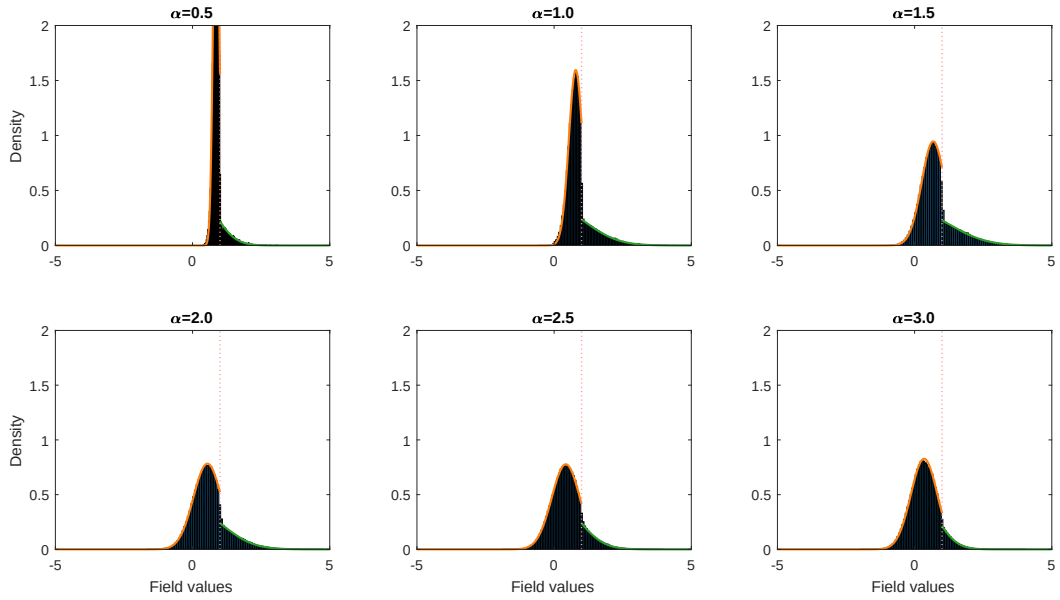


FIG. S2: Field distribution in soft classification of points. The distribution predicted by theory (solid lines; orange for the "touching" regime, green for the "interior" regime) and the histogram from simulation results (black area) at different values of α (panels) and $c = 10$.

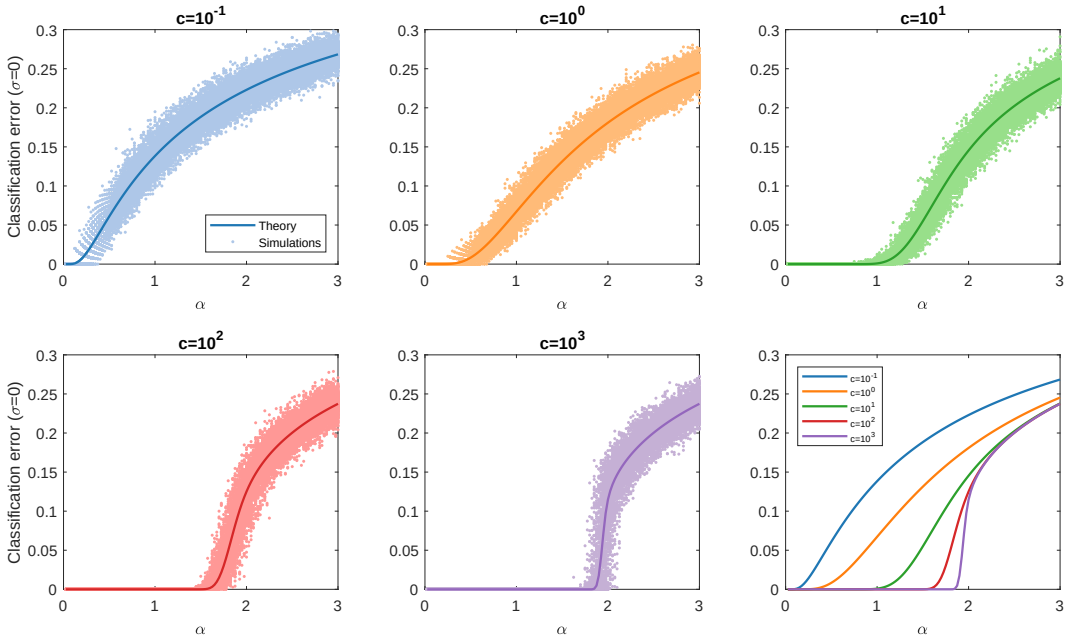


FIG. S3: Training errors in soft classification of points. Classification error without noise (y-axis) at different values of α (x-axis) and choices of c (color coded). Compares theoretical prediction (solid dark lines) and simulation results (light dots). The last panel overlays the theoretical prediction for different choices of c.

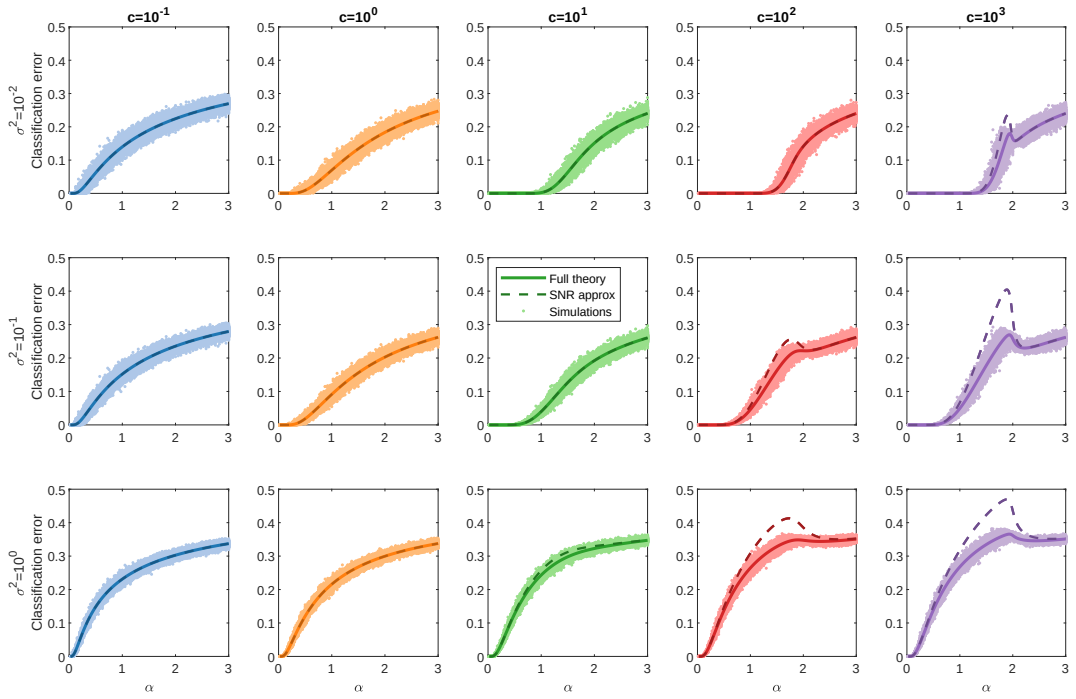


FIG. S4: Test errors in soft classification of points. Classification error (y-axis) at different values of α (x-axis) at different levels of noise σ^2 (rows) and choices of c (columns). Compares theoretical predictions (solid dark lines), the SNR approximation (dashed lines), and simulation results (light dots).

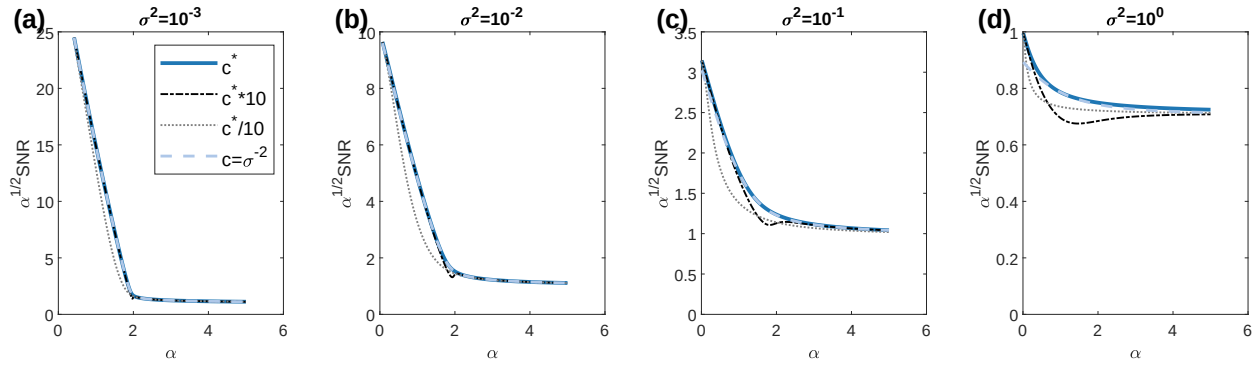


FIG. S5: Classification error using different choices of c in soft classification of points. Classification error presented as scaled SNR $\sqrt{\alpha}\mathcal{S}$ (y-axis, higher values imply lower error, where $\mathcal{S} = H^{-1}(\varepsilon)$ using the inverse of the Gaussian tail function H), at different levels of noise σ^2 (panels), using the optimal choice c^* (solid colored lines), the canonical choice $c = \sigma^{-2}$ (dashed colored lines), and two sub-optimal choices $10c^*$ and $0.1c^*$ (dashed and dotted black lines).

2. Spheres

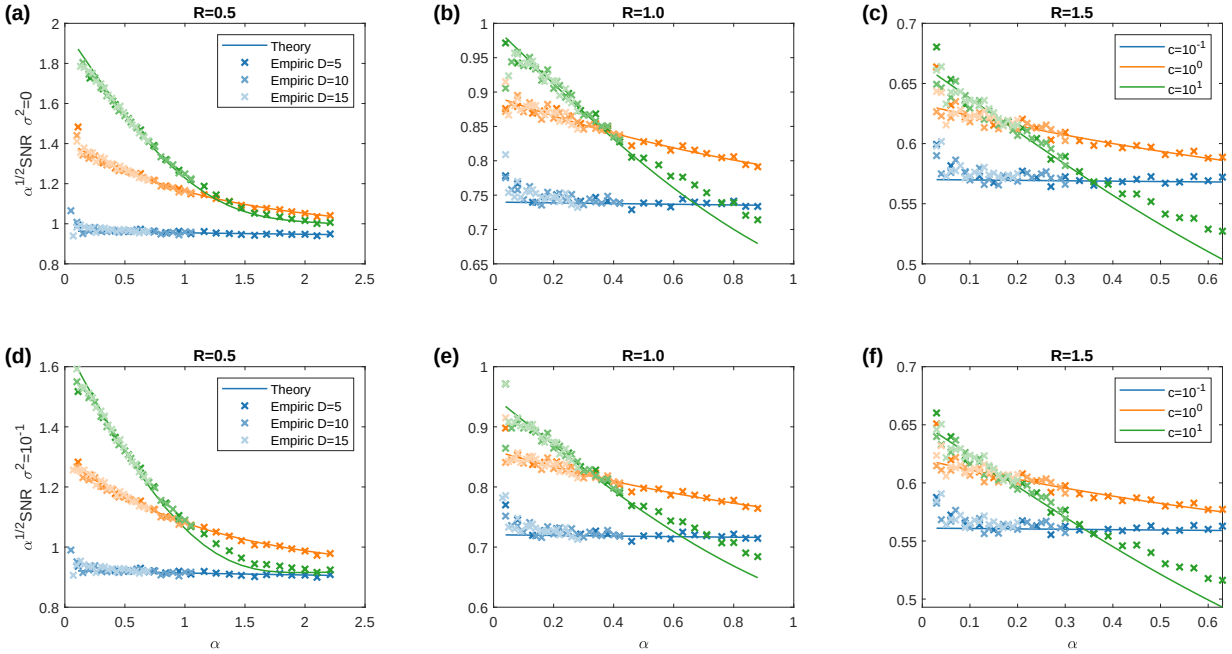


FIG. S6: Errors in soft classification of spheres using center-slacks. Classification error presented as scaled SNR $\sqrt{\alpha}\mathcal{S}$ (y-axis, higher values imply lower error, where $\mathcal{S} = H^{-1}(\varepsilon)$ using the inverse of the Gaussian tail function H), at different values of α (x-axis), choices of c (color coded), and values of R (panels, R indicated in the title). Compares theoretical predictions (solid dark lines) and simulation results (crosses) using different values of D (coded in lightness). (a-c) Results without noise $\sigma^2 = 0$. (d-f) Results with noise $\sigma^2 = 0.1$.

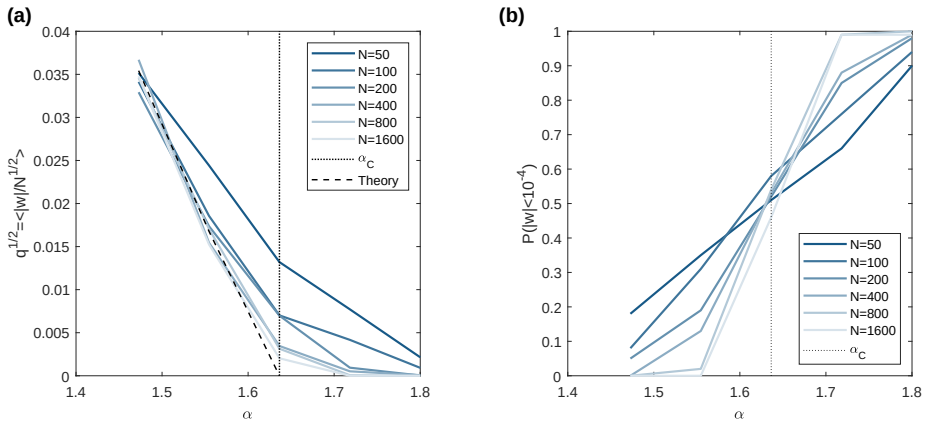


FIG. S7: Finite-size effects for the weights' norm around the phase transition using manifold-slacks. (a) The weights' norm $q^{1/2}$ (y-axis) at different values of α (y-axis) around the phase transition (dotted line). The theory (dashed line) is compared to simulation results, using different choices of N (solid lines, color coded). (b) The fraction of simulation results below 10^{-4} (y-axis) at different values of α (y-axis) around the phase transition (dotted line), using different choices of N (color coded).

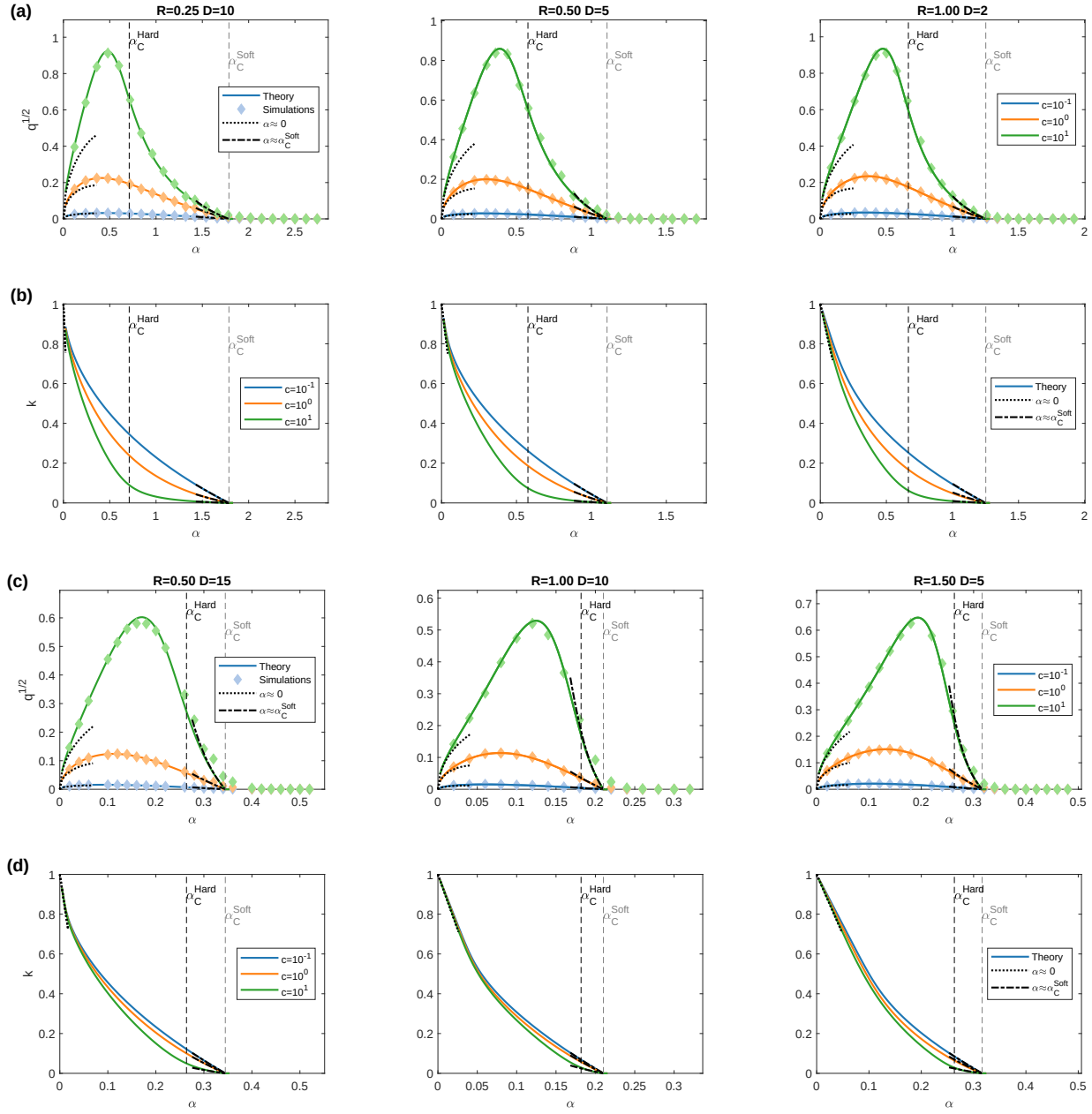


FIG. S8: Order parameters in soft classification of spheres using manifold-slacks. (a,c) The weights' norm $q^{1/2}$ (y-axis) at different values of α (x-axis), choices of c (color coded), and values of R, D (indicated in title). Theory results (solid lines) are compared both to simulation results (diamonds) and the theory derived in the limits of either $\alpha \to 0$ or $\alpha \to \alpha_C^{Soft}$ (black dotted and dash-dot lines, respectively). (b,d) The order parameter k (y-axis) at different values of α (x-axis), choices of c (color coded), and values of R, D (indicated in title of the above panel). Compares full theory results (solid lines) with results derived in the limits of either $\alpha \to 0$ or $\alpha \to \alpha_C^{Soft}$ (black dotted and dash-dot lines, respectively).

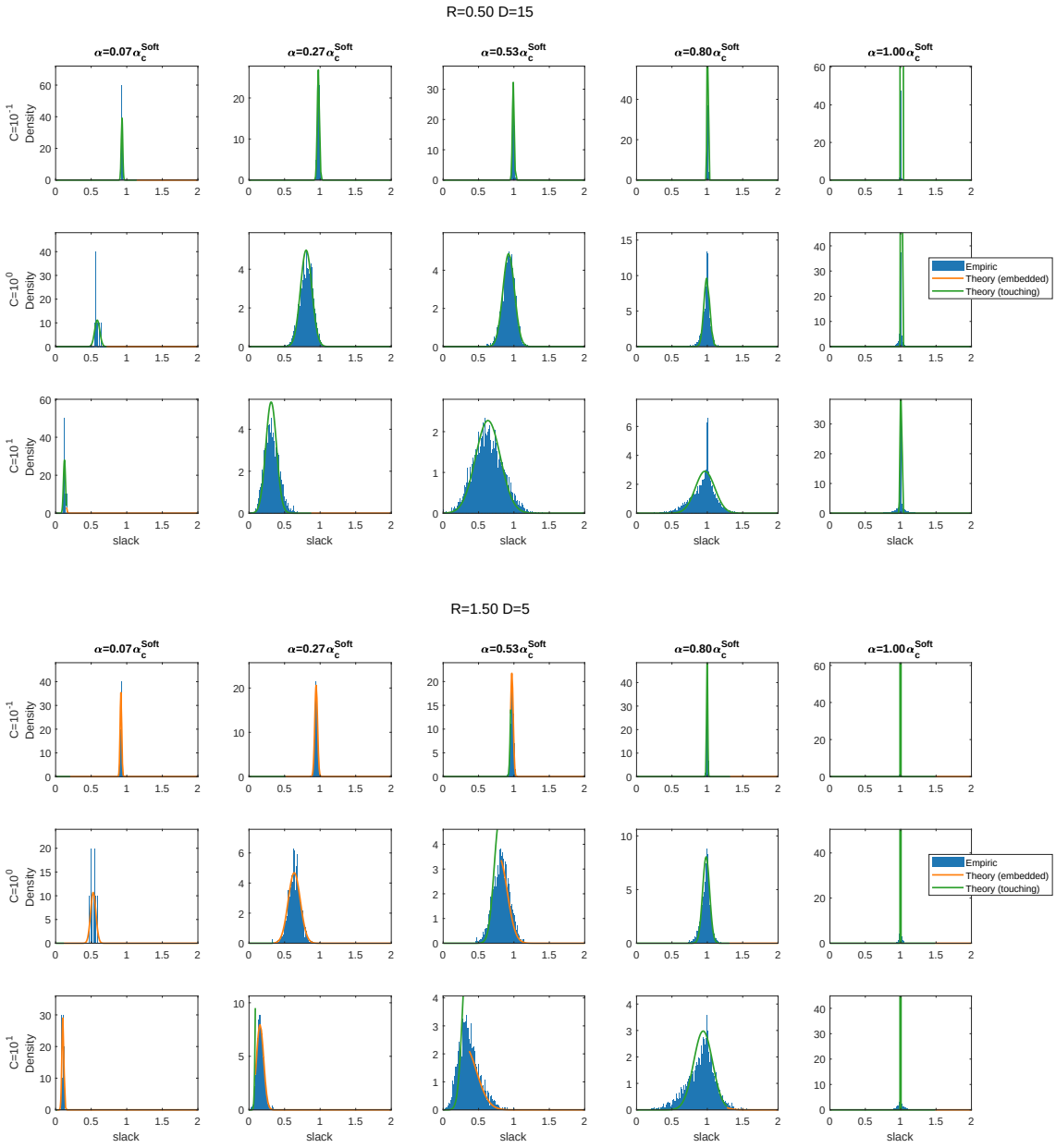


FIG. S9: Distribution of slack variables in soft classification of spheres using manifold-slacks. Distribution of slack variables at different values of α relative to α_C^{Soft} (columns), choices of c (rows), for $R = 0.5, D = 15$ (top half) and $R = 1.5, D = 5$ (bottom half). Compares theory (solid dark line, orange for the "embedded" regime, green for the "touching" regime), and simulation results (blue histogram).

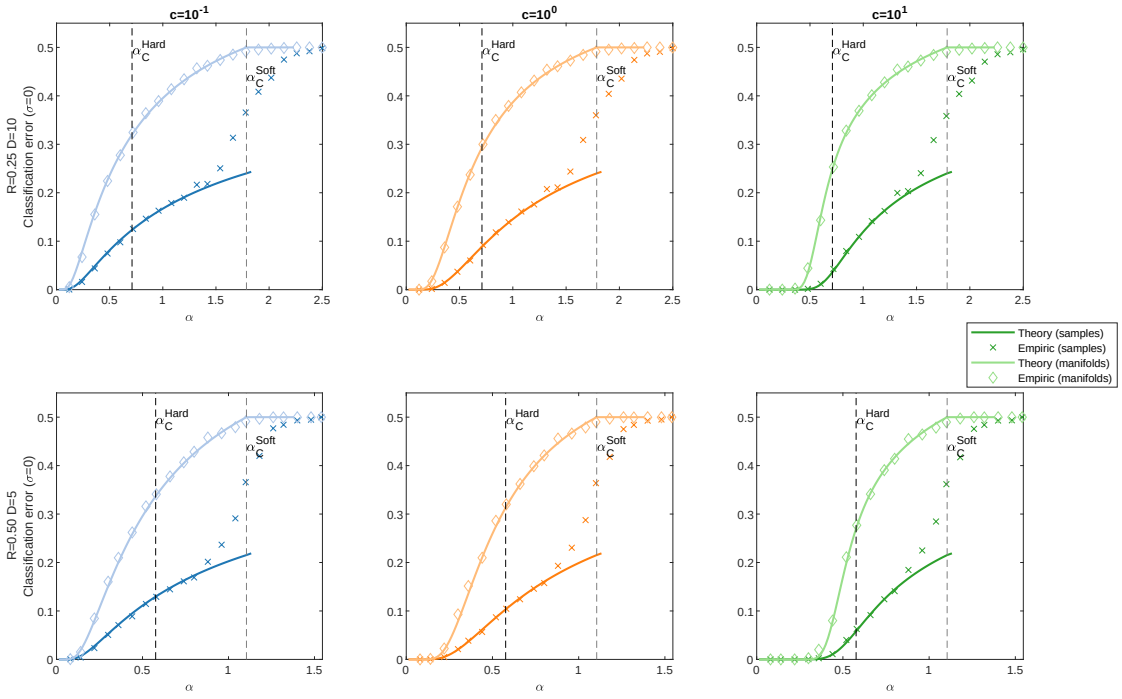


FIG. S10: Training errors in soft classification of spheres using manifold-slacks. Classification error without noise (y-axis) at different values of α (x-axis) for several values of R, D (rows) and choices of c (columns). Compares samples' classification-error theory (solid dark lines) with simulation results (crosses), and entire-manifold classification-error theory (solid light lines) with simulation results (diamonds).

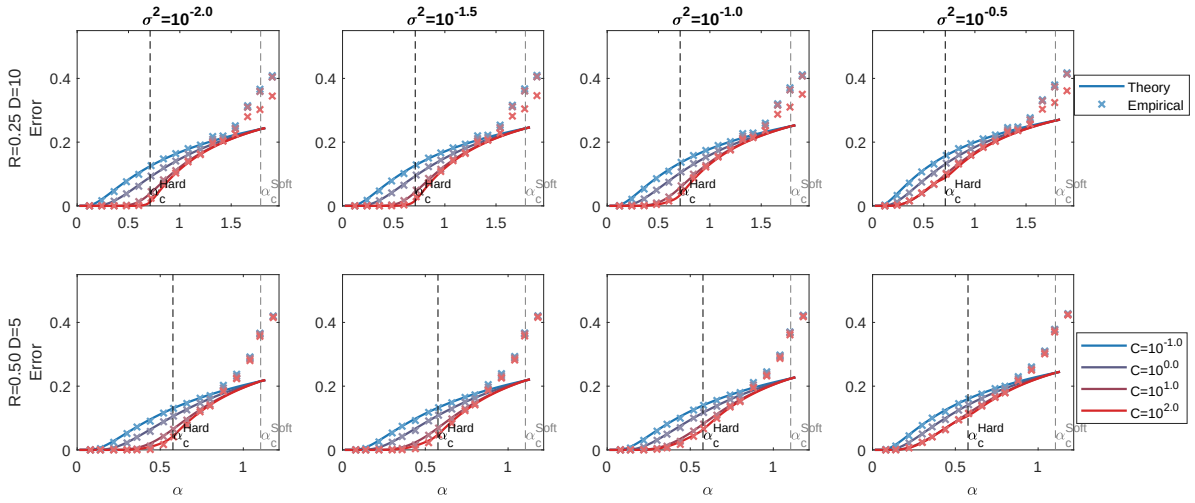


FIG. S11: Test errors in soft classification of spheres using manifold-slacks. Classification error (y-axis) at different values of α (x-axis) for several values of R, D (rows) and levels of noise σ^2 (columns). Compares classification error theory (solid lines) with simulation results (crosses), for different choices of c (color coded).

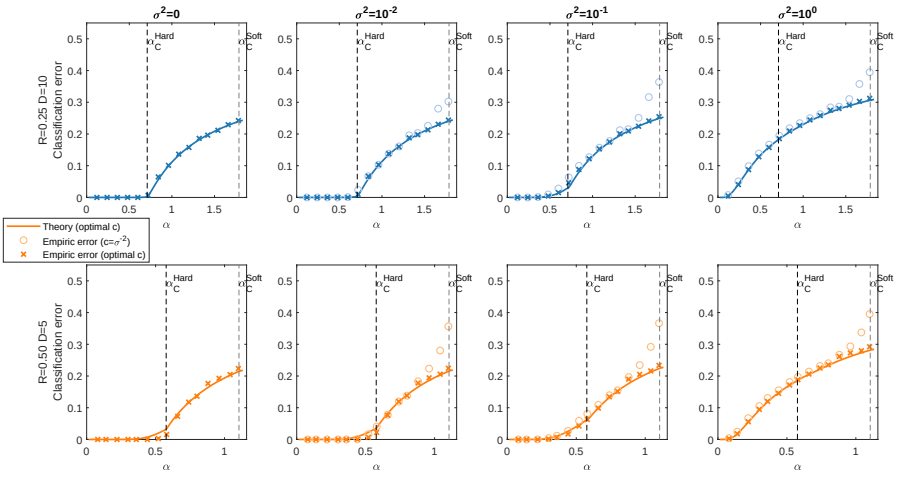


FIG. S12: Errors in soft classification of spheres using the optimal choice of c using manifold-slacks. Classification error (y-axis) at different values of α (x-axis) for several values of R, D (rows) and different levels of noise σ^2 (columns). Compares classification error theory, using the optimal c (solid lines), with simulation results, using either the optimal c (crosses), or the canonical choice $c = \sigma^{-2}$ (circles).

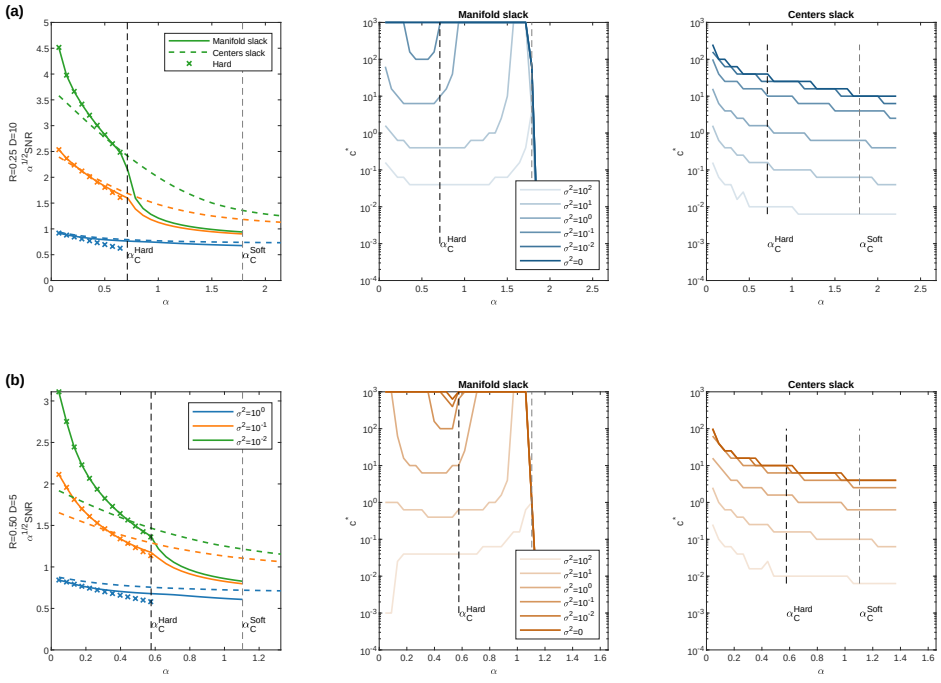


FIG. S13: Comparison of soft classification of spheres using manifold-slacks and center-slacks. Left column: classification error presented as scaled SNR $\sqrt{\alpha}\mathcal{S}$ (y-axis, higher values imply lower error, where $\mathcal{S} = H^{-1}(\varepsilon)$ using the inverse of the Gaussian tail function H) at different values of α (x-axis), levels of noise σ^2 (color coded) and values of R, D (rows). Compares simulation results of manifold-slack classifiers (solid lines), center-slack classifiers (dashed lines) and max-margin classifiers (crosses). Middle and right columns: the corresponding optimal choice of c (y-axis, log scale) when using manifold-slacks (middle) and center-slacks (right) at different values of α (x-axis) and noise levels σ^2 (color coded).

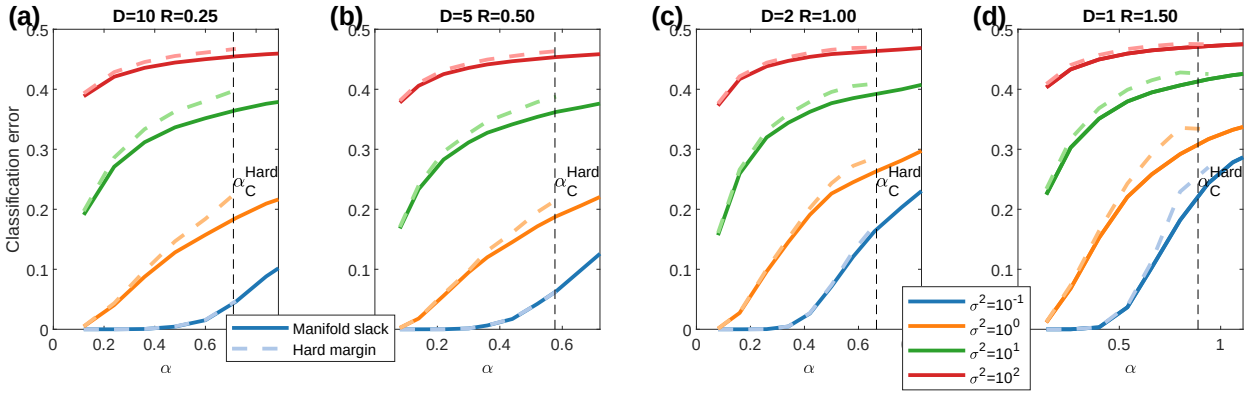


FIG. S14: Errors in classification of spheres using the manifold-slack and max-margin methods. Classification error (y-axis) at different values of α (x-axis) and different combinations of R, D (panels, values indicated in title). Compares results for manifold-slack classifiers using the optimal choice of c (solid lines) and max-margin classifiers (dashed lines), at different noise levels (color coded).

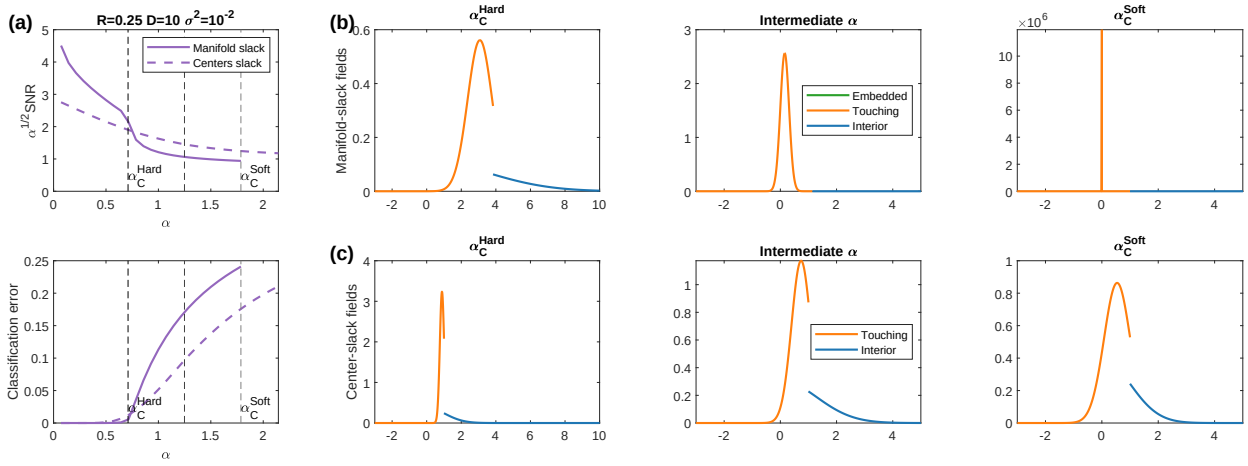


FIG. S15: Differences in errors and field distribution between manifold-slacks and center-slacks. (a) Classification error (y-axis) using manifold-slacks (solid lines) or center-slacks (dashed lines) at different values of α (x-axis) with $R = 0.25, D = 10$ and $\sigma^2 = 0.01$. Top: classification error presented as scaled SNR $\sqrt{\alpha}\mathcal{S}$ (higher values imply lower error, where $\mathcal{S} = H^{-1}(\varepsilon)$ using the inverse of the Gaussian tail function H); bottom: classification error presented as ε. The vertical dashed lines indicate 3 values of α: α_C^{Hard}, α_C^{Soft} and their average value. (b-c) Field distribution at the manifold center using the optimal choice of c, at those 3 values of α, color coded by the different regimes (see legends), using manifold-slacks (b) and center-slacks (c).

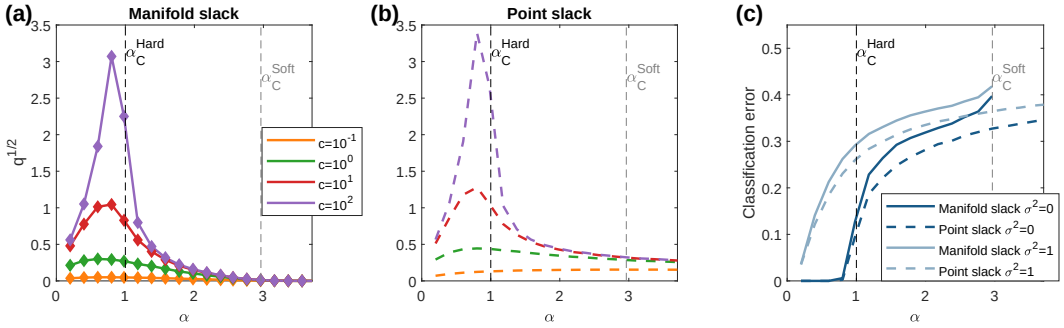


FIG. S16: Comparison of soft classification of line segments using the manifold-slack and point-slack methods. Results for classification of line segments (spheres with dimension $D = 1$ and radius $R = 1$). (a-b) The weights' norm $q^{1/2}$ (y-axis) at different values of α (x-axis) and choices of c (color coded). (a) Compares theory results of manifold-slacks (solid lines) to simulation results (diamonds). (b) Presents simulation results using the point-slack method (dashed lines) classifying $2P$ samples of the line end-points. (c) Classification error (y-axis) using manifold-slack classifiers (solid lines) or point-slack classifiers (dashed lines) at different values of α (x-axis) and noise levels (color coded), using the optimal choice of c for each method.

3. General manifolds

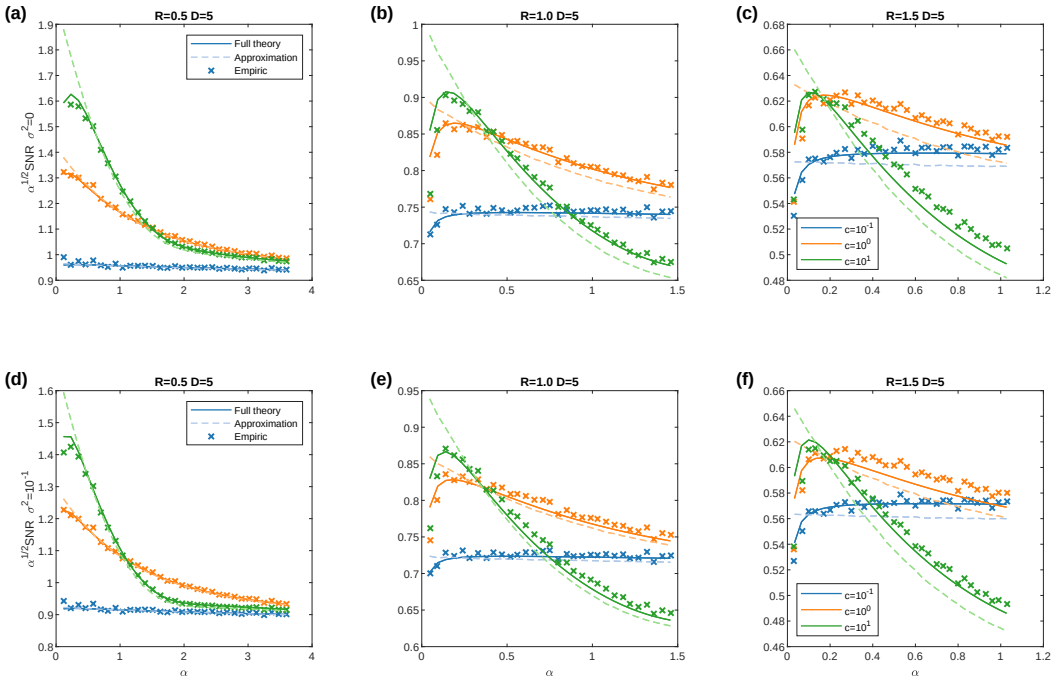


FIG. S17: Errors in soft classification of point-cloud manifolds using center-slacks. Classification error presented as scaled SNR $\sqrt{\alpha}\mathcal{S}$ (y-axis, higher values imply lower error, where $\mathcal{S} = H^{-1}(\varepsilon)$ using the inverse of the Gaussian tail function H), at different values of α (x-axis) and choices of c (color coded). Compares the full theory (equation 49, solid lines), an approximation (equation 50, dashed lines), and simulation results (crosses). Results for manifolds of $M = 100$ points from an ellipsoid with $\gamma = 0.5$, radius R and dimension D (indicated in panel title), without noise $\sigma^2 = 0$ (a-c) and with noise $\sigma^2 = 0.1$ (d-f).

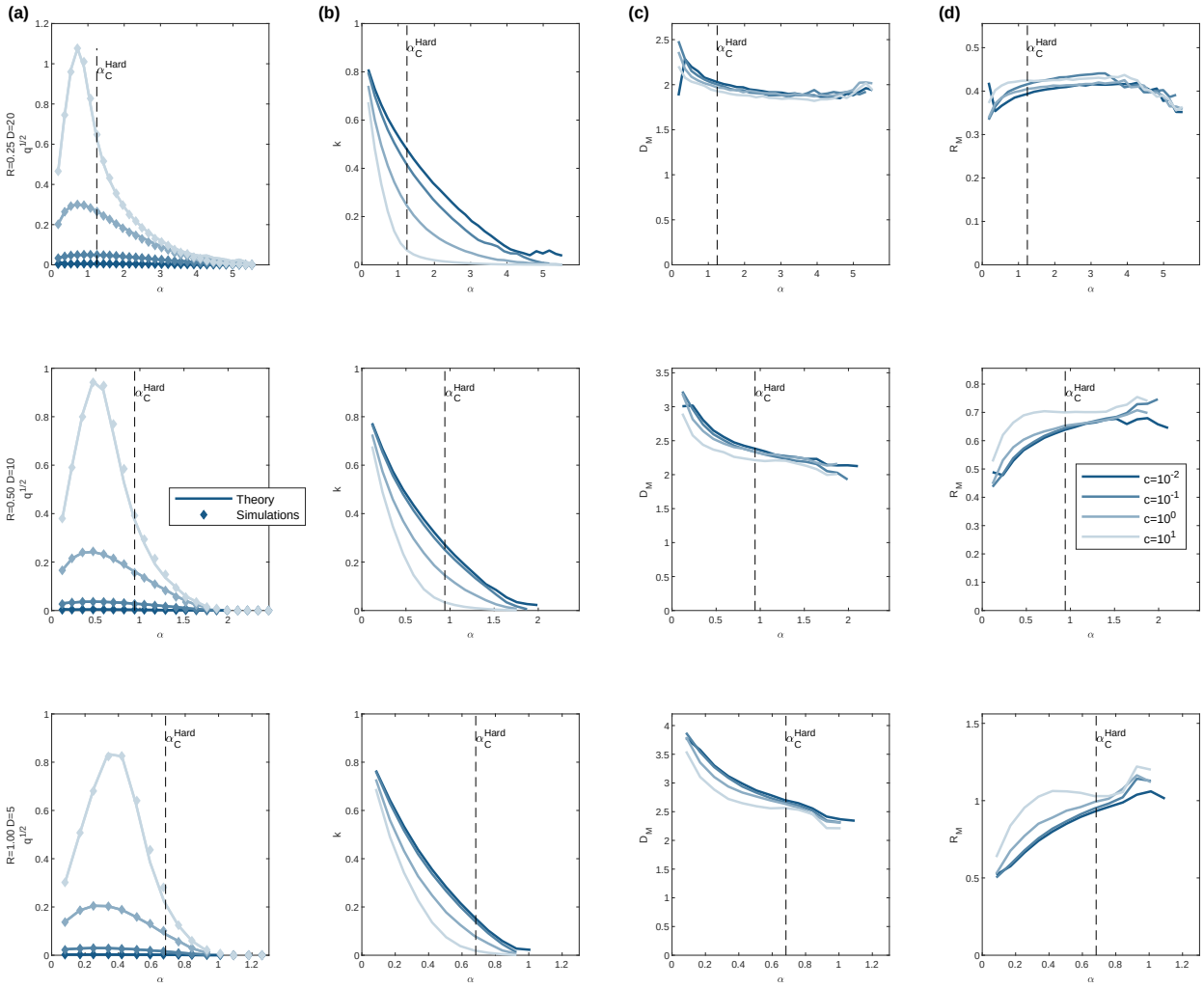


FIG. S18: Order parameters and manifold properties for point-cloud manifolds. Results for manifolds of $M = 100$ points from an ellipsoid with $\gamma = 1.5$, radius R, and dimension D (indicated to the left of each row). (a) The weights' norm $q^{1/2}$ (y-axis) at different values of α (x-axis) and choices of c (color coded). Compares theory (the least-squares algorithm, solid lines) and simulation results (diamonds). (b-d) The corresponding values of the order parameter k (b), manifold dimension D_M (c), and manifold radius R_M (d) at different values of α (x-axis) and choices of c (color coded).

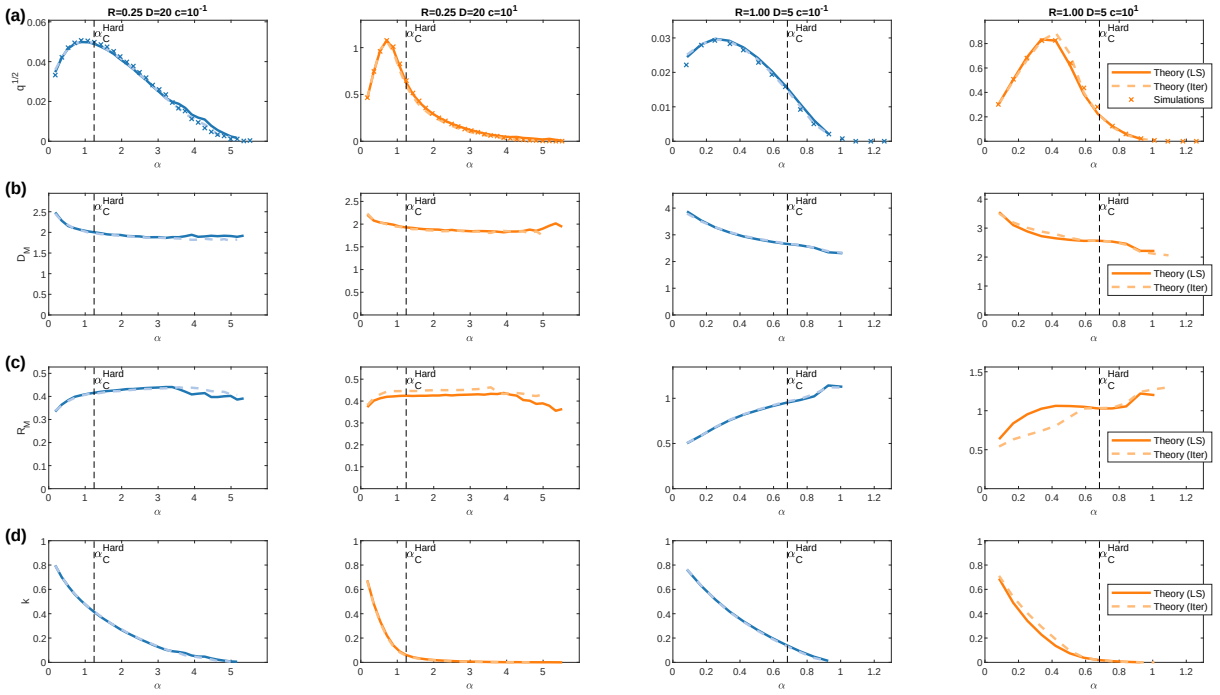


FIG. S19: Order parameters and manifold properties for point-cloud manifolds using different algorithms. Results for manifolds of $M = 100$ points from an ellipsoid with $\gamma = 1.5$, radius R and dimension D. (a) The weights' norm $q^{1/2}$ (y-axis) at different values of α (x-axis) for different values of R, D and c (indicated in the top panel title). Compares simulation results (crosses) with theoretical results using the least-squares algorithm (solid lines) and the iterative algorithm (dashed lines). (b-d) The corresponding results for manifold dimension (b), manifold radius (c), and the order parameter k (d) at different values of α (x-axis). Compares theory using the least-squares algorithm (solid lines) and the iterative algorithm (dashed lines).

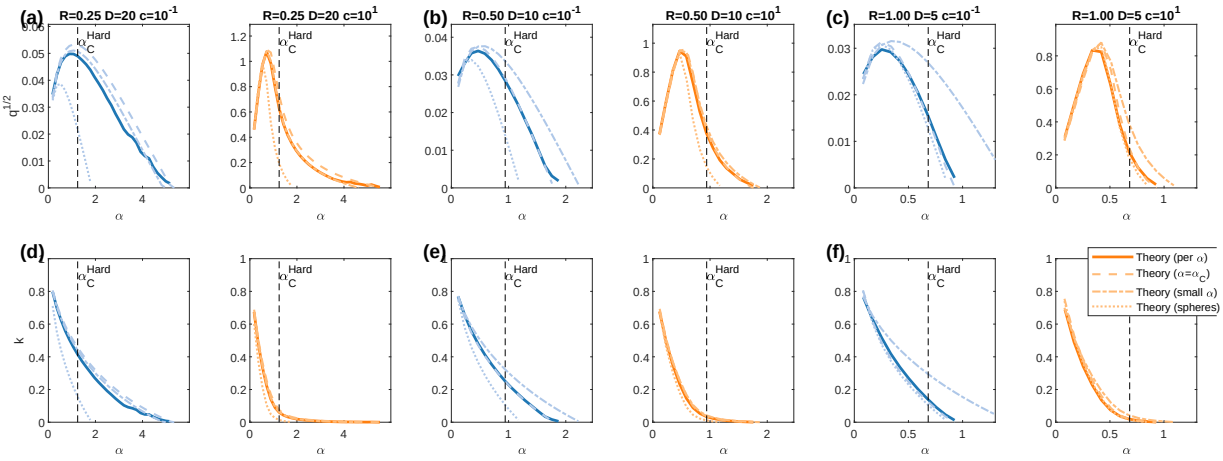


FIG. S20: Manifold properties dependence on α for point-cloud manifolds. Results for manifolds of $M = 100$ points from an ellipsoid with $\gamma = 1.5$, radius R and dimension D. Compares theory calculated per α (the least-squares algorithm, solid lines), theory calculated at $\alpha \approx \alpha_C^{Soft}$ (dashed lines) or at small α (dash-dot lines), and naive application of the theory of spheres (dotted lines). (a-c) The weights' norm $q^{1/2}$ (y-axis) at different values of α (x-axis) for different values of R, D and c (indicated in the top panel title). (d-f) The corresponding order parameter k (y-axis) at different values of α (x-axis) for different values of R, D and c.

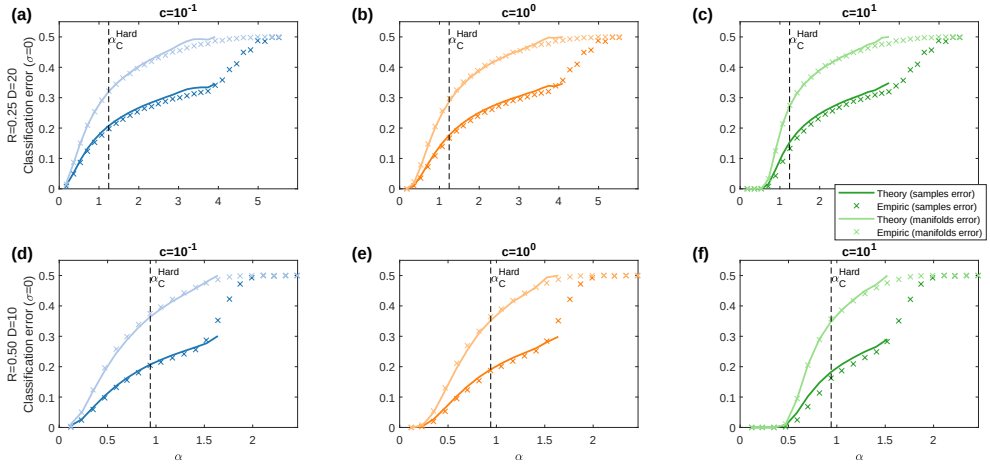


FIG. S21: Training errors for point-cloud manifolds using manifold-slacks. Results for manifolds of $M = 100$ points from an ellipsoid with $\gamma = 1.5$, radius R and dimension D (indicated to the left of each row). Classification error without noise $\sigma^2 = 0$ (y-axis) at different values of α (x-axis) and choices of c (columns). Compares samples' classification-error theory (solid dark lines) with simulation results (dark crosses), and entire-manifolds classification-error theory (solid light lines) with simulation results (light crosses).

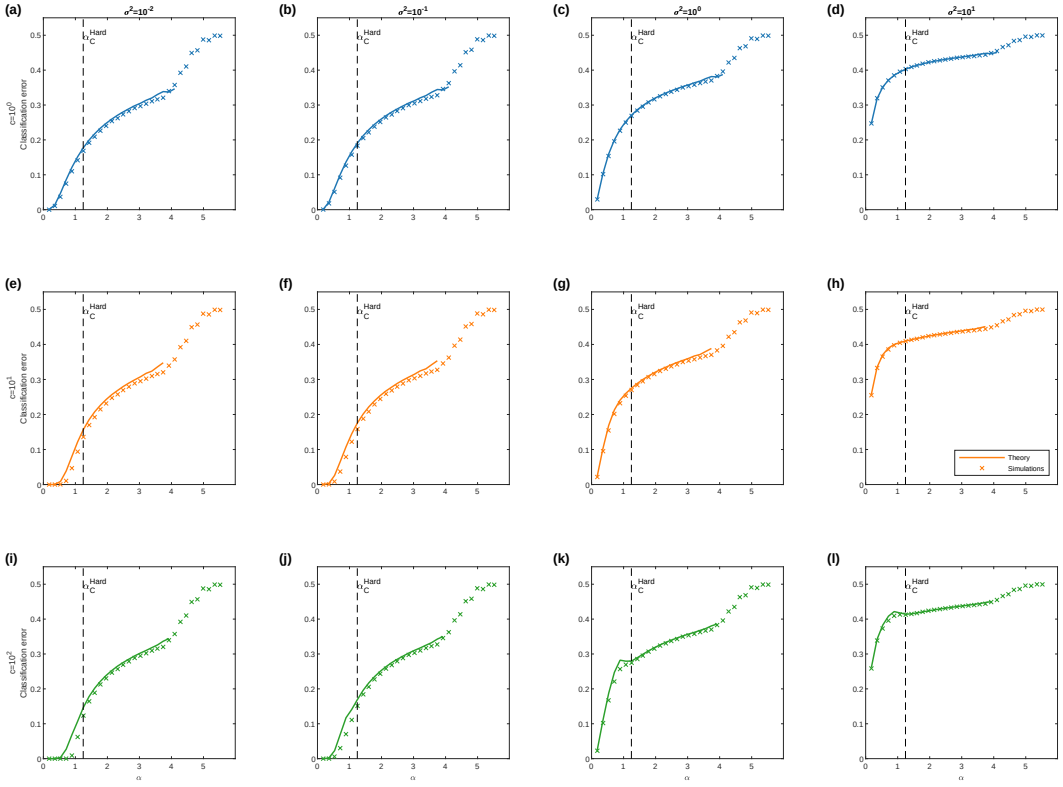


FIG. S22: Test errors for point-cloud manifolds using manifold-slacks. Results for manifolds of $M = 100$ points from an ellipsoid with $\gamma = 1.5$, radius $R = 0.25$ and dimension $D = 20$. Classification error (y-axis) at different values of α (x-axis), levels of noise σ^2 (columns) and choices of c (rows). Compares classification error theory (solid dark lines) with simulation results (dark crosses).

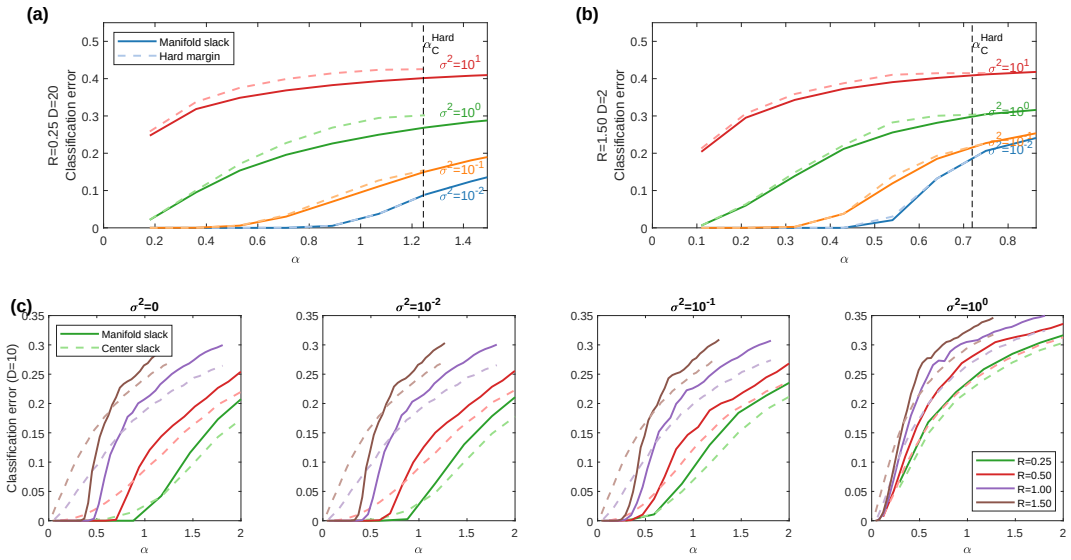


FIG. S23: Classification errors for point-cloud manifolds using different methods. Results for manifolds of $M = 100$ points from an ellipsoid with $\gamma = 1.5$, different choices for radius R, dimension D. (a-b) Classification error (y-axis) at different values of α (x-axis) and levels of noise σ^2 (color coded). Compares manifold-slack classifiers using the optimal choice of c (solid dark lines) and max-margin classifiers (light dashed lines) for $R = 0.25$ and $D = 20$ (a), $R = 1.5$ and $D = 2$ (b). (c) Classification error using the optimal choice of c (y-axis) at different values of α (x-axis), levels of noise σ^2 (columns) and values of R (color coded, dimension is $D = 10$). Compares manifold-slack classifiers (solid dark lines) and center-slack classifiers (light dashed lines).

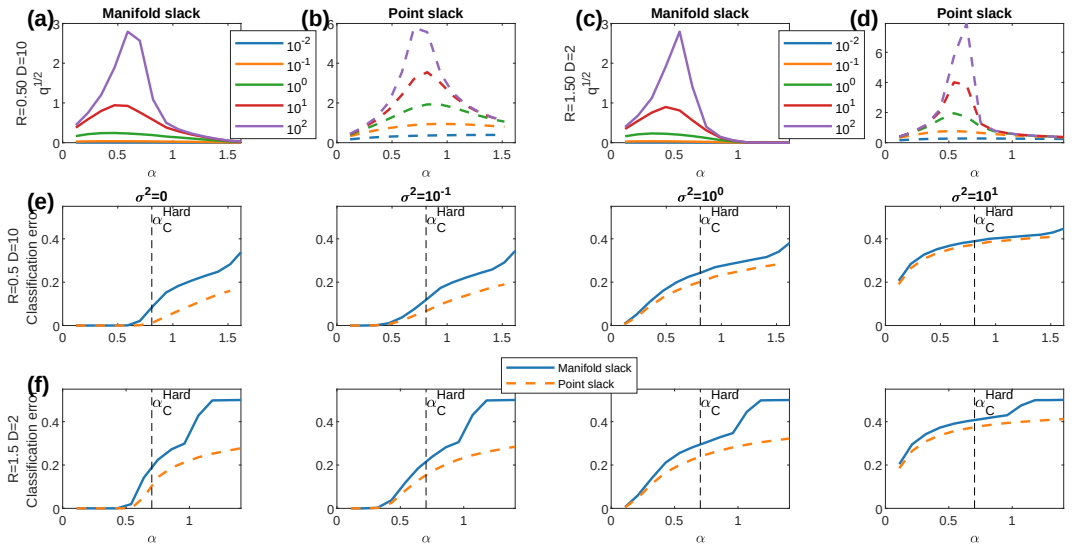


FIG. S24: Comparison of soft classification of point-cloud manifolds using the manifold-slack and point-slack methods. Results for manifolds of $M = 100$ points from an ellipsoid with $\gamma = 1.5$, different radius R and dimension D. (a-d) The weights' norm $q^{1/2}$ (y-axis) using manifold-slack classifiers (solid lines, (a,c)) and point-slack classifiers (dashed lines, (b,d)) for different choices of c (color coded), using $R = 0.5$ and $D = 10$ (a-b) or $R = 1$ and $D = 2$ (c-d). (e-f) Classification error (y-axis) at different values of α (x-axis) using the optimal choice of c at different levels of noise σ^2 (columns) and values of R, D (indicated to the left of each row). Compares manifold-slack classifiers (solid lines) and point-slack classifiers (dashed lines).

Appendix B: Algorithms

1. Self-consistent solution of points equations

We rewrite the self-consistent equations for points 7,8 as iterative update formulas.
Given scalars c, α:

1. Initialize $q_0 = 1$.
2. Update iteratively:

$$a_{n-1} = \alpha H\left(-1/\sqrt{q_{n-1}}\right) \tag{B1}$$

$$k_n = \frac{1}{2}\left(1 - a_{n-1} - c^{-1}\right) + \frac{1}{2}\sqrt{\left(1 + a_{n-1} + c^{-1}\right)^2 - 4a_{n-1}} \tag{B2}$$

$$q_n = \kappa_0^{-2}\left(\alpha\left(ck_n\right)^2 / \left(1 + ck_n\right)^2\right) \tag{B3}$$

   where $\kappa_0(\alpha)$ is the inverse function of $\alpha_0(\kappa)$.
3. Repeat updating until convergence, defined as a change of less that 10^{-12} in q.

2. Self-consistent solution of spheres equations

The self-consistent equations for spheres C277,C279 take the form $1 = A(q,k)$ and $1 = B(q,k)$ and may be solved numerically by minimizing $\mathcal{L} = \frac{1}{2}\left(A(q,k) - 1\right)^2 + \frac{1}{2}\left(B(q,k) - 1\right)^2$ with respect to q, k. Those non-linear equations depend on the initial conditions q_0, k_0, which we choose as follows.
Given a scalar c and a sorted set of $\{\alpha_i\}$ values:

1. For the minimal α_0, initialize q, k using the expressions from the small α regime in the theory for points: $k_0 = 1 - \alpha c/(1+c)$ and $q_0 = \alpha c^2/(1+c)^2$.
2. Minimize $\mathcal{L}(q,k)$ from initial conditions q_0, k_0.
3. If this optimization finds a solution with $\mathcal{L} > 10^{-4}$ interpret this as a failure and exit.
4. Use the previous solution as initial conditions for the next α_i: $q_0(\alpha_i) = q(\alpha_{i-1})$, $k_0(\alpha_i) = k(\alpha_{i-1})$
5. Go back to (2).

3. Classification of synthetic sphere manifolds

Simulation results for spheres use a cutting-plane approach to find the classifier which optimally separates the entire spheres, i.e., corresponds to the case of an infinite number of samples, and is brought here for completeness.
Given P spheres defined by their centers $\left\{\boldsymbol{x}_0^\mu \in \mathbb{R}^N\right\}$ and axes $\left\{U^\mu \in \mathbb{R}^{N\times D}\right\}$, with the radius absorbed into each axis, classification of the entire spheres with respect to target labels $\{y^\mu\}$ is done such that at stage K, exactly K points from each sphere $X^\mu \in \mathbb{R}^{N\times K}$ are used:

1. At $K = 1$ we initialize $X^\mu = \{\boldsymbol{x}_0^\mu\}$.
2. Get an optimal classifier:

$$\boldsymbol{w}^* = \arg \min_{\forall \boldsymbol{x}^\mu \in X^\mu} \min_{y^\mu \boldsymbol{w}\cdot\boldsymbol{x}^\mu \geq 1 - s^\mu} \|\boldsymbol{w}\|^2 + c\|\vec{s}\|^2 \tag{B4}$$

   and denote the achieved margin $\kappa_0 = \min_\mu \min_{\boldsymbol{x}^\mu \in X^\mu} y^\mu \boldsymbol{w}\cdot\boldsymbol{x}^\mu + s^\mu$ (which is usually 1).
3. Find the worst point with respect to the current $\boldsymbol{w}^*$, $\boldsymbol{x}_{worst}^\mu = \boldsymbol{x}_0^\mu - U^\mu \hat{S}^\mu$ where $\vec{S}^\mu = y^\mu \boldsymbol{w}^{*T} U^\mu$ and $\hat{S}^\mu = \vec{S}^\mu / \|\vec{S}^\mu\|$ and add it to each set $X^\mu = X^\mu \cup \{\boldsymbol{x}_{worst}^\mu\}$. Denote the margin on the worst points $\kappa_1 = \min_\mu y^\mu \boldsymbol{w}^* \cdot \boldsymbol{x}_{worst}^\mu + s^\mu$.
4. Go back to (2) as long as $\kappa_0 \geq 0$ and $\kappa_1 \leq (1-\epsilon)\kappa_0$ (where $\epsilon = 10^{-4}$ was used).

4. Least-squares calculation of anchor points for point-cloud manifolds

Given $\vec{t} \in \mathbb{R}^N, t_0 \in \mathbb{R}$ and scalars c, k, q:

1. Use least-squares optimization with linear constraints:

$$\vec{v}^*, v_0^* = \arg\min \left\{ \|\vec{v} - \vec{t}\|^2 + \frac{ck}{1+ck} \left(v_0 - t_0\right)^2 \right\} \tag{B5}$$

$$\cdots s.t.\ \forall \vec{S} \in M\ v_0 + \vec{v} \cdot \vec{S} \geq 1/\sqrt{q} \tag{B6}$$

2. Calculate $\tilde{S}$:

$$\tilde{S} = \frac{\vec{v}^* - \vec{t}}{\frac{ck}{1+ck}\left(v_0^* - t_0\right)} \tag{B7}$$

5. Iterative calculation of anchor points for point-cloud manifolds

Given $\vec{t} \in \mathbb{R}^N, t_0 \in \mathbb{R}$ and scalars c, k, q:

1. Initialize: $\vec{v} = \vec{t}$
2. Update iteratively:

$$\tilde{S} = \arg\min_{\vec{S} \in M} \vec{S} \cdot \vec{v} \tag{B8}$$

$$\vec{v} = \vec{t} + \frac{ck}{1+ck} \left(1/\sqrt{q} - \vec{v} \cdot \tilde{S} - t_0\right) \tilde{S} \tag{B9}$$

$$v_0 = t_0 + \frac{ck}{1+ck} \left(1/\sqrt{q} - \vec{v} \cdot \tilde{S} - t_0\right) \tag{B10}$$

3. Repeat until convergence, defined by a change of less than $\max \Delta\vec{v} < 10^{-6}$ or reaching 100 iterations.

6. Iterative algorithm for the properties of point-cloud manifolds

An iterative algorithm for the calculation of R_M, D_M, k, q at specific values of α and c.

1. Initialize $k^{(0)} = 1$ and $q^{(0)} = \alpha$.
2. For each iteration n use $k^{(n)}, q^{(n)}$. Sample T values of standard Gaussian variables $\vec{t} \in \mathbb{R}^N, t_0 \in \mathbb{R}$:
   (a) Use one of the above methods (from section B 4 or section B 5) to sample anchor points $\tilde{S}\left(\vec{t}, t_0\right)$.
   (b) Collect the resulting statistics $\left(\vec{t} \cdot \tilde{S}\right)^2 / \tilde{S}^2, \tilde{S}^2$.
3. Calculate current estimation of manifold geometry:

$$R_M^2 = \left\langle \|\delta\tilde{S}\|^2 \right\rangle_{\vec{t}, t_0} \tag{B11}$$

$$D_M = \left\langle \left(\vec{t} \cdot \delta\tilde{S}\right)^2 / \|\delta\tilde{S}\|^2 \right\rangle_{\vec{t}, t_0} \tag{B12}$$

4. Find the order parameters $k^{(n+1)}, q^{(n+1)}$ which solve the self-consistent equations using the current estimation of R_M, D_M, as described in section B 2.
5. Repeat until convergence, defined by a change of less than 10^{-3} in both k and q or reaching 50 iterations.

Appendix C: Detailed derivations

1. Replica theory for points

Consider P points $\boldsymbol{x}^\mu \in \mathbb{R}^N$ and labels $y^\mu \in \{\pm 1\}$; soft-margin classification is defined as solving:

$$\boldsymbol{w}^*, \vec{s}^* = \arg\min_{\boldsymbol{w}} \|\boldsymbol{w}\|^2 + c\|\vec{s}\|^2 \; s.t. \; h^\mu \geq 1 - s^\mu \tag{C1}$$

where $\boldsymbol{w}^* \in \mathbb{R}^N$ and $\vec{s}^* \in \mathbb{R}_+^P$ and the fields:

$$h^\mu = y^\mu \left(\boldsymbol{w} \cdot \boldsymbol{x}^\mu + b\right) \tag{C2}$$

where we will assume $b = 0$ for brevity. Denote the optimal loss:

$$L^* = \min_{\boldsymbol{w}} \|\boldsymbol{w}\|^2/N + c\|\vec{s}\|^2/N \; s.t. \; h^\mu \geq 1 - s^\mu \tag{C3}$$

We write an expression for the volume $V\left(L, c\right)$ for $L = \|\boldsymbol{w}\|^2/N + c\|\vec{s}\|^2/N$ which would vanish for $L < L^*$:

$$V\left(L, c\right) = \int d^N \boldsymbol{w} \int d^P \vec{s} \prod_\mu^P \Theta\left(h^\mu - 1 + s^\mu\right) \delta\left(\|\boldsymbol{w}\|^2 + c\|\vec{s}\|^2 - NL\right) \tag{C4}$$

$$= \int d^N \boldsymbol{w} \int d^P \vec{s} \int_{1-s^\mu}^\infty d^P h^\mu \int \frac{d^P \hat{h}^\mu}{2\pi} e^{i(y^\mu \boldsymbol{w}\cdot\boldsymbol{x}^\mu - h^\mu)\hat{h}^\mu} \int \frac{d\hat{l}}{2\pi} e^{i\left(\|\boldsymbol{w}\|^2 + c\|\vec{s}\|^2 - NL\right)\hat{l}} \tag{C5}$$

We wish to calculate the values for which the volume vanishes assuming random (Gaussian) points $\boldsymbol{x}^\mu$ and random (binary) labels y^μ. Using the replica identity:

$$\left[\log V\right]_{x,y} = \lim_{n\to 0} \left[\frac{1}{n}\left(V^n - 1\right)\right]_{x,y} \tag{C6}$$

it is enough to find G which satisfies $[V^n] = e^{nG}$, to have that $[\log V] \approx G$. Thus we consider V^n:

$$V^n = \int d^{n\times N} \boldsymbol{w}^\alpha \int d^{n\times P} \vec{s}^{\boldsymbol{\alpha}} \int_{1-s^{\alpha,\mu}}^\infty d^{n\times P} h^{\alpha,\mu} \int \frac{d^{n\times P}\hat{h}^{\alpha,\mu}}{2\pi} \int \frac{d^n \hat{l}^\alpha}{2\pi} \tag{C7}$$

$$\cdots e^{\sum_\alpha^n \sum_\mu^P i\left(y^\mu \sum_i^N w_i^\alpha x_i^\mu - h^{\alpha,\mu}\right)\hat{h}^{\alpha,\mu} + \sum_\alpha^n i\left(\|\boldsymbol{w}^\alpha\|^2 + c\|\vec{s}^\alpha\|^2 - NL\right)\hat{l}^\alpha} \tag{C8}$$

Gaussian integral on $x_i^\mu \sim \mathcal{N}\left(0, 1/N\right)$:

$$\left[e^{\sum_\alpha^n \sum_\mu^P i y^\mu \sum_i^N w_i^\alpha x_i^\mu \hat{h}^{\alpha,\mu}}\right]_x = e^{-\frac{1}{2}\sum_\mu^P \left(\sum_{\alpha,\beta}^n \left(\frac{1}{N}\sum_i^N w_i^\alpha w_i^\beta\right)\hat{h}^{\alpha,\mu}\hat{h}^{\beta,\mu}\right)} \tag{C9}$$

so denote:

$$q_{\alpha\beta} = \frac{1}{N}\sum_i^N w_i^\alpha w_i^\beta \tag{C10}$$

we have:

$$\left[V^n\right]_x = \int d^{n\times n} q_{\alpha\beta} \int \frac{d^{n\times n}\hat{q}_{\alpha\beta}}{2\pi} \int d^{n\times N} \boldsymbol{w}^\alpha \int d^{n\times P} \vec{s}^{\boldsymbol{\alpha}} \int_{1-s^{\alpha,\mu}}^\infty d^{n\times P} h^{\alpha,\mu} \int \frac{d^{n\times P}\hat{h}^{\alpha,\mu}}{2\pi} \int \frac{d^n \hat{l}^\alpha}{2\pi} \tag{C11}$$

$$\cdots e^{-i\sum_{\alpha,\beta}^n N q_{\alpha\beta}\hat{q}_{\alpha\beta} - i\sum_\alpha^n \sum_\mu^P h^{\alpha,\mu}\hat{h}^{\alpha,\mu} - iN\sum_\alpha^n L\hat{l}^\alpha} \tag{C12}$$

$$\cdots e^{-\frac{1}{2}\sum_\mu^P \sum_{\alpha,\beta}^n q_{\alpha\beta}\hat{h}^{\alpha,\mu}\hat{h}^{\beta,\mu} + i\sum_\alpha^n c\sum_\mu^P (s^{\alpha,\mu})^2\hat{l}^\alpha + i\sum_\alpha^n \sum_i^N w_i^\alpha w_i^\alpha \hat{l}^\alpha + i\sum_{\alpha,\beta}^n \sum_i^N w_i^\alpha w_i^\beta \hat{q}_{\alpha\beta}} \tag{C13}$$

Integration over $\hat{h}^{\alpha,\mu}$, w_i^α using $\int \frac{d^n x}{\sqrt{2\pi}} e^{-x^T Ax/2 + b^T x} = e^{-\frac{1}{2}\log\det A + b^T A^{-1} b/2}$:

$$I_1 \doteq \int \frac{d^{n\times P}\hat{h}^{\alpha,\mu}}{\sqrt{2\pi}} e^{-\frac{1}{2}\sum_\mu^P \sum_{\alpha,\beta}^n q_{\alpha\beta}\hat{h}^{\alpha,\mu}\hat{h}^{\beta,\mu} - i\sum_\alpha^n \sum_\mu^P h^{\alpha,\mu}\hat{h}^{\alpha,\mu}} \tag{C14}$$

$$= e^{-\frac{1}{2}\sum_\mu^P \sum_{\alpha,\beta}^n q^{-1}_{\alpha\beta} h^{\alpha,\mu}h^{\beta,\mu} - \frac{P}{2}\log\det q} \tag{C15}$$

$$I_2 \doteq \int d^{n\times N}\boldsymbol{w}^\alpha e^{i\sum_{\alpha,\beta}^n \sum_i^N w_i^\alpha w_i^\beta \hat{q}_{\alpha\beta} + i\sum_\alpha^n \sum_i^N w_i^\alpha w_i^\alpha \hat{l}^\alpha} \tag{C16}$$

$$= \int d^{n\times N}\boldsymbol{w}^\alpha e^{-\frac{1}{2}\sum_{\alpha,\beta}^n \sum_i^N w_i^\alpha w_i^\beta \left(-2i\hat{q}_{\alpha\beta} - \delta_{\alpha\beta} 2i\hat{l}^\alpha\right)} \tag{C17}$$

$$= e^{-\frac{N}{2}\log\det\left(-2i\hat{q}_{\alpha\beta} - \delta_{\alpha\beta}2i\hat{l}^\alpha\right)} \tag{C18}$$

so that:

$$[V^n]_x = \int d^{n\times n} q_{\alpha\beta} \int \frac{d^{n\times n}\hat{q}_{\alpha\beta}}{2\pi} \int d^{n\times P}\vec{s}^\alpha \int_{1-s^{\alpha,\mu}}^\infty d^{n\times P} h^{\alpha,\mu} \int \frac{d^n \hat{l}^\alpha}{2\pi} \tag{C19}$$

$$\cdots e^{-\frac{N}{2}\log\det\left(-2i\hat{q}_{\alpha\beta} - \delta_{\alpha\beta}2i\hat{l}^\alpha\right) - iN\sum_{\alpha,\beta}^n q_{\alpha\beta}\hat{q}_{\alpha\beta} - iN\sum_\alpha^n L\hat{l}^\alpha} \tag{C20}$$

$$\cdots e^{i\sum_\alpha^n c\sum_\mu^P (s^{\alpha,\mu})^2 \hat{l}^\alpha - \frac{1}{2}\sum_\mu^P \sum_{\alpha,\beta}^n q^{-1}_{\alpha\beta} h^{\alpha,\mu}h^{\beta,\mu} - \frac{P}{2}\log\det q} \tag{C21}$$

Rewrite it such that the all the μ-s are decoupled:

$$I \doteq e^{-\frac{P}{2}\log\det q} \int \frac{d^{n\times P}\vec{s}^\alpha}{\sqrt{2\pi}} \int_{1-s^{\alpha,\mu}}^\infty e^{-\frac{1}{2}\sum_\mu^P \sum_{\alpha,\beta}^n q^{-1}_{\alpha\beta} h^{\alpha,\mu}h^{\beta,\mu} + i\sum_\alpha^n c\sum_\mu^P (s^{\alpha,\mu})^2\hat{l}^\alpha} \tag{C22}$$

$$= \left(e^{-\frac{1}{2}\log\det q} \int \frac{d^n s^\alpha}{\sqrt{2\pi}} \int_{1-s^\alpha}^\infty e^{-\frac{1}{2}\sum_{\alpha,\beta}^n q^{-1}_{\alpha\beta} h^\alpha h^\beta + i\sum_\alpha^n c(s^\alpha)^2\hat{l}^\alpha}\right)^P \tag{C23}$$

we have:

$$[V^n]_x = \int d^{n\times n} q_{\alpha\beta} \int \frac{d^{n\times n}\hat{q}_{\alpha\beta}}{2\pi} \int \frac{d^n\hat{l}^\alpha}{\sqrt{2\pi}} e^{-nNG_0 - nNG_1} \tag{C24}$$

$$G_0 = \frac{i}{n}\sum_{\alpha,\beta}^n q_{\alpha\beta}\hat{q}_{\alpha\beta} + \frac{1}{2n}\log\det\left(-2i\hat{q}_{\alpha\beta} - \delta_{\alpha\beta}2i\hat{l}^\alpha\right) + \frac{i}{n}\sum_\alpha^n L\hat{l}^\alpha \tag{C25}$$

$$G_1 = \frac{\alpha}{2n}\log\det q - \frac{\alpha}{n}\log\int \frac{d^n s^\alpha}{\sqrt{2\pi}} \int_{1-s^\alpha}^\infty d^n h^\alpha e^{iC\sum_\alpha^n (s^\alpha)^2\hat{l}^\alpha - \frac{1}{2}\sum_{\alpha,\beta}^n q^{-1}_{\alpha\beta} h^\alpha h^\beta} \tag{C26}$$

Assuming replica symmetry:

$$q_{\alpha\beta} = q + (q_0 - q)\delta_{\alpha\beta} \tag{C27}$$

$$\hat{q}_{\alpha\beta} = \hat{q} + (\hat{q}_0 - \hat{q})\delta_{\alpha\beta} \tag{C28}$$

$$\hat{l}^\alpha = \hat{l} \tag{C29}$$

we have:

$$\frac{1}{n}\sum_{\alpha,\beta}^n q_{\alpha\beta}\hat{q}_{\alpha\beta} \approx \hat{q}_0 q_0 - \hat{q}q \tag{C30}$$

$$\log\det[q] \approx n\log(q_0 - q) + n\frac{q}{q_0 - q} \tag{C31}$$

$$\log\det|-2i\hat{q} - 2i\hat{l}| \approx n\log\left(-2i\hat{l} - 2i\hat{q}_0 + 2i\hat{q}\right) + n\frac{-2i\hat{q}}{-2i\hat{l} - 2i\hat{q}_0 + 2i\hat{q}} \tag{C32}$$

$$q^{-1}_{\alpha\beta} \approx \frac{1}{(q_0 - q)}\delta_{\alpha\beta} - \frac{q}{(q_0 - q)^2} \tag{C33}$$

so that we get, changing all $-i\hat{l} \to \hat{l}$,$-i\hat{q} \to \hat{q}$,$-i\hat{q}_0 \to \hat{q}_0$:

$$[V^n]_x = \int dq \int dq_0 \int d\hat{q} \int d\hat{q}_0 \int \frac{d\hat{l}}{\sqrt{2\pi}} e^{-nNG_0 - nNG_1} \tag{C34}$$

$$G_0 = -\left[\hat{q}_0 q_0 - \hat{q}q\right] + \frac{1}{2}\left[\log\left(2\hat{l} + 2\hat{q}_0 - 2\hat{q}\right) + \frac{2\hat{q}}{2\hat{l} + 2\hat{q}_0 - 2\hat{q}}\right] - L\hat{l} \tag{C35}$$

$$G_1 = \frac{\alpha}{2}\left[\log\left(q_0 - q\right) + \frac{q}{q_0 - q}\right] - \frac{\alpha}{n}\log\int \frac{d^n s^\alpha}{\sqrt{2\pi}} \int_{1-s^\alpha}^{\infty} \frac{d^n h^\alpha}{\sqrt{2\pi}} e^{-\frac{1}{2}\frac{1}{q_0-q}\sum_\alpha^n (h^\alpha)^2 + \frac{1}{2}\frac{q}{(q_0-q)^2}\left(\sum_\alpha^n h^\alpha\right)^2 - c\sum_\alpha^n (s^\alpha)^2 \hat{l}} \tag{C36}$$

Assuming the behavior in the thermodynamic limit $N \to \infty$ is dominated by the maximum of the integral, we calculate the derivatives of G_0:

$$0 = \frac{\partial G_0}{\partial \hat{q}} = q + \frac{1}{2}\left[-\frac{1}{\hat{l} + \hat{q}_0 - \hat{q}} + \frac{\left(\hat{l} + \hat{q}_0 - \hat{q}\right) + \hat{q}}{\left(\hat{l} + \hat{q}_0 - \hat{q}\right)^2}\right] \tag{C37}$$

$$0 = \frac{\partial G_0}{\partial \hat{q}_0} = -q_0 + \frac{1}{2}\left[\frac{1}{\hat{l} + \hat{q}_0 - \hat{q}} - \frac{\hat{q}}{\left(\hat{l} + \hat{q}_0 - \hat{q}\right)^2}\right] \tag{C38}$$

so that:

$$q = -\frac{1}{2}\frac{\hat{q}}{\left(\hat{l} + \hat{q}_0 - \hat{q}\right)^2} \tag{C39}$$

$$q_0 = \frac{1}{2}\frac{1}{\hat{l} + \hat{q}_0 - \hat{q}} + q \tag{C40}$$

$$q_0 - q = \frac{1}{2}\frac{1}{\hat{l} + \hat{q}_0 - \hat{q}} \tag{C41}$$

$$\frac{q}{\left(q_0 - q\right)^2} = -\frac{1}{2}\frac{\hat{q}}{\left(\hat{l} + \hat{q}_0 - \hat{q}\right)^2} \Big/ \frac{1}{4}\frac{1}{\left(\hat{l} + \hat{q}_0 - \hat{q}\right)^2} = -2\hat{q} \tag{C42}$$

$$q_0\hat{q}_0 - q\hat{q} = \frac{1}{2}\frac{\hat{q}_0}{\hat{l} + \hat{q}_0 - \hat{q}} - \frac{1}{2}\frac{\hat{q}\hat{q}_0}{\left(\hat{l} + \hat{q}_0 - \hat{q}\right)^2} + \frac{1}{2}\frac{\hat{q}\hat{q}}{\left(\hat{l} + \hat{q}_0 - \hat{q}\right)^2} = \frac{1}{2} - \hat{l}q_0 \tag{C43}$$

and G_0 becomes:

$$G_0 = -\frac{1}{2} + \left(q_0 - L\right)\hat{l} - \frac{1}{2}\log\left(q_0 - q\right) - \frac{1}{2}\frac{q}{q_0 - q} \tag{C44}$$

For G_1 we have:

$$G_1 = \frac{\alpha}{2}\log\left(q_0 - q\right) + \frac{\alpha}{2}\frac{q}{q_0 - q} - \frac{\alpha}{n}\log\int \frac{d^n s^\alpha}{\sqrt{2\pi}} \int_{1-s^\alpha}^{\infty} \frac{d^n h^\alpha}{\sqrt{2\pi}} e^{-\frac{1}{2}\frac{1}{q_0-q}\sum_\alpha^n (h^\alpha)^2 + \frac{1}{2}\frac{q}{(q_0-q)^2}\left(\sum_\alpha^n h^\alpha\right)^2 - c\sum_\alpha^n (s^\alpha)^2 \hat{l}} \tag{C45}$$

and using the Hubbard-Stratonovich transform $e^{ay^2/2} = \int \frac{dt}{\sqrt{2\pi}} e^{-t^2/2 + \sqrt{a}yt}$:

$$I = \int \frac{d^n s^\alpha}{\sqrt{2\pi}} \int_{1-s^\alpha}^{\infty} \frac{d^n h^\alpha}{\sqrt{2\pi}} e^{-\frac{1}{2}\frac{1}{q_0-q}\sum_\alpha^n (h^\alpha)^2 + \frac{1}{2}\frac{q}{(q_0-q)^2}\left(\sum_\alpha^n h^\alpha\right)^2 - c\sum_\alpha^n (s^\alpha)^2 \hat{l}} \tag{C46}$$

$$= \int Dt \int \frac{d^n s^\alpha}{\sqrt{2\pi}} \int_{1-s^\alpha}^{\infty} \frac{d^n h^\alpha}{\sqrt{2\pi}} e^{-\frac{1}{2}\frac{1}{q_0-q}\sum_\alpha^n (h^\alpha)^2 + t\frac{\sqrt{q}}{q_0-q}\sum_\alpha^n h_\mu^\alpha - c\sum_\alpha^n (s^\alpha)^2 \hat{l}} \tag{C47}$$

so that G_1 decouples into n terms:

$$G_1 = \frac{\alpha}{2}\log(q_0-q) + \frac{\alpha}{2}\frac{q}{q_0-q} - \frac{\alpha}{n}\log\int\frac{d^n s^\alpha}{\sqrt{2\pi}}\int_{1-s^\alpha}^{\infty}\frac{d^n h^\alpha}{\sqrt{2\pi}}e^{-\frac{1}{2}\frac{1}{q_0-q}\sum_\alpha^n (h^\alpha)^2 + t\frac{\sqrt{q}}{q_0-q}\sum_\alpha^n h_\mu^\alpha - c\sum_\alpha^n (s^\alpha)^2\hat{l}} \tag{C48}$$

$$= \frac{\alpha}{2}\log(q_0-q) + \frac{\alpha}{2}\frac{q}{q_0-q} - \frac{\alpha}{n}\log\int Dt\left(\int\frac{ds}{\sqrt{2\pi}}\int_{1-s}^{\infty}\frac{dh}{\sqrt{2\pi}}e^{-\frac{1}{2}\frac{1}{q_0-q}h^2 + t\frac{\sqrt{q}}{q_0-q}h - Cs^2\hat{l}}\right)^n \tag{C49}$$

and using the replica identity $\log\int Dt\, z(t)^n \approx \log\left[1+n\int Dt\log z(t)\right] \approx n\int Dt\log z(t)$ for $n\to 0$:

$$G_1 = \frac{\alpha}{2}\log(q_0-q) + \frac{\alpha}{2}\frac{q}{q_0-q} - \alpha\int Dt\log\int\frac{ds}{\sqrt{2\pi}}\int_{1-s}^{\infty}\frac{dh}{\sqrt{2\pi}}e^{-\frac{1}{2}\frac{1}{q_0-q}h^2 + t\frac{\sqrt{q}}{q_0-q}h - Cs^2\hat{l}} \tag{C50}$$

by changing $h\to h-s$ and integrating over s using $\int\frac{dx}{\sqrt{2\pi}}e^{-x^2/2a+bx} = e^{\frac{1}{2}\log a+\frac{1}{2}b^2 a}$:

$$I \doteq \int\frac{ds}{\sqrt{2\pi}}\int_{1-s}^{\infty}\frac{dh}{\sqrt{2\pi}}e^{-\frac{1}{2}\frac{1}{q_0-q}h^2 + t\frac{\sqrt{q}}{q_0-q}h - Cs^2\hat{l}} \tag{C51}$$

$$= \int\frac{ds}{\sqrt{2\pi}}\int_{1}^{\infty}\frac{dh}{\sqrt{2\pi}}e^{-\frac{1}{2}\frac{1}{q_0-q}h^2 + \frac{1}{q_0-q}hs - \frac{1}{2}\frac{1}{q_0-q}s^2 + t\frac{\sqrt{q}}{q_0-q}h - t\frac{\sqrt{q}}{q_0-q}s - c\hat{l}s^2} \tag{C52}$$

$$= \int_{1}^{\infty}\frac{dh}{\sqrt{2\pi}}e^{-\frac{1}{2}\frac{1}{q_0-q}h^2 + t\frac{\sqrt{q}}{q_0-q}h + \frac{1}{2}\log\frac{q_0-q}{1+2C\hat{l}(q_0-q)} + \frac{1}{2}\frac{q_0-q}{1+2C\hat{l}(q_0-q)}\left(\frac{h-t\sqrt{q}}{q_0-q}\right)^2} \tag{C53}$$

and by completion to square:

$$G_1 = \frac{\alpha}{2}\log(q_0-q) + \frac{\alpha}{2}\frac{q}{q_0-q} - \alpha\int Dt\log\int_{1}^{\infty}\frac{dh}{\sqrt{2\pi}}e^{-\frac{1}{2}\frac{1}{q_0-q}h^2 + t\frac{\sqrt{q}}{q_0-q}h + \frac{1}{2}\log\frac{q_0-q}{1+2C\hat{l}(q_0-q)} + \frac{1}{2}\frac{q_0-q}{1+2C\hat{l}(q_0-q)}\left(\frac{h-t\sqrt{q}}{q_0-q}\right)^2} \tag{C54}$$

$$= \frac{\alpha}{2}\frac{q}{q_0-q} - \alpha\int Dt\log e^{\frac{1}{2}\frac{t^2 q}{q_0-q}}\int_{1}^{\infty}\frac{dh}{\sqrt{2\pi}}e^{-\frac{1}{2}\frac{(h-t\sqrt{q})^2}{q_0-q}\left(1-\frac{1}{1+2C\hat{l}(q_0-q)}\right) - \frac{1}{2}\log(q_0-q) - \frac{1}{2}\log\frac{1+2C\hat{l}(q_0-q)}{q_0-q}} \tag{C55}$$

$$= \frac{\alpha}{2}\frac{q}{q_0-q} - \alpha\int Dt\left[\frac{1}{2}\frac{t^2 q}{q_0-q} + \log\int_{1}^{\infty}\frac{dh}{\sqrt{2\pi}}e^{-\frac{1}{2}\frac{(h-t\sqrt{q})^2 2C\hat{l}}{1+2C\hat{l}(q_0-q)} - \frac{1}{2}\log\left(1+2C\hat{l}(q_0-q)\right)}\right] \tag{C56}$$

$$= -\alpha\int Dt\log\int_{1}^{\infty}\frac{dh}{\sqrt{2\pi}}e^{-\frac{1}{2}\frac{(h-t\sqrt{q})^2 2C\hat{l}}{1+2C\hat{l}(q_0-q)} - \frac{1}{2}\log\left(1+2C\hat{l}(q_0-q)\right)} \tag{C57}$$

and by a change of variable $h = h_0\sqrt{q}$:

$$G_1 = -\alpha\int Dt\log\int_{1/\sqrt{q}}^{\infty}\frac{dh_0\sqrt{q}}{\sqrt{2\pi}}e^{-\frac{1}{2}\frac{(h_0\sqrt{q}-t\sqrt{q})^2 2C\hat{l}}{1+2C\hat{l}(q_0-q)} - \frac{1}{2}\log\left(1+2C\hat{l}(q_0-q)\right)} \tag{C58}$$

$$= -\alpha\int Dt\log\int_{1/\sqrt{q}}^{\infty}\frac{dh_0}{\sqrt{2\pi}}e^{-\frac{1}{2}\frac{(h_0-t)^2 2C\hat{l}q}{1+2C\hat{l}(q_0-q)} - \frac{1}{2}\log\left(1+2C\hat{l}(q_0-q)\right)/q} \tag{C59}$$

Thus we conclude:

$$[V^n]_x = \int dq\int dq_0\int d\hat{q}\int d\hat{q}_0\int\frac{d\hat{l}}{\sqrt{2\pi}}e^{-nNG_0 - nNG_1} \tag{C60}$$

$$G_0 = -\frac{1}{2} + (q_0-L)\,\hat{l} - \frac{1}{2}\log(q_0-q) - \frac{1}{2}\frac{q}{q_0-q} \tag{C61}$$

$$G_1 = -\alpha\int Dt\log\int_{1/\sqrt{q}}^{\infty}\frac{dh_0}{\sqrt{2\pi}}e^{-\frac{1}{2}\frac{(h_0-t)^2 2C\hat{l}q}{1+2C\hat{l}(q_0-q)} - \frac{1}{2}\log\left(1+2C\hat{l}(q_0-q)\right)/q} \tag{C62}$$

Now $G = G_0 + G_1$ is thus, renaming $\hat{l} = \hat{l}_0/(q_0 - q)$ and h_0 to h:

$$G = -\frac{1}{2} + (q_0 - L)\frac{\hat{l}_0}{q_0 - q} - \frac{1}{2}\log(q_0 - q) - \frac{1}{2}\frac{q}{q_0 - q} \tag{C63}$$

$$\cdots - \alpha \int Dt \log \int_{1/\sqrt{q}}^{\infty} \frac{dh}{\sqrt{2\pi}} e^{-\frac{1}{2}\frac{(h-t)^2}{q_0 - q}\frac{2C\hat{l}_0 q}{1+2C\hat{l}_0} - \frac{1}{2}\log\left(1+2C\hat{l}_0\right)/q} \tag{C64}$$

so the limit of $q \to q_0$:

$$\lim_{q\to q_0}(q_0 - q)\, G_0 = (q_0 - L)\,\hat{l}_0 - \frac{1}{2}q_0 \tag{C65}$$

$$\lim_{q\to q_0}(q_0 - q)\, G_1 = -\alpha \lim_{q\to q_0}(q_0 - q) \int Dt \log \int_{1/\sqrt{q}}^{\infty} \frac{dh}{\sqrt{2\pi}} e^{-\frac{1}{2}\frac{(h-t)^2}{q_0 - q}\frac{2C\hat{l}_0 q}{1+2C\hat{l}_0} - \frac{1}{2}\log\left(1+2C\hat{l}_0\right)/q} \tag{C66}$$

$$= -\alpha \int Dt \lim_{q\to q_0}(q_0 - q) \log \max_{h>1/\sqrt{q}} e^{-\frac{1}{2}\frac{(h-t)^2}{q_0 - q}\frac{2C\hat{l}_0 q}{1+2C\hat{l}_0} - \frac{1}{2}\log\left(1+2C\hat{l}_0\right)/q} \tag{C67}$$

$$= -\alpha \int Dt \lim_{q\to q_0}(q_0 - q) \max_{h>1/\sqrt{q}} -\frac{1}{2}\frac{(h-t)^2}{q_0 - q}\frac{2C\hat{l}_0 q}{1+2C\hat{l}_0} - \frac{1}{2}\log\left(1+2C\hat{l}_0\right)/q \tag{C68}$$

$$= \frac{\alpha}{2}\frac{2C\hat{l}_0 q_0}{1+2C\hat{l}_0} \int Dt \min_{h>1/\sqrt{q}} (h-t)^2 \tag{C69}$$

So to sum up:

$$\lim_{q\to q_0}(q_0 - q)\, G = (q_0 - L)\,\hat{l}_0 - \frac{1}{2}q_0 + \frac{\alpha}{2}\frac{2C\hat{l}_0 q_0}{1+2C\hat{l}_0}\alpha_0^{-1}(1/\sqrt{q}) \tag{C70}$$

for Gardner's α_0:

$$\alpha_0^{-1}(\kappa) = \int_{-\infty}^{\kappa} Dt\,(\kappa - t)^2 \tag{C71}$$

Thus we have:

$$1 = (1 - L/q)\,2\hat{l}_0 + \alpha\frac{2C\hat{l}_0}{1+2C\hat{l}_0}\alpha_0^{-1}(1/\sqrt{q}) \tag{C72}$$

and denoting $k = 2\hat{l}_0$ we have the mean-field equation:

$$L/q = 1 - \frac{1}{k} + \alpha\frac{c}{1+ck}\alpha_0^{-1}(1/\sqrt{q}) \tag{C73}$$

2. Self-consistent equations for points

The self-consistent equations for points, equations 7-8, are derived directly from the mean-field equation 6 by assuming that for the optimal loss we expect saddle-point conditions on $L(q,k)$, namely that $0=\frac{\partial L}{\partial q}=\frac{\partial L}{\partial k}$:

$$0=\frac{\partial}{\partial k}L=-q\alpha\frac{1}{(c+k)^2}\alpha_0^{-1}\left(1/\sqrt{q}\right)+q/k^2 \tag{C74}$$

$$1=\frac{(ck)^2}{(1+ck)^2}\alpha\alpha_0^{-1}\left(1/\sqrt{q}\right) \tag{C75}$$

$$0=\frac{\partial}{\partial q}L=1-1/k+\frac{c\alpha}{1+ck}\frac{\partial}{\partial q}\left[q\alpha_0^{-1}\left(1/\sqrt{q}\right)\right] \tag{C76}$$

$$=\frac{k-1}{k}+\frac{c\alpha}{1+ck}\int_{-\infty}^{1/\sqrt{q}}Dt\left(1/\sqrt{q}-t\right)t \tag{C77}$$

$$=\frac{k-1}{k}+\frac{c\alpha}{1+ck}H\left(-1/\sqrt{q}\right) \tag{C78}$$

$$1-k=\frac{ck}{1+ck}\alpha H\left(-1/\sqrt{q}\right) \tag{C79}$$

Those self-consistent equations can be evaluated for the limits $\alpha\to 0$ and $\alpha\to\infty$.
When $\alpha\to 0$ we have $k\to 1$ and $q\to 0$ so that $\alpha_0^{-1}\left(1/\sqrt{q}\right)\approx 1/q$ and thus:

$$k=1-\frac{ck}{1+ck}\alpha\approx=1-\frac{c}{1+c}\alpha \tag{C80}$$

$$\sqrt{q}=\frac{ck}{1+ck}\sqrt{\alpha}\approx\frac{c}{1+c}\sqrt{\alpha} \tag{C81}$$

When $\alpha\to\infty$ we have $k\to 0$ and $q\to 0$ so that scaling $k=k_0/\alpha$ we have:

$$1=\frac{ck_0}{(1-k_0/\alpha)(1+ck_0/\alpha)}\approx ck_0 \tag{C82}$$

$$k=1/c\alpha \tag{C83}$$

$$q=\frac{(ck)^2}{(1+ck)^2}\alpha=\frac{(1/\alpha)^2}{(1+1/\alpha)^2}\alpha=\frac{\alpha}{(\alpha+1)^2}\approx 1/\alpha \tag{C84}$$

So the limits:

$$k=\begin{cases}1-\frac{c}{1+c}\alpha & \alpha\to 0\\ 1/c\alpha & \alpha\to\infty\end{cases} \tag{C85}$$

$$q=\begin{cases}\frac{c^2}{(1+c)^2}\alpha & \alpha\to 0\\ 1/\alpha & \alpha\to\infty\end{cases} \tag{C86}$$

The limit $c\to\infty$ exhibit different behavior for $\alpha<2$ and $\alpha>2$. For $\alpha<2$ the solution satisfies

$$1=\alpha\alpha_0^{-1}\left(1/\sqrt{q}\right) \tag{C87}$$

which is the max-margin solution. On the other hand, for $\alpha\geq 2$ and $c\to\infty$ we have that $\lim_{c\to\infty}k=0$ with finite $q, K=\lim_{c\to\infty}ck$, which obey the self-consistent equations:

$$1=\frac{K^2}{(1+K)^2}\alpha\alpha_0^{-1}\left(1/\sqrt{q}\right) \tag{C88}$$

$$1=\frac{K}{1+K}\alpha H\left(-1/\sqrt{q}\right) \tag{C89}$$

The relation between α and q thus becomes:

$$\alpha=\alpha_0^{-1}\left(1/\sqrt{q}\right)/H^2\left(-1/\sqrt{q}\right) \tag{C90}$$

3. Field and slack distribution for points

Note we have in the theory the inner integral given as, using our notation $k = 2\hat{l}_0 = 2\hat{l}\,(q_0 - q)$:

$$I \doteq \int \frac{ds}{\sqrt{2\pi}} \int_{1-s}^{\infty} \frac{dh}{\sqrt{2\pi}} e^{-\frac{1}{2}\frac{1}{q_0-q}h^2 + \frac{\sqrt{qt}}{q_0-q}h - Cs^2\hat{l}} \tag{C91}$$

$$= \int \frac{ds}{\sqrt{2\pi}} \int_{1-s}^{\infty} \frac{dh}{\sqrt{2\pi}} e^{-\frac{1}{2}\frac{1}{q_0-q}\left(h-\sqrt{qt}\right)^2 + \frac{1}{2}\frac{qt^2}{q_0-q} - \frac{1}{2}\frac{1}{q_0-q}cks^2} \tag{C92}$$

So that:

$$G_1 = \frac{\alpha}{2}\log\left(q_0 - q\right) + \frac{\alpha}{2}\frac{q}{q_0-q} - \alpha \int Dt \log I \tag{C93}$$

$$= \frac{\alpha}{2}\frac{q}{q_0-q} - \alpha \int Dt \log e^{\frac{1}{2}\frac{qt^2}{q_0-q}} \int \frac{ds}{\sqrt{2\pi}} \int_{1-s}^{\infty} \frac{dh}{\sqrt{2\pi}} e^{-\frac{1}{2}\log(q_0-q) - \frac{1}{2}\frac{1}{q_0-q}\left(h-\sqrt{qt}\right)^2 - \frac{1}{2}\frac{1}{q_0-q}cks^2} \tag{C94}$$

$$= -\alpha \int Dt \log \int \frac{ds}{\sqrt{2\pi}} \int_{1-s}^{\infty} \frac{dh}{\sqrt{2\pi}} e^{-\frac{1}{2}\log(q_0-q) - \frac{1}{2}\frac{1}{q_0-q}\left(h-\sqrt{qt}\right)^2 - \frac{1}{2}\frac{1}{q_0-q}cks^2} \tag{C95}$$

so the limit:

$$\lim_{q_0 \to q}\left(q_0 - q\right) G_1 = -\alpha \int Dt \lim_{q_0 \to q}\left(q_0 - q\right) \log \int \frac{ds}{\sqrt{2\pi}} \int_{1-s}^{\infty} \frac{dh}{\sqrt{2\pi}} e^{-\frac{1}{2}\log(q_0-q) - \frac{1}{2}\frac{1}{q_0-q}\left(h-\sqrt{qt}\right)^2 - \frac{1}{2}\frac{1}{q_0-q}cks^2} \tag{C96}$$

$$= -\alpha \int Dt \lim_{q_0 \to q}\left(q_0 - q\right) \max_{s>1-h}\left\{-\frac{1}{2}\log\left(q_0 - q\right) - \frac{1}{2}\frac{1}{q_0-q}\left(h-\sqrt{qt}\right)^2 - \frac{1}{2}\frac{1}{q_0-q}cks^2\right\} \tag{C97}$$

$$= \alpha \int Dt \min_{s>1-h}\left\{\frac{1}{2}\left(h-\sqrt{qt}\right)^2 + \frac{1}{2}cks^2\right\} \tag{C98}$$

with Lagrangian:

$$h^*, s^* = \arg\min_{s>1-h} \frac{1}{2}\left(h - t\sqrt{q}\right)^2 + \frac{1}{2}cks^2 \tag{C99}$$

$$\mathcal{L} = \frac{1}{2}\left(h - t\sqrt{q}\right)^2 + \frac{1}{2}cks^2 + \lambda\left(1 - h - s\right) \tag{C100}$$

and derivatives:

$$\frac{\partial \mathcal{L}}{\partial h} = \left(h - t\sqrt{q}\right) - \lambda = 0 \tag{C101}$$

$$\frac{\partial \mathcal{L}}{\partial s} = cks - \lambda = 0 \tag{C102}$$

so from KKT conditions:

$$0 = \lambda\left(1 - h - s\right) \tag{C103}$$

$$\lambda = h - t\sqrt{q} \tag{C104}$$

$$\lambda = cks \tag{C105}$$

so either $\lambda = 0$ and then:

$$s = 0 \tag{C106}$$

$$1 \leq h = t\sqrt{q} \tag{C107}$$

or $\lambda \geq 0$ and then:

$$s \geq 0 \tag{C108}$$

$$1 \geq h = \frac{ck}{1+ck} + \frac{\sqrt{q}}{1+ck}t \tag{C109}$$

so that we can write:

$$h = \begin{cases} \frac{ck}{1+ck} + \frac{\sqrt{q}}{1+ck}t_0 & -\infty \leq t_0 \leq 1/\sqrt{q} \\ \sqrt{q}t_0 & 1/\sqrt{q} \leq t_0 \end{cases} \tag{C110}$$

which can be written equivalently as equation 12. The slack variables satisfy $s = \max\{1-h, 0\}$ which yields

$$s = \begin{cases} \frac{1}{1+ck} - \frac{\sqrt{q}}{1+ck}t_0 & -\infty \leq t_0 \leq 1/\sqrt{q} \\ 0 & 1/\sqrt{q} \leq t_0 \end{cases} \tag{C111}$$

Interestingly, the slack distribution allows to derive the self-consistent equations 7-8 without saddle-point assumption (i.e., without taking derivatives of L). From the definition of L we have that:

$$L = \|\boldsymbol{w}\|^2/N + c\|\vec{s}\|^2/N = q + \alpha c \left\langle s^2 \right\rangle \tag{C112}$$

$$\left\langle s^2 \right\rangle = \frac{q}{(1+ck)^2} \int_{-\infty}^{1/\sqrt{q}} Dt_0 \left(1/\sqrt{q} - t_0\right)^2 \tag{C113}$$

and the following equation is true for the optimal loss L^* (see details in section C 4):

$$L = \frac{c}{N}\sum_{\mu}^{P} s_\mu = \alpha c \langle s \rangle \tag{C114}$$

$$\langle s \rangle = \frac{\sqrt{q}}{1+ck} \int_{-\infty}^{1/\sqrt{q}} Dt_0 \left(1/\sqrt{q} - t_0\right) \tag{C115}$$

Combining equations C112,6 and C114 yields equations 7-8.

Furthermore, from the expression for $\left\langle s^2 \right\rangle$ and the self-consistent equation $\frac{1}{(ck)^2} = \frac{1}{(1+ck)^2}\alpha\alpha_0^{-1}\left(1/\sqrt{q}\right)$ we have:

$$\frac{q}{c^2k^2} = \alpha \left\langle s^2 \right\rangle \tag{C116}$$

4. Optimal loss at classification of points and spheres

We show the optimal loss satisfies $L^* = \alpha c \langle s \rangle$ for both points (equation C114) and spheres (equation C283).

We write a Lagrangian for the problem, assuming no bias for brevity, i.e. $v_0^\mu = y^\mu \boldsymbol{w} \cdot \boldsymbol{u}_0^\mu$. For spheres we have the constraint on the minimal field $h_{min}^\mu = v_0^\mu - R\|v^\mu\| \geq 1 - s^\mu$ so that both cases are captured by the same Lagrangian (with $R = 0$ for points):

$$L^* = \min_{\boldsymbol{w}} \|\boldsymbol{w}\|^2/N + c\|\vec{s}\|^2/N \ s.t. \ v_0^\mu - Rv^\mu \geq 1 - s^\mu \ \forall \mu \tag{C117}$$

$$\mathcal{L} = \frac{1}{2}\|\boldsymbol{w}\|^2/N + \frac{1}{2}c\|\vec{s}\|^2/N + \sum_{\mu}^{P} \lambda_\mu \left(1 - s^\mu - v_0^\mu + R\|v^\mu\|\right) \tag{C118}$$

KKT conditions yield 3 equations:

$$0 = \frac{\partial \mathcal{L}}{\partial w_i} = w_i + \sum_\mu \lambda_\mu \left(-y^\mu u_{0i}^\mu + y^\mu R \sum_l^D \frac{v_l^\mu u_{li}^\mu}{\|v^\mu\|} \right) \tag{C119}$$

$$0 = \frac{\partial \mathcal{L}}{\partial s^\mu} = 2cs^\mu/N + 2\lambda_\mu \tag{C120}$$

$$\forall \mu \; 0 = \lambda_\mu \left(1 - s^\mu - v_0^\mu + R\|v^\mu\|\right) \tag{C121}$$

Denoting $h_\mu = v_0^\mu - R\|v^\mu\|$ those can be written as:

$$0 = \vec{\lambda}\left(1 - \vec{s} - \vec{h}\right) \tag{C122}$$

$$\vec{\lambda} = \vec{s}c/N \tag{C123}$$

$$\boldsymbol{w} = \sum_\mu \lambda_\mu y^\mu \left(\boldsymbol{u}_0^\mu - R \sum_l^D \frac{v_l^\mu}{\|v^\mu\|} \boldsymbol{u}_l^\mu \right) \tag{C124}$$

$$\boldsymbol{w}^T \boldsymbol{w} = \sum_\mu \lambda_\mu \left(v_0^\mu - R\|v^\mu\|\right) = \vec{\lambda}^T \vec{h} \tag{C125}$$

so that we have that the optimal solution L^* satisfies:

$$L^* = \boldsymbol{w}^T \boldsymbol{w} + c\|\vec{s}\|^2/N + 2\sum_\mu^P \lambda_\mu \left(1 - s^\mu - h_\mu\right) \tag{C126}$$

$$= \vec{\lambda}^T \left(1 - \vec{s} - \vec{h}\right) + \sum_\mu^P \lambda_\mu = \frac{c}{N} \sum_\mu^P s_\mu \tag{C127}$$

Yielding the result:

$$L^* = c\alpha \langle s \rangle \tag{C128}$$

5. Classification error for points

We seek to derive the classification error for training ε_{tr} and testing $\varepsilon_g(\sigma)$ with respect to Gaussian noise $\mathcal{N}\left(0, \sigma^2/N\right)$ applied to the training set.

The training error has contribution only from the "touching" regime of the field distribution (equation 12):

$$\varepsilon_{tr} = \int_{-\infty}^0 dh e^{-(h-\mu_1)^2/2\sigma_1^2} / \sqrt{2\pi\sigma_1^2} = H\left(\mu_1/\sigma_1\right) \tag{C129}$$

with $\mu_1 = \frac{ck}{1+ck}$ and $\sigma_1^2 = \frac{q}{(1+ck)^2}$, so that:

$$\varepsilon_{tr} = H\left(ck/\sqrt{q}\right) \tag{C130}$$

When i.i.d Gaussian noise $\mathcal{N}\left(0, \sigma^2/N\right)$ is applied to each input component, as the weights are independent of this noise, the fields are affected by i.i.d Gaussian noise $\mathcal{N}\left(0, \sigma^2 q\right)$:

$$h = h^\mu + \sigma\sqrt{q}\eta^\mu \tag{C131}$$

when η^μ are standard Gaussian variables. The noisy field distribution can be written explicitly, denoted $P_g(h)$:

$$P_g(h) = e^{-(h-\mu_1)^2/2\left(\sigma_1^2+\sigma^2 q\right)}/\sqrt{2\pi\left(\sigma_1^2+\sigma^2 q\right)}H\left(\frac{(h-1)\left(\sigma^2 q+\sigma_1^2\right)-\sigma^2 q(h-\mu_1)}{\sigma\sqrt{q}\sigma_1\sqrt{\sigma^2 q+\sigma_1^2}}\right) \tag{C132}$$

$$+ e^{-(h-\mu_2)^2/2\left(\sigma_2^2+\sigma^2 q\right)}/\sqrt{2\pi\left(\sigma_2^2+\sigma^2 q\right)}H\left(-\frac{(h-1)\left(\sigma^2 q+\sigma_2^2\right)-\sigma^2 q(h-\mu_2)}{\sigma\sqrt{q}\sigma_2\sqrt{\sigma^2 q+\sigma_2^2}}\right) \tag{C133}$$

so the error is given by:

$$\varepsilon_g = \int_{-\infty}^{0} dh P_g(h) \tag{C134}$$

which is useful for numerical evaluation. For the analytic derivation below it is more useful to consider a different formalism, using the field distribution (equation 12):

$$\varepsilon_g = \int_{-\infty}^{\infty} dh P_{tr}(h) H\left(h/\sigma\sqrt{q}\right) \tag{C135}$$

$$= \int_{-\infty}^{1} dh e^{-(h-ck/(1+ck))^2/2q/(1+ck)^2}/\sqrt{2\pi q/(1+ck)^2}\int_{h/\sigma\sqrt{q}}^{\infty} dx e^{-x^2/2}/\sqrt{2\pi} \tag{C136}$$

$$+ \int_{1}^{\infty} dh e^{-h^2/2q}/\sqrt{2\pi q}\int_{h/\sigma\sqrt{q}}^{\infty} dx e^{-x^2/2}/\sqrt{2\pi} \tag{C137}$$

so that replacing $g = h(1+ck)/\sqrt{q} - ck/\sqrt{q}$ and $g = h/\sqrt{q}$:

$$\varepsilon_g = \int_{-\infty}^{1/\sqrt{q}} Dg_1 H\left(\frac{g_1\sqrt{q}+ck}{\sigma\sqrt{q}(1+ck)}\right) + \int_{1/\sqrt{q}}^{\infty} Dg_2 H\left(g_2/\sigma\right) \tag{C138}$$

so using identity 10,010.4 from [20]:

$$\int_h^k DxH(a+bx) = \int_{a/\sqrt{b^2+1}}^{\infty} DxH\left(h\sqrt{b^2+1}+bx\right) - \int_{a/\sqrt{b^2+1}}^{\infty} DxH\left(k\sqrt{b^2+1}+bx\right) \tag{C139}$$

we have an exact expression:

$$\varepsilon_g = H\left(1/\sqrt{q/(ck)^2 + q\sigma^2(1+ck)^2/(ck)^2}\right) + \int_0^{\infty} DxH\left(\frac{\sqrt{1+\sigma^2}}{\sqrt{q}\sigma}+\frac{x}{\sigma}\right) \tag{C140}$$

$$- \int_{1/\sqrt{q/(ck)^2+q\sigma^2(1+ck)^2/(ck)^2}}^{\infty} DxH\left(\frac{\sqrt{1+\sigma^2(1+ck)^2}}{\sqrt{q}\sigma(1+ck)}+\frac{x}{\sigma(1+ck)}\right) \tag{C141}$$

where in the second and third integrals we have only positive terms, with $x \geq 0$ and $\sqrt{1+\sigma^2}, \sqrt{1+\sigma^2(1+ck)^2} \geq 1$. Thus if $\sqrt{q}\sigma \ll 1$ we expect a good approximation:

$$\varepsilon_g \approx H(\mathcal{S}) \tag{C142}$$

$$\mathcal{S} = ck/\sqrt{q\left(1+(1+ck)^2\sigma^2\right)} \tag{C143}$$

6. Optimal choice of c for points

The optimal SNR $\mathcal{S}$ should be optimized with respect to c:

$$c^* = \arg\min_c \mathcal{S}^{-2} \tag{C144}$$

so that taking its derivative should satisfy $0 = \frac{\partial \mathcal{S}^{-2}}{\partial c}$:

$$\frac{\partial q}{\partial c}\frac{\left(\sigma^2\left(1+ck\right)^2+1\right)}{\left(ck\right)^2} = 2q\left(k+c\frac{\partial k}{\partial c}\right)\frac{\left(\sigma^2\left(1+ck\right)^2+1\right)-\left(\sigma^2\left(1+ck\right)\right)\left(ck\right)}{\left(ck\right)^3} \tag{C145}$$

$$\frac{\partial q}{\partial c} = 2q\left(k+c\frac{\partial k}{\partial c}\right)\frac{\left(\sigma^2\left(1+ck\right)+1\right)}{\left(ck\right)\left(\sigma^2\left(1+ck\right)^2+1\right)} \tag{C146}$$

Starting from the self-consistent equations 7, 8 we rewrite them as:

$$q\left(1+ck\right)^2 = \left(ck\right)^2\alpha q\alpha_0^{-1}\left(1/\sqrt{q}\right) \tag{C147}$$

$$\left(1-k\right)\left(1+ck\right) = \left(ck\right)\alpha H\left(-1/\sqrt{q}\right) \tag{C148}$$

where we have multiplied the first equation by q, so that we may use the identity $\frac{\partial}{\partial c}q\alpha_0^{-1}\left(1/\sqrt{q}\right) = H\left(-1/\sqrt{q}\right)\frac{\partial q}{\partial c}$ when taking its derivative:

$$\frac{\partial q}{\partial c}\left(1+ck\right)^2 + q2\left(1+ck\right)\left(k+c\frac{\partial k}{\partial c}\right) = 2\left(ck\right)\left(k+c\frac{\partial k}{\partial c}\right)\alpha q\alpha_0^{-1}\left(1/\sqrt{q}\right) + \left(ck\right)^2\alpha H\left(-1/\sqrt{q}\right)\frac{\partial q}{\partial c} \tag{C149}$$

in order to get:

$$\frac{\partial q}{\partial c} = 2q\left(k+c\frac{\partial k}{\partial c}\right)\frac{\left(ck\right)\alpha\alpha_0^{-1}\left(1/\sqrt{q}\right)-\left(1+ck\right)}{\left(1+ck\right)^2-\left(ck\right)^2\alpha H\left(-1/\sqrt{q}\right)} \tag{C150}$$

which yields for the optimal SNR an expression without $\frac{\partial q}{\partial c}$ or $\frac{\partial k}{\partial c}$:

$$\frac{\left(\sigma^2\left(1+ck\right)+1\right)}{\left(ck\right)\left(\sigma^2\left(1+ck\right)^2+1\right)} = \frac{\left(ck\right)\alpha\alpha_0^{-1}\left(1/\sqrt{q}\right)-\left(1+ck\right)}{\left(1+ck\right)^2-\left(ck\right)^2\alpha H\left(-1/\sqrt{q}\right)} \tag{C151}$$

Using the self-consistent equations again to substitute $\alpha\alpha_0^{-1}\left(1/\sqrt{q}\right)$ and $\alpha H\left(-1/\sqrt{q}\right)$ we get:

$$\frac{\left(\sigma^2\left(1+ck\right)+1\right)}{\left(ck\right)\left(\sigma^2\left(1+ck\right)^2+1\right)} = \frac{\frac{\left(1+ck\right)^2}{\left(ck\right)}-\left(1+ck\right)}{\left(1+ck\right)^2-\left(ck\right)\left(1-k\right)\left(1+ck\right)} \tag{C152}$$

so that for $\sigma = 0$ we have no solution with both $c > 0$ and $q > 0$ (thus proving the ε_{tr} is monotonic in c for any α) while for $\sigma > 0$ we have:

$$\sigma^{-2}ck^2 = \left(1+ck\right)^2 - \left(1+ck\right)\left[1+ck^2\right] \tag{C153}$$

and the optimal c should satisfy:

$$c = \frac{\sigma^{-2}}{1-k} - \frac{1}{k} \tag{C154}$$

which needs to be solved self-consistently as k depends on c.

7. Replica theory for spheres

We write an expression for the volume $V(L,c)$ for $L = \|\boldsymbol{w}\|^2/N + c\|\vec{s}\|^2/N$ which would vanish for $L < L^*$:

$$V(L,c) = \int d^N \boldsymbol{w} \int d^P \vec{s} \int d^{P\times D}\vec{v} \prod_{\mu}^{P}\prod_{l}^{D} \delta\left(y^\mu \boldsymbol{w}\cdot \boldsymbol{u}_l^\mu - v_l^\mu\right) \times \tag{C155}$$

$$\cdots \prod_{\mu}^{P} \Theta\left(v_0^\mu - R\|\vec{v}^\mu\| \geq 1 - s^\mu\right) \delta\left(\|\boldsymbol{w}\|^2 + c\|\vec{s}\|^2 - NL\right) \tag{C156}$$

$$= \int d^N \boldsymbol{w} \int d^P \vec{s} \int d^{P\times D}\vec{v}_l^\mu \int \frac{d^{P\times D}\hat{v}_l^\mu}{2\pi} e^{i\sum_\mu^P \sum_l^D \left(y^\mu \boldsymbol{w}\cdot \boldsymbol{u}_l^\mu - v_l^\mu\right)\hat{v}_l^\mu} \times \tag{C157}$$

$$\cdots \int_{1-s^\mu}^{\infty} d^P h^\mu \int \frac{d^P \hat{h}^\mu}{2\pi} e^{i\left(v_0^\mu - R\|\vec{v}^\mu\| - h^\mu\right)\hat{h}^\mu} \int \frac{d\hat{l}}{2\pi} e^{i\left(\|\boldsymbol{w}\|^2 + c\|\vec{s}\|^2 - NL\right)\hat{l}} \tag{C158}$$

We wish to calculate the values for which the volume vanishes assuming random (Gaussian) axes $\boldsymbol{u}_l^\mu$ and random (binary) labels y^μ. Using the replica identity:

$$[\log V]_{x,y} = \lim_{n\to 0}\left[\frac{1}{n}\left(V^n - 1\right)\right]_{x,y} \tag{C159}$$

it is enough to find G which satisfies $[V^n] = e^{nG}$, to have that $[\log V] \approx G$. Thus we consider V^n:

$$V^n = \int d^{n\times N}\boldsymbol{w}^\alpha \int d^{n\times P}\vec{s}^\alpha \int d^{n\times P\times D}\vec{v}_l^{\alpha,\mu} \int \frac{d^{n\times P\times D}\hat{v}_l^{\alpha,\mu}}{2\pi} \int_{1-s^{\alpha,\mu}}^{\infty} d^{n\times P}h^{\alpha,\mu} \int \frac{d^{n\times P}\hat{h}^{\alpha,\mu}}{2\pi} \int \frac{d^n\hat{l}^\alpha}{2\pi} \tag{C160}$$

$$\cdots e^{i\sum_\alpha^n \sum_\mu^P \sum_l^D \left(y^\mu \boldsymbol{w}^\alpha\cdot \boldsymbol{u}_l^\mu - v_l^{\alpha,\mu}\right)\hat{v}_l^{\alpha,\mu} + \sum_\alpha^n \sum_\mu^P i\left(v_0^{\alpha,\mu} - R\|\vec{v}^{\alpha,\mu}\| - h^{\alpha,\mu}\right)\hat{h}^{\alpha,\mu} + \sum_\alpha^n i\left(\|\boldsymbol{w}^\alpha\|^2 + c\|\vec{s}^\alpha\|^2 - NL\right)\hat{l}^\alpha} \tag{C161}$$

Using Gaussian integral on the exes $u_{li}^\mu \sim \mathcal{N}(0, 1/N)$ for $l = 0..D$ and $\mu = 1..P$:

$$\left[e^{\sum_\alpha^n \sum_\mu^P iy^\mu \sum_i^N w_i^\alpha u_{li}^\mu \hat{v}_l^{\alpha,\mu}}\right]_u = e^{-\frac{1}{2}\sum_\mu^P\left(\sum_{\alpha,\beta}^n\left(\frac{1}{N}\sum_i^N w_i^\alpha w_i^\beta\right)\hat{v}_l^{\alpha,\mu}\hat{v}_l^{\beta,\mu}\right)} \tag{C162}$$

so denoting as usual:

$$q_{\alpha\beta} = \frac{1}{N}\sum_i^N w_i^\alpha w_i^\beta \tag{C163}$$

we have:

$$[V^n]_x = \int d^{n\times n}q_{\alpha\beta} \int \frac{d^{n\times n}\hat{q}_{\alpha\beta}}{2\pi} \int d^{n\times N}\boldsymbol{w}^\alpha \int d^{n\times P}\vec{s}^\alpha \int d^{n\times P\times D}\vec{v}_l^{\alpha,\mu} \times \tag{C164}$$

$$\cdots \int \frac{d^{n\times P\times D}\hat{v}_l^{\alpha,\mu}}{2\pi} \int_{1-s^{\alpha,\mu}}^{\infty} d^{n\times P}h^{\alpha,\mu} \int \frac{d^{n\times P}\hat{h}^{\alpha,\mu}}{2\pi} \int \frac{d^n\hat{l}^\alpha}{2\pi} \times \tag{C165}$$

$$\cdots e^{-i\sum_\alpha^n \sum_\mu^P \sum_l^D v_l^{\alpha,\mu}\hat{v}_l^{\alpha,\mu} - i\sum_{\alpha,\beta}^n Nq_{\alpha\beta}\hat{q}_{\alpha\beta} - i\sum_\alpha^n \sum_\mu^P h^{\alpha,\mu}\hat{h}^{\alpha,\mu} - iN\sum_\alpha^n L\hat{l}^\alpha} \tag{C166}$$

$$\cdots e^{-\frac{1}{2}\sum_\mu^P \sum_{\alpha,\beta}^n q_{\alpha\beta}\hat{v}_0^{\alpha,\mu}\hat{v}_0^{\beta,\mu} - \frac{1}{2}\sum_\mu^P \sum_l^D \sum_{\alpha,\beta}^n q_{\alpha\beta}\hat{v}_l^{\alpha,\mu}\hat{v}_l^{\beta,\mu} + i\sum_\alpha^n \sum_\mu^P\left(v_0^{\alpha,\mu} - R\|\vec{v}^{\alpha,\mu}\|\right)\hat{h}^{\alpha,\mu}} \tag{C167}$$

$$\cdots e^{+i\sum_\alpha^n c\sum_\mu^P (s^{\alpha,\mu})^2\hat{l}^\alpha + i\sum_\alpha^n \sum_i^N w_i^\alpha w_i^\alpha \hat{l}^\alpha + i\sum_{\alpha,\beta}^n \sum_i^N w_i^\alpha w_i^\beta \hat{q}_{\alpha\beta}} \tag{C168}$$

Integration over $\hat{v}_l^{\alpha,\mu}$, w_i^α using $\int \frac{d^n x}{\sqrt{2\pi}} e^{-x^T Ax/2 + b^T x} = e^{-\frac{1}{2}\log\det A + b^T A^{-1} b/2}$:

$$\int \frac{d^{n\times P}\hat{h}^{\alpha,\mu}}{\sqrt{2\pi}} e^{-\frac{1}{2}\sum_\mu^P \sum_{\alpha,\beta}^n q_{\alpha\beta}\hat{v}_0^{\alpha,\mu}\hat{v}_0^{\beta,\mu} - i\sum_\alpha^n \sum_\mu^P v_0^{\alpha,\mu}\hat{v}_0^{\alpha,\mu}} = e^{-\frac{1}{2}\sum_\mu^P \sum_{\alpha,\beta}^n q_{\alpha\beta}^{-1} v_0^{\alpha,\mu} v_0^{\beta,\mu} - \frac{P}{2}\log\det q} \tag{C169}$$

$$\int \frac{d^{n\times P}\hat{h}^{\alpha,\mu}}{\sqrt{2\pi}} e^{-\frac{1}{2}\sum_\mu^P \sum_l^D \sum_{\alpha,\beta}^n q_{\alpha\beta}\hat{v}_l^{\alpha,\mu}\hat{v}_l^{\beta,\mu} - i\sum_\alpha^n \sum_\mu^P \sum_l^D v_l^{\alpha,\mu}\hat{v}_l^{\alpha,\mu}} = e^{-\frac{1}{2}\sum_\mu^P \sum_l^D \sum_{\alpha,\beta}^n q_{\alpha\beta}^{-1} v_l^{\alpha,\mu} v_l^{\beta,\mu} - \frac{DP}{2}\log\det q} \tag{C170}$$

$$\int d^{n\times N}\boldsymbol{w}^\alpha e^{i\sum_{\alpha,\beta}^n \sum_i^N w_i^\alpha w_i^\beta \hat{q}_{\alpha\beta} + i\sum_\alpha^n \sum_i^N w_i^\alpha w_i^\alpha \hat{l}^\alpha} = e^{-\frac{N}{2}\log\det\left(-2i\hat{q}_{\alpha\beta} - \delta_{\alpha\beta}2i\hat{l}^\alpha\right)} \tag{C171}$$

so that:

$$[V^n]_x = \int d^{n\times n} q_{\alpha\beta} \int \frac{d^{n\times n}\hat{q}_{\alpha\beta}}{2\pi} \int d^{n\times P}\vec{s}^{\alpha} \int d^{n\times P\times D}\vec{v}_l^{\alpha,\mu} \int_{1-s^{\alpha,\mu}}^{\infty} d^{n\times P} h^{\alpha,\mu} \int \frac{d^{n\times P}\hat{h}^{\alpha,\mu}}{2\pi} \int \frac{d^n \hat{l}^{\alpha}}{2\pi} \tag{C172}$$

$$\cdots e^{-i\sum_{\alpha,\beta}^{n} N q_{\alpha\beta}\hat{q}_{\alpha\beta} - i\sum_{\alpha}^{n}\sum_{\mu}^{P} h^{\alpha,\mu}\hat{h}^{\alpha,\mu} - iN\sum_{\alpha}^{n} L\hat{l}^{\alpha} - \frac{1}{2}\sum_{\mu}^{P}\sum_{\alpha,\beta}^{n} q_{\alpha\beta}^{-1} v_0^{\alpha,\mu} v_0^{\beta,\mu} - \frac{1}{2}\sum_{\mu}^{P}\sum_{l}^{D}\sum_{\alpha,\beta}^{n} q_{\alpha\beta}^{-1} v_l^{\alpha,\mu} v_l^{\beta,\mu}} \tag{C173}$$

$$\cdots e^{+i\sum_{\alpha}^{n}\sum_{\mu}^{P}\left(v_0^{\alpha,\mu} - R\|\vec{v}^{\alpha,\mu}\|\right)\hat{h}^{\alpha,\mu} + i\sum_{\alpha}^{n} c\sum_{\mu}^{P}(s^{\alpha,\mu})^2\hat{l}^{\alpha} - \frac{N}{2}\log\det\left(-2i\hat{q}_{\alpha\beta} - \delta_{\alpha\beta}2i\hat{l}^{\alpha}\right) - \frac{(D+1)P}{2}\log\det q} \tag{C174}$$

This can be rewritten such that all the μ-s are decoupled:

$$I \doteq \int d^{n\times P}\vec{s}^{\alpha} \int d^{n\times P\times D}\vec{v}_l^{\alpha,\mu} \int_{1-s^{\alpha,\mu}}^{\infty} d^{n\times P} h^{\alpha,\mu} \int \frac{d^{n\times P}\hat{h}^{\alpha,\mu}}{2\pi} \tag{C175}$$

$$\cdots e^{-i\sum_{\alpha}^{n}\sum_{\mu}^{P}\sum_{l}^{D} v_l^{\alpha,\mu}\hat{v}_l^{\alpha,\mu} - i\sum_{\alpha,\beta}^{n} N q_{\alpha\beta}\hat{q}_{\alpha\beta} - i\sum_{\alpha}^{n}\sum_{\mu}^{P} h^{\alpha,\mu}\hat{h}^{\alpha,\mu} - \frac{1}{2}\sum_{\mu}^{P}\sum_{\alpha,\beta}^{n} q_{\alpha\beta}^{-1} v_0^{\alpha,\mu} v_0^{\beta,\mu} - \frac{1}{2}\sum_{\mu}^{P}\sum_{l}^{D}\sum_{\alpha,\beta}^{n} q_{\alpha\beta}^{-1} v_l^{\alpha,\mu} v_l^{\beta,\mu}} \tag{C176}$$

$$\cdots e^{+i\sum_{\alpha}^{n}\sum_{\mu}^{P}\left(v_0^{\alpha,\mu} - R\|\vec{v}^{\alpha,\mu}\|\right)\hat{h}^{\alpha,\mu} + i\sum_{\alpha}^{n} c\sum_{\mu}^{P}(s^{\alpha,\mu})^2\hat{l}^{\alpha} - \frac{(D+1)P}{2}\log\det q} \tag{C177}$$

$$= \left(\int d^n \bar{s}^{\alpha} \int d^{n\times D}\vec{v}_l^{\alpha} \int_{1-s^{\alpha}}^{\infty} d^n h^{\alpha} \int \frac{d^n\hat{h}^{\alpha}}{2\pi} e^{F}\right)^{P} \tag{C178}$$

$$F \doteq -i\sum_{\alpha}^{n} h^{\alpha}\hat{h}^{\alpha} - \frac{1}{2}\sum_{l=0}^{D}\sum_{\alpha,\beta}^{n} q_{\alpha\beta}^{-1} v_l^{\alpha} v_l^{\beta} + i\sum_{\alpha}^{n}\left(v_0^{\alpha} - R\|\vec{v}^{\alpha}\|\right)\hat{h}^{\alpha} + i\sum_{\alpha}^{n} c\,(s^{\alpha})^2\,\hat{l}^{\alpha} - \frac{D+1}{2}\log\det q \tag{C179}$$

note that replacing $v_0^{\alpha} = h^{\alpha,\mu} + R\|\vec{v}^{\alpha}\|$ we can write:

$$I \doteq \int d^n \vec{v}_0^{\alpha} \int_{1-s^{\alpha}}^{\infty} d^n h^{\alpha} \int \frac{d^n\hat{h}^{\alpha}}{2\pi} e^{-i\sum_{\alpha}^{n} h^{\alpha}\hat{h}^{\alpha} + i\sum_{\alpha}^{n}(v_0^{\alpha} - R\|\vec{v}^{\alpha}\|)\hat{h}^{\alpha} - \frac{1}{2}\sum_{\alpha,\beta}^{n} q_{\alpha\beta}^{-1} v_0^{\alpha} v_0^{\beta}} \tag{C180}$$

$$= \int_{1-s^{\alpha}+R\|\vec{v}^{\alpha}\|}^{\infty} d^n v_0^{\alpha} e^{-\frac{1}{2}\sum_{\alpha,\beta}^{n} q_{\alpha\beta}^{-1} v_0^{\alpha} v_0^{\beta}} \tag{C181}$$

so that we have:

$$[V^n]_x = \int d^{n\times n} q_{\alpha\beta} \int \frac{d^{n\times n}\hat{q}_{\alpha\beta}}{2\pi} \int \frac{d^n\hat{l}^{\alpha}}{\sqrt{2\pi}} e^{-nNG_0 - nNG_1} \tag{C182}$$

$$G_0 = \frac{i}{n}\sum_{\alpha,\beta}^{n} q_{\alpha\beta}\hat{q}_{\alpha\beta} + \frac{1}{2n}\log\det\left(-2i\hat{q}_{\alpha\beta} - \delta_{\alpha\beta}2i\hat{l}^{\alpha}\right) + \frac{i}{n}\sum_{\alpha}^{n} L\hat{l}^{\alpha} \tag{C183}$$

$$G_1 = \frac{\alpha}{2n}(D+1)\log\det q - \frac{\alpha}{n}\log\int \frac{d^n\bar{s}^{\alpha}}{\sqrt{2\pi}} \int d^{n\times D}\vec{v}_l^{\alpha} \int_{1-s^{\alpha}+R\|\vec{v}^{\alpha}\|}^{\infty} \frac{d^n v_0^{\alpha}}{\sqrt{2\pi}} e^{-\frac{1}{2}\sum_{\alpha,\beta}^{n} q_{\alpha\beta}^{-1} v_0^{\alpha} v_0^{\beta} - \frac{1}{2}\sum_{l}^{D}\sum_{\alpha,\beta}^{n} q_{\alpha\beta}^{-1} v_l^{\alpha} v_l^{\beta} + i\sum_{\alpha}^{n} c(s^{\alpha})^2\hat{l}^{\alpha}} \tag{C184}$$

Assuming replica symmetry:

$$q_{\alpha\beta} = q + (q_0 - q)\delta_{\alpha\beta} \tag{C185}$$

$$\hat{q}_{\alpha\beta} = \hat{q} + (\hat{q}_0 - \hat{q})\delta_{\alpha\beta} \tag{C186}$$

$$\hat{l}^{\alpha} = \hat{l} \tag{C187}$$

we have:

$$\frac{1}{n}\sum_{\alpha,\beta}^{n} q_{\alpha\beta}\hat{q}_{\alpha\beta} \approx \hat{q}_0 q_0 - \hat{q}q \tag{C188}$$

$$\log\det\left[q\right] \approx n\log\left(q_0-q\right) + n\frac{q}{q_0-q} \tag{C189}$$

$$\log\det\left|-2i\hat{q}-2i\hat{l}\right| \approx n\log\left(-2i\hat{l}-2i\hat{q}_0+2i\hat{q}\right) + n\frac{-2i\hat{q}}{-2i\hat{l}-2i\hat{q}_0+2i\hat{q}} \tag{C190}$$

$$q^{-1}_{\alpha\beta} \approx \frac{1}{\left(q_0-q\right)}\delta_{\alpha\beta} - \frac{q}{\left(q_0-q\right)^2} \tag{C191}$$

so that after changing $-i\hat{l}\to\hat{l}$,$-i\hat{q}\to\hat{q}$,$-i\hat{q}_0\to\hat{q}_0$ we get:

$$\left[V^n\right]_x = \int dq\int dq_0\int d\hat{q}\int d\hat{q}_0\int\frac{d\hat{l}}{\sqrt{2\pi}}e^{-nNG_0-nNG_1} \tag{C192}$$

$$G_0 = -\left[\hat{q}_0 q_0-\hat{q}q\right] + \frac{1}{2}\left[\log\left(2\hat{l}+2\hat{q}_0-2\hat{q}\right)+\frac{2\hat{q}}{2\hat{l}+2\hat{q}_0-2\hat{q}}\right] - L\hat{l} \tag{C193}$$

$$G_1 = \frac{\alpha\left(D+1\right)}{2}\left[\log\left(q_0-q\right)+\frac{q}{q_0-q}\right] \tag{C194}$$

$$\cdots - \frac{\alpha}{n}\log\int\frac{d^n\vec{s}^{\alpha}}{\sqrt{2\pi}}\int d^{n\times D}\vec{v}^{\alpha}_l e^{-\frac{1}{2}\frac{1}{q_0-q}\sum_l^D\sum_\alpha^n(v_l^\alpha)^2+\frac{1}{2}\frac{q}{(q_0-q)^2}\sum_l^D\left(\sum_\alpha^n v_l^\alpha\right)^2-c\sum_\alpha^n(s^\alpha)^2\hat{l}}\times \tag{C195}$$

$$\cdots\times\int_{1-s^\alpha+R\|\vec{v}^\alpha\|}^{\infty}\frac{d^n v_0^\alpha}{\sqrt{2\pi}}e^{-\frac{1}{2}\frac{1}{q_0-q}\sum_\alpha^n(v_0^\alpha)^2+\frac{1}{2}\frac{q}{(q_0-q)^2}\left(\sum_\alpha^n v_0^\alpha\right)^2} \tag{C196}$$

Assuming the behavior in the thermodynamic limit $N\to\infty$ is dominated by the maximum of the integral, we calculate the derivatives of G_0:

$$0 = \frac{\partial G_0}{\partial\hat{q}} = q+\frac{1}{2}\left[-\frac{1}{\hat{l}+\hat{q}_0-\hat{q}}+\frac{\left(\hat{l}+\hat{q}_0-\hat{q}\right)+\hat{q}}{\left(\hat{l}+\hat{q}_0-\hat{q}\right)^2}\right] \tag{C197}$$

$$0 = \frac{\partial G_0}{\partial\hat{q}_0} = -q_0+\frac{1}{2}\left[\frac{1}{\hat{l}+\hat{q}_0-\hat{q}}-\frac{\hat{q}}{\left(\hat{l}+\hat{q}_0-\hat{q}\right)^2}\right] \tag{C198}$$

so that:

$$q = -\frac{1}{2}\frac{\hat{q}}{\left(\hat{l}+\hat{q}_0-\hat{q}\right)^2} \tag{C199}$$

$$q_0 = \frac{1}{2}\frac{1}{\hat{l}+\hat{q}_0-\hat{q}}+q \tag{C200}$$

$$q_0-q = \frac{1}{2}\frac{1}{\hat{l}+\hat{q}_0-\hat{q}} \tag{C201}$$

$$\frac{q}{\left(q_0-q\right)^2} = -\frac{1}{2}\frac{\hat{q}}{\left(\hat{l}+\hat{q}_0-\hat{q}\right)^2}\Big/\frac{1}{4}\frac{1}{\left(\hat{l}+\hat{q}_0-\hat{q}\right)^2} = -2\hat{q} \tag{C202}$$

$$q_0\hat{q}_0-q\hat{q} = \frac{1}{2}\frac{\hat{q}_0}{\hat{l}+\hat{q}_0-\hat{q}}-\frac{1}{2}\frac{\hat{q}\hat{q}_0}{\left(\hat{l}+\hat{q}_0-\hat{q}\right)^2}+\frac{1}{2}\frac{\hat{q}\hat{q}}{\left(\hat{l}+\hat{q}_0-\hat{q}\right)^2} = \frac{1}{2}-\hat{l}q_0 \tag{C203}$$

and G_0 becomes:

$$G_0 = -\left[\frac{1}{2} - \hat{l}\,(q_0 - q) - q\hat{l}\right] + \frac{1}{2}\left[\log\left(\frac{1}{q_0 - q}\right) - (q_0 - q)\,\frac{q}{(q_0 - q)^2}\right] - L\hat{l} \tag{C204}$$

$$= -\frac{1}{2} + (q_0 - L)\,\hat{l} - \frac{1}{2}\log(q_0 - q) - \frac{1}{2}\frac{q}{q_0 - q} \tag{C205}$$

For G_1 we have:

$$G_1 = \frac{\alpha\,(D+1)}{2}\log(q_0 - q) + \frac{\alpha\,(D+1)}{2}\frac{q}{q_0 - q} \tag{C206}$$

$$\cdots - \frac{\alpha}{n}\log\int\frac{d^n\vec{s}^{\alpha}}{\sqrt{2\pi}}\int\frac{d^{n\times D}\vec{v}_l^{\alpha}}{\sqrt{2\pi}}e^{-\frac{1}{2}\frac{1}{q_0-q}\sum_l^D\sum_\alpha^n(v_l^\alpha)^2+\frac{1}{2}\frac{q}{(q_0-q)^2}\sum_l^D\left(\sum_\alpha^n v_l^\alpha\right)^2-c\sum_\alpha^n(s^\alpha)^2\hat{l}}\times \tag{C207}$$

$$\cdots\times\int_{1-s^\alpha+R\|\vec{v}^\alpha\|}^{\infty}\frac{d^n v_0^\alpha}{\sqrt{2\pi}}e^{-\frac{1}{2}\frac{1}{q_0-q}\sum_\alpha^n(v_0^\alpha)^2+\frac{1}{2}\frac{q}{(q_0-q)^2}\left(\sum_\alpha^n v_0^\alpha\right)^2} \tag{C208}$$

and using the Hubbard-Stratonovich transform $e^{ay^2/2} = \int\frac{dt}{\sqrt{2\pi}}e^{-t^2/2+\sqrt{a}yt}$ for $l = 0..D$:

$$e^{\frac{1}{2}\frac{q}{(q_0-q)^2}\left(\sum_\alpha^n v_l^\alpha\right)^2} = \int Dt_l e^{t\frac{\sqrt{q}}{q_0-q}\sum_\alpha^n v_l^\alpha} \tag{C209}$$

so that G_1 decouples into n terms:

$$G_1 = \frac{\alpha\,(D+1)}{2}\log(q_0 - q) + \frac{\alpha\,(D+1)}{2}\frac{q}{q_0 - q} \tag{C210}$$

$$\cdots - \frac{\alpha}{n}\log\int\frac{d^n\vec{s}^{\alpha}}{\sqrt{2\pi}}\int\frac{d^{n\times D}\vec{v}_l^{\alpha}}{\sqrt{2\pi}}\int D^D\vec{t}\,e^{-\frac{1}{2}\frac{1}{q_0-q}\sum_l^D\sum_\alpha^n(v_l^\alpha)^2+t_l\frac{\sqrt{q}}{q_0-q}\sum_\alpha^n v_l^\alpha-c\sum_\alpha^n(s^\alpha)^2\hat{l}}\times \tag{C211}$$

$$\cdots\times\int_{1-s^\alpha+R\|\vec{v}^\alpha\|}^{\infty}\frac{d^n v_0^\alpha}{\sqrt{2\pi}}\int Dt_0 e^{-\frac{1}{2}\frac{1}{q_0-q}\sum_\alpha^n(v_0^\alpha)^2+t_0\frac{\sqrt{q}}{q_0-q}\sum_\alpha^n v_0^\alpha} \tag{C212}$$

$$= \frac{\alpha\,(D+1)}{2}\log(q_0 - q) + \frac{\alpha\,(D+1)}{2}\frac{q}{q_0 - q} - \frac{\alpha}{n}\log\int D^D\vec{t}\int Dt_0\times \tag{C213}$$

$$\cdots\times\left(\int\frac{ds}{\sqrt{2\pi}}\int\frac{d^D\vec{v}_l}{\sqrt{2\pi}}e^{-\frac{1}{2}\frac{1}{q_0-q}\sum_l^D(v_l)^2+t_l\frac{\sqrt{q}}{q_0-q}v_l-Cs^2\hat{l}}\int_{1-s+R\|\vec{v}\|}^{\infty}\frac{dv_0}{\sqrt{2\pi}}e^{-\frac{1}{2}\frac{1}{q_0-q}v_0^2+t_0\frac{\sqrt{q}}{q_0-q}v_0}\right)^n \tag{C214}$$

and using the replica identity $\log\int Dt\,z(t)^n \approx \log\left[1 + n\int Dt\log z(t)\right] \approx n\int Dt\log z(t)$ for $n\to 0$:

$$G_1 = \frac{\alpha\,(D+1)}{2}\log(q_0 - q) + \frac{\alpha\,(D+1)}{2}\frac{q}{q_0 - q} \tag{C215}$$

$$\cdots - \alpha\int D^D\vec{t}\int Dt_0\log\int\frac{d^D\vec{v}_l}{\sqrt{2\pi}}e^{-\frac{1}{2}\frac{1}{q_0-q}\sum_l^D(v_l)^2+t_l\frac{\sqrt{q}}{q_0-q}v_l}\int\frac{ds}{\sqrt{2\pi}}\int_{1-s+R\|\vec{v}\|}^{\infty}\frac{dv_0}{\sqrt{2\pi}}e^{-\frac{1}{2}\frac{1}{q_0-q}v_0^2+t_0\frac{\sqrt{q}}{q_0-q}v_0-Cs^2\hat{l}} \tag{C216}$$

by changing $v_0 \to v_0 - s$ and integrating over s using $\int\frac{dx}{\sqrt{2\pi}}e^{-x^2/2a+bx} = e^{\frac{1}{2}\log a+\frac{1}{2}b^2 a}$:

$$I \doteq \int \frac{ds}{\sqrt{2\pi}} \int_{1-s+R\|\vec{v}\|}^{\infty} \frac{dv_0}{\sqrt{2\pi}} e^{-\frac{1}{2}\frac{1}{q_0-q}v_0^2 + t_0\frac{\sqrt{q}}{q_0-q}v_0 - Cs^2\hat{l}} \tag{C217}$$

$$= \int \frac{ds}{\sqrt{2\pi}} \int_{1+R\|\vec{v}\|}^{\infty} \frac{dv_0}{\sqrt{2\pi}} e^{-\frac{1}{2}\frac{1}{q_0-q}(v_0-s)^2 + t\frac{\sqrt{q}}{q_0-q}(v_0-s) - Cs^2\hat{l}} \tag{C218}$$

$$= \int_{1+R\|\vec{v}\|}^{\infty} \frac{dv_0}{\sqrt{2\pi}} e^{-\frac{1}{2}\frac{1}{q_0-q}v_0^2 + t\frac{\sqrt{q}}{q_0-q}v_0} \int \frac{ds}{\sqrt{2\pi}} e^{-\frac{1}{2}\left(\frac{1}{q_0-q}+2C\hat{l}\right)s^2 + \frac{1}{q_0-q}\left(v_0 - t\sqrt{q}\right)s} \tag{C219}$$

$$= \int_{1+R\|\vec{v}\|}^{\infty} \frac{dv_0}{\sqrt{2\pi}} e^{-\frac{1}{2}\frac{1}{q_0-q}v_0^2 + t\frac{\sqrt{q}}{q_0-q}v_0 + \frac{1}{2}\log\frac{q_0-q}{1+2C\hat{l}(q_0-q)} + \frac{1}{2}\frac{q_0-q}{1+2C\hat{l}(q_0-q)}\left(\frac{v_0-t\sqrt{q}}{q_0-q}\right)^2} \tag{C220}$$

and by completion to square:

$$\int \frac{dv_0}{\sqrt{2\pi}} e^{-\frac{1}{2}\frac{1}{q_0-q}v_0^2 + t_0\frac{\sqrt{q}}{q_0-q}v_0 + \frac{1}{2}\log\frac{q_0-q}{1+2C\hat{l}(q_0-q)} + \frac{1}{2}\frac{(v_0-t_0\sqrt{q})^2}{1+2C\hat{l}(q_0-q)}} = \int \frac{dv_0}{\sqrt{2\pi}} e^{\frac{1}{2}\frac{qt_0^2}{q_0-q} - \frac{1}{2}\frac{(v_0-t_0\sqrt{q})^2 2C\hat{l}}{1+2C\hat{l}(q_0-q)} - \frac{1}{2}\log\frac{1+2C\hat{l}(q_0-q)}{q_0-q}} \tag{C221}$$

$$\int \frac{d^D\vec{v}_l}{\sqrt{2\pi}} e^{-\frac{1}{2}\frac{1}{q_0-q}\sum_l^D v_l^2 + t_l\frac{\sqrt{q}}{q_0-q}v_l} = \int \frac{d^D\vec{v}_l}{\sqrt{2\pi}} e^{-\frac{1}{2}\frac{1}{q_0-q}\|\vec{v}-\sqrt{q}\vec{t}\|^2 + \frac{1}{2}\frac{1}{q_0-q}q\|\vec{t}\|^2} \tag{C222}$$

so that by inserting the $\log(q_0-q)$ into the integral and taking out the term which depends only on $\vec{t}, t_0$:

$$G_1 = \frac{\alpha(D+1)}{2}\log(q_0-q) + \frac{\alpha(D+1)}{2}\frac{q}{q_0-q} \tag{C223}$$

$$\cdots - \alpha \int D^D\vec{t} \int Dt_0 \log \int \frac{d^D\vec{v}_l}{\sqrt{2\pi}} e^{-\frac{1}{2}\frac{1}{q_0-q}\|\vec{v}-\sqrt{q}\vec{t}\|^2 + \frac{1}{2}\frac{1}{q_0-q}q\|\vec{t}\|^2} \times \tag{C224}$$

$$\cdots \int_{1+R\|\vec{v}\|}^{\infty} \frac{dv_0}{\sqrt{2\pi}} e^{\frac{1}{2}\frac{qt_0^2}{q_0-q} - \frac{1}{2}\frac{(v_0-t_0\sqrt{q})^2 2C\hat{l}}{1+2C\hat{l}(q_0-q)} - \frac{1}{2}\log\frac{1+2C\hat{l}(q_0-q)}{q_0-q}} \tag{C225}$$

$$= \frac{\alpha(D+1)}{2}\frac{q}{q_0-q} - \alpha\left[\frac{1}{2}\frac{q}{q_0-q}D + \frac{1}{2}\frac{q}{q_0-q}\right] - \alpha \int D^D\vec{t} \int Dt_0 \log \int \frac{d^D\vec{v}_l}{\sqrt{2\pi(q_0-q)}} e^{-\frac{1}{2}\frac{1}{q_0-q}\|\vec{v}-\sqrt{q}\vec{t}\|^2} \times \tag{C226}$$

$$\cdots \int_{1+R\|\vec{v}\|}^{\infty} \frac{dv_0}{\sqrt{2\pi}} e^{-\frac{1}{2}\frac{(v_0-t_0\sqrt{q})^2 2C\hat{l}}{1+2C\hat{l}(q_0-q)} - \frac{1}{2}\log(q_0-q) - \frac{1}{2}\log\frac{1+2C\hat{l}(q_0-q)}{q_0-q}} \tag{C227}$$

$$= -\alpha \int D^D\vec{t} \int Dt_0 \log \int \frac{d^D\vec{v}_l}{\sqrt{2\pi(q_0-q)}} \int_{1+R\|\vec{v}\|}^{\infty} \frac{dv_0}{\sqrt{2\pi}} e^{-\frac{1}{2}\frac{1}{q_0-q}\|\vec{v}-\sqrt{q}\vec{t}\|^2 - \frac{1}{2}\frac{(v_0-t_0\sqrt{q})^2 2C\hat{l}}{1+2C\hat{l}(q_0-q)} - \frac{1}{2}\log\left(1+2C\hat{l}(q_0-q)\right)} \tag{C228}$$

and by a change of variable $v_l = v_l\sqrt{q}$ for $l = 0..D$:

$$G_1 = -\alpha \int D^D\vec{t} \int Dt_0 \log \int \frac{d^D\vec{v}_l\sqrt{q}}{\sqrt{2\pi(q_0-q)}} \int_{1/\sqrt{q}+R\|\vec{v}\|}^{\infty} \frac{dv_0\sqrt{q}}{\sqrt{2\pi}} e^{-\frac{1}{2}\frac{1}{q_0-q}\|\sqrt{q}\vec{v}-\sqrt{q}\vec{t}\|^2 - \frac{1}{2}\frac{(\sqrt{q}v_0-\sqrt{q}t_0)^2 2C\hat{l}}{1+2C\hat{l}(q_0-q)} - \frac{1}{2}\log\left(1+2C\hat{l}(q_0-q)\right)} \tag{C229}$$

$$= -\alpha \int D^D\vec{t} \int Dt_0 \log \int \frac{d^D\vec{v}_l}{\sqrt{2\pi}} \int_{1/\sqrt{q}+R\|\vec{v}\|}^{\infty} \frac{dv_0}{\sqrt{2\pi}} e^{-\frac{1}{2}\frac{q}{q_0-q}\|\vec{v}-\vec{t}\|^2 - \frac{1}{2}\frac{(v_0-t_0)^2 2C\hat{l}q}{1+2C\hat{l}(q_0-q)} - \frac{1}{2}\log\left(1+2C\hat{l}(q_0-q)\right)/q - \frac{D}{2}\log(q_0-q)/q} \tag{C230}$$

Thus we conclude:

$$[V^n]_x = \int dq \int dq_0 \int d\hat{q} \int d\hat{q}_0 \int \frac{d\hat{l}}{\sqrt{2\pi}} e^{-nNG_0 - nNG_1} \tag{C231}$$

$$G_0 = -\frac{1}{2} + (q_0 - L)\,\hat{l} - \frac{1}{2}\log(q_0 - q) - \frac{1}{2}\frac{q}{q_0 - q} \tag{C232}$$

$$G_1 = -\alpha \int D^D\vec{t} \int Dt_0 \log \int \frac{d^D\vec{v}_l}{\sqrt{2\pi}} \int_{1/\sqrt{q}+R\|\vec{v}\|}^{\infty} \frac{dv_0}{\sqrt{2\pi}} e^{-\frac{1}{2}\frac{q}{q_0-q}\|\vec{v}-\vec{t}\|^2 - \frac{1}{2}\frac{(v_0-t_0)^2 2C\hat{l}q}{1+2C\hat{l}(q_0-q)} - \frac{1}{2}\log\left(1+2C\hat{l}(q_0-q)\right)/q - \frac{D}{2}\log(q_0-q)} \tag{C233}$$

Now we rename $\hat{l} = \hat{l}_0/(q_0 - q)$ and take the limit $q \to q_0$:

$$\lim_{q\to q_0}(q_0 - q)\,G_0 = (q_0 - L)\,\hat{l}_0 - \frac{1}{2}q_0 \tag{C234}$$

$$F \doteq -\frac{1}{2}\frac{q}{q_0 - q}\|\vec{v} - \vec{t}\|^2 - \frac{1}{2}\frac{(v_0 - t_0)^2 2C\hat{l}_0 q}{\left(1 + 2C\hat{l}_0\right)(q_0 - q)} - \frac{1}{2}\log\left(1 + 2C\hat{l}_0\right)/q - \frac{D}{2}\log(q_0 - q) \tag{C235}$$

$$\lim_{q\to q_0}(q_0 - q)\,G_1 = -\alpha \lim_{q\to q_0}(q_0 - q) \int D^D\vec{t} \int Dt_0 \log \int \frac{d^D\vec{v}_l}{\sqrt{2\pi}} \int_{1/\sqrt{q}+R\|\vec{v}\|}^{\infty} \frac{dv_0}{\sqrt{2\pi}} e^F \tag{C236}$$

$$= -\alpha \int D^D\vec{t} \int Dt_0 \lim_{q\to q_0}(q_0 - q) \log \max_{v_0 \geq 1/\sqrt{q}+R\|\vec{v}\|} e^F \tag{C237}$$

$$= -\alpha \int D^D\vec{t} \int Dt_0 \lim_{q\to q_0}(q_0 - q) \max_{v_0 \geq 1/\sqrt{q}+R\|\vec{v}\|} F \tag{C238}$$

$$= \frac{\alpha q_0}{2} \int D^D\vec{t} \int Dt_0 \min_{v_0 \geq 1/\sqrt{q}+R\|\vec{v}\|} \left\{ \|\vec{v} - \vec{t}\|^2 + \frac{2C\hat{l}_0}{\left(1 + 2C\hat{l}_0\right)}(v_0 - t_0)^2 \right\} \tag{C239}$$

So combined into $G = G_1 + G_2$:

$$\lim_{q\to q_0}(q_0 - q)\,G = (q - L)\,\hat{l}_0 - \frac{1}{2}q + \frac{\alpha q}{2} \int D^D\vec{t} \int Dt_0 \min_{v_0 \geq 1/\sqrt{q}+R\|\vec{v}\|} \left\{ \|\vec{v} - \vec{t}\|^2 + \frac{2C\hat{l}_0}{\left(1 + 2C\hat{l}_0\right)}(v_0 - t_0)^2 \right\} \tag{C240}$$

Thus we have from $\lim_{q\to q_0}(q_0 - q)\,G = 0$:

$$1 = (1 - L/q)\,2\hat{l}_0 + \alpha \int D^D\vec{t} \int Dt_0 \min_{v_0 \geq 1/\sqrt{q}+R\|\vec{v}\|} \left\{ \|\vec{v} - \vec{t}\|^2 + \frac{2C\hat{l}_0}{\left(1 + 2C\hat{l}_0\right)}(v_0 - t_0)^2 \right\} \tag{C241}$$

and denoting $k = 2\hat{l}_0$:

$$L = q + \frac{q\alpha}{k} \int D^D\vec{t} \int Dt_0 \min_{v_0 \geq 1/\sqrt{q}+R\|\vec{v}\|} \left\{ \|\vec{v} - \vec{t}\|^2 + \frac{ck}{1 + ck}(v_0 - t_0)^2 \right\} - \frac{q}{k} \tag{C242}$$

8. Solving the mean-field minimization problem for spheres

Let us solve the following problem, so that we can write for it a closed form expression:

$$F\left(\vec{t}, t_0; ck, q\right) = \min_{v_0 \geq 1/\sqrt{q}+R\|\vec{v}\|} \left\{ \|\vec{v} - \vec{t}\|^2 + \frac{ck}{1 + ck}(v_0 - t_0)^2 \right\} \tag{C243}$$

$$\mathcal{L} = \frac{1}{2}\|\vec{v} - \vec{t}\|^2 + \frac{1}{2}\frac{ck}{1 + ck}(v_0 - t_0)^2 + \lambda\left(1/\sqrt{q} + R\|\vec{v}\| - v_0\right) \tag{C244}$$

From KKT conditions by taking derivatives we have the equations:

$$0 = \frac{\partial L}{\partial v_0} = \frac{ck}{1+ck}(v_0 - t_0) - \lambda \tag{C245}$$
$$0 = \frac{\partial L}{\partial v_l} = (v_l - t_l) + \frac{\lambda R 2 v_l}{2\|\vec{v}\|} \tag{C246}$$
$$0 = \lambda\left(1/\sqrt{q} + R\|\vec{v}\| - v_0\right) \tag{C247}$$

so that denoting $v = \|\vec{v}\| \geq 0$ and $t = \|\vec{t}\|$ the constraints are:

$$\lambda = \frac{ck}{1+ck}(v_0 - t_0) \tag{C248}$$
$$t_l = \frac{v + \lambda R}{v} v_l \tag{C249}$$
$$0 = \lambda\left(1/\sqrt{q} + Rv - v_0\right) \tag{C250}$$
$$v \geq 0 \tag{C251}$$

We solve for different regimes:

1. "Interior" regime defined by $\lambda = 0$:

$$v_0 = t_0 \tag{C252}$$
$$v_l = t_l \tag{C253}$$
$$v_0 \geq 1/\sqrt{q} + Rv \tag{C254}$$
$$t_0 \geq 1/\sqrt{q} + Rt \tag{C255}$$
$$F = 0 \tag{C256}$$

2. "Embedded" regime defined by $\lambda > 0$ and $v = 0$:

$$v_0 = 1/\sqrt{q} \tag{C257}$$
$$F = \frac{ck}{1+ck}\left(1/\sqrt{q} - t_0\right)^2 + t^2 \tag{C258}$$

3. "Touching" regime defined by $\lambda > 0$ and $v > 0$:

$$v_0 = 1/\sqrt{q} + Rv \tag{C259}$$
$$v_l = \frac{v}{v + \lambda R} t_l \tag{C260}$$
$$\|\vec{v} - \vec{t}\|^2 = \left(\frac{-\lambda R}{v + \lambda R}\right)^2 t^2 \tag{C261}$$
$$t - \lambda R = v = \frac{v}{v + \lambda R} t \tag{C262}$$
$$v_0 = 1/\sqrt{q} + \frac{\left(t_0 - 1/\sqrt{q}\right) R^2 + \frac{1+ck}{ck} tR}{\frac{1+ck}{ck} + R^2} \tag{C263}$$
$$t_0 \leq 1/\sqrt{q} + Rt \tag{C264}$$
$$t_0 \geq 1/\sqrt{q} - \frac{1+ck}{ck} t/R \tag{C265}$$
$$F = \frac{\left(1/\sqrt{q} + Rt - t_0\right)^2}{\frac{1+ck}{ck} + R^2} \tag{C266}$$

so that we got that the minimization problem depends only on t_0 and the norm $t = \|\vec{t}\|$:

$$F\left(t_0, t\right) = \begin{cases} \frac{ck}{1+ck}\left(1/\sqrt{q} - t_0\right)^2 + t^2 & -\infty < t_0 \leq 1/\sqrt{q} - \frac{1+ck}{ck}t/R \\ \frac{ck}{1+ck(1+R^2)}\left(1/\sqrt{q} + Rt - t_0\right)^2 & 1/\sqrt{q} - \frac{1+ck}{ck}t/R \leq t_0 \leq 1/\sqrt{q} + Rt \\ 0 & 1/\sqrt{q} + Rt \leq t_0 \leq \infty \end{cases} \tag{C267}$$

As $t \sim \chi_D$ the Chi distribution with D degrees of freedom, denoting $\chi_D\left(t\right) = \Gamma\left(D/2\right)^{-1} 2^{1-D/2} t^{D-1} e^{-t^2/2} dt$:

$$f\left(R, D, ck, q\right) = \int \chi_D\left(t\right) \int_{-\infty}^{1/\sqrt{q} - \frac{1+ck}{ck}t/R} Dt_0 \left[\frac{ck}{1+ck}\left(1/\sqrt{q} - t_0\right)^2 + t^2\right] \cdots \tag{C268}$$

$$+ \int \chi_D\left(t\right) \int_{1/\sqrt{q} - \frac{1+ck}{ck}t/R}^{1/\sqrt{q}+Rt} Dt_0 \frac{ck}{1+ck+ckR^2}\left(1/\sqrt{q} + Rt - t_0\right)^2 \tag{C269}$$

For $R = 0$ we recover the result for soft classification of points $f = \frac{ck}{1+ck}\alpha_0^{-1}\left(1/\sqrt{q}\right)$ and for $c \to \infty$ we recover the expression for max-margin classifiers [6], denoting $\kappa = 1/\sqrt{q}$:

$$\alpha\left(\kappa\right)^{-1} = \int \chi_D(t) \int_{-\infty}^{\kappa - tR^{-1}} Dt_0 \left[\left(\kappa - t_0\right)^2 + t^2\right] + \int_{\kappa - tR^{-1}}^{\kappa + Rt} Dt_0 \frac{\left(\kappa - t_0 + Rt\right)^2}{1+R^2} \tag{C270}$$

9. Self-consistent equations for spheres

Assuming the optimal loss satisfies the saddle-point equations $0 = \frac{\partial L}{\partial k} = \frac{\partial L}{\partial q}$ we have:

$$1 = \alpha f - \alpha k \frac{\partial}{\partial k} f \tag{C271}$$

$$1 - k = \alpha f + \alpha q \frac{\partial}{\partial q} f \tag{C272}$$

Taking the derivatives of f with respect to k, q we have that:

$$\frac{\partial}{\partial k} f = \frac{c}{\left(1+ck\right)^2} \int \chi_D\left(t\right) \int_{-\infty}^{1/\sqrt{q} - \frac{1+ck}{ck}t/R} Dt_0 \left(1/\sqrt{q} - t_0\right)^2 \tag{C273}$$

$$+ \frac{c}{\left(1+ck\left(1+R^2\right)\right)^2} \int \chi_D\left(t\right) \int_{1/\sqrt{q} - \frac{1+ck}{ck}t/R}^{1/\sqrt{q}+Rt} Dt_0 \left(1/\sqrt{q} + Rt - t_0\right)^2 \tag{C274}$$

$$\frac{\partial}{\partial q} f = -q^{-3/2} \frac{ck}{1+ck} \int \chi_D\left(t\right) \int_{-\infty}^{1/\sqrt{q} - \frac{1+ck}{ck}t/R} Dt_0 \left(1/\sqrt{q} - t_0\right) \tag{C275}$$

$$- q^{-3/2} \frac{ck}{1+ck\left(1+R^2\right)} \int \chi_D\left(t\right) \int_{1/\sqrt{q} - \frac{1+ck}{ck}t/R}^{1/\sqrt{q}+Rt} Dt_0 \left(1/\sqrt{q} + Rt - t_0\right) \tag{C276}$$

so the self-consistent equations:

$$1 = \alpha \frac{(ck)^2 \left(1+R^2\right)}{\left(1+ck\left(1+R^2\right)\right)^2} \int \chi_D(t) \int_{1/\sqrt{q}-\frac{1+ck}{ck}t/R}^{1/\sqrt{q}+Rt} Dt_0 \left(1/\sqrt{q}+Rt-t_0\right)^2 \tag{C277}$$

$$+\alpha \int \chi_D(t) \int_{-\infty}^{1/\sqrt{q}-\frac{1+ck}{ck}t/R} Dt_0 \left[\frac{(ck)^2}{(1+ck)^2}\left(1/\sqrt{q}-t_0\right)^2 + t^2\right] \tag{C278}$$

$$1-k = \alpha \int \chi_D(t) \int_{1/\sqrt{q}-\frac{1+ck}{ck}t/R}^{1/\sqrt{q}+Rt} Dt_0 \frac{ck}{1+ck\left(1+R^2\right)} \left(1/\sqrt{q}+Rt-t_0\right)\left(Rt-t_0\right) \tag{C279}$$

$$+\alpha \int \chi_D(t) \int_{-\infty}^{1/\sqrt{q}-\frac{1+ck}{ck}t/R} Dt_0 \left[t^2 - \frac{ck}{1+ck}\left(1/\sqrt{q}-t_0\right)t_0\right] \tag{C280}$$

As for points, those equations can also be derived by combining the equations for the optimal loss, namely the loss definition, the mean-field equation 35, and an optimality condition for the loss (see details in section C 4):

$$L = q + \alpha c \left\langle s^2 \right\rangle \tag{C281}$$

$$L = q + \frac{q}{k}\left(\alpha f - 1\right) \tag{C282}$$

$$L = c\alpha \left\langle s \right\rangle \tag{C283}$$

where the slack moment equations C358-C360 can be written as:

$$\left\langle s^2 \right\rangle = \frac{q}{c}\frac{\partial}{\partial k} f \tag{C284}$$

$$\left\langle s \right\rangle = -\frac{q}{ck} q \frac{\partial}{\partial q} f \tag{C285}$$

which leads to the self-consistent equations C271,C272.

10. Interesting regimes of the self-consistent equations for spheres

The self-consistent equations C277-C279 can be simplified for several interesting cases.

In the limit $c \to \infty$ for $\alpha > \alpha_C^{Hard}$ the equations which can be derived by a replica theory from the Lagrangian:

$$L = \|\vec{s}\|^2/N \quad s.t.\ \forall \mu\ h_{min}^{\mu} \geq 1 - s^{\mu} \tag{C286}$$

the resulting equations are as follows, which are related to self-consistent equations from soft classification theory through $\lim_{c\to\infty} k = 0$ while $q, K = \lim_{c\to\infty} ck$ are finite:

$$1 = \alpha \frac{(K)^2 \left(1+R^2\right)}{\left(1+K\left(1+R^2\right)\right)^2} \int \chi_D(t) \int_{1/\sqrt{q}-\frac{1+K}{K}t/R}^{1/\sqrt{q}+Rt} Dt_0 \left(1/\sqrt{q}+Rt-t_0\right)^2 \tag{C287}$$

$$+\alpha \int \chi_D(t) \int_{-\infty}^{1/\sqrt{q}-\frac{1+K}{K}t/R} Dt_0 \left[\frac{(K)^2}{(1+K)^2}\left(1/\sqrt{q}-t_0\right)^2 + t^2\right] \tag{C288}$$

$$1 = \alpha \int \chi_D(t) \int_{1/\sqrt{q}-\frac{1+K}{K}t/R}^{1/\sqrt{q}+Rt} Dt_0 \frac{K}{1+K\left(1+R^2\right)} \left(1/\sqrt{q}+Rt-t_0\right)\left(Rt-t_0\right) \tag{C289}$$

$$+\alpha \int \chi_D(t) \int_{-\infty}^{1/\sqrt{q}-\frac{1+K}{K}t/R} Dt_0 \left[t^2 - \frac{K}{1+K}\left(1/\sqrt{q}-t_0\right)t_0\right] \tag{C290}$$

When $D \gg 1$ the distribution of χ_D is narrow with a mode at $\sqrt{D-1}$ and a mean just below $\sqrt{D}$, so we will assume $t = \sqrt{D}$ and $\alpha_C \approx \frac{1+R^2}{R^2 D}$ (equation 42). We consider several different cases:

1. For the case of "large D, small R" we assume $R\sqrt{D} = O(1)$ with $\sqrt{D}/R \gg 1$. In this case F is dominated by the contribution of the "touching" regime and $\frac{1+ck}{ck}\sqrt{D}/R - 1/\sqrt{q} \gg 1$, and the equations become:

$$1 = \frac{(ck)^2 \left(1+R^2\right)}{\left(1+ck+ckR^2\right)^2} \alpha \alpha_0^{-1} \left(1/\sqrt{q} + R\sqrt{D}\right) \tag{C291}$$

$$1-k = \alpha \int_{-\infty}^{1/\sqrt{q}+R\sqrt{D}} Dt_0 \frac{ck\left(1/\sqrt{q} + R\sqrt{D} - t_0\right)}{1+ck+ckR^2} \left(R\sqrt{D} - t_0\right) \tag{C292}$$

   In this case q, k are non-trivial functions of $R, \sqrt{D}, \alpha$.

2. For the case of "large D, regular R" we assume $R = O(1)$ with $R\sqrt{D} \gg 1$. Again the leading contribution comes from the "touching" regime, but this time leading to the following equations:

$$1 = \alpha \frac{(ck)^2 \left(1+R^2\right)}{\left(1+ck\left(1+R^2\right)\right)^2} \left(1/\sqrt{q} + R\sqrt{D}\right)^2 \tag{C293}$$

$$1-k = \alpha \frac{ckR\sqrt{D}}{1+ck\left(1+R^2\right)} \left(1/\sqrt{q} + R\sqrt{D}\right) \tag{C294}$$

   which are combined as (for α_C given by equation 42):

$$k \approx 1 - \sqrt{\alpha/\alpha_C} \tag{C295}$$

$$\sqrt{q} \approx \frac{1+R^2}{R\sqrt{D}} \frac{ck\sqrt{\alpha/\alpha_C}}{1+ck^2\left(1+R^2\right)} \tag{C296}$$

3. In the limit of $\alpha \to 0$ we expect to have $q \to 0$ and $k \to 1$, as in the case of soft classification of points, so that $1/\sqrt{q} - \frac{1+ck}{ck}\sqrt{D}/R \gg 1$ and $1/\sqrt{q} + R\sqrt{D} \gg 1$, and the self-consistent equations are simplified to:

$$1 = \alpha \left[D + \frac{(ck)^2}{(1+ck)^2}(1+1/q)\right] \tag{C297}$$

$$1-k = \alpha \left[D + \frac{ck}{1+ck}\right] \tag{C298}$$

   and the resulting first-order approximations for small α are:

$$k \approx 1 - \alpha(1+D) \tag{C299}$$

$$\sqrt{q} \approx \sqrt{\alpha} \frac{ck}{1+ck} \tag{C300}$$

4. On the other hand, for $\alpha \to \alpha_C^{Soft}$ we expect both $q \to 0$ and $k \to 0$, so that we need to assume $1/\sqrt{q} + R\sqrt{D} \gg 1$ and $\frac{1+ck}{ck}\sqrt{D}/R - 1/\sqrt{q} \gg 1$, leading to different simplified equations:

$$1 = \frac{\alpha(ck)^2\left(1+R^2\right)}{\left(1+ck\left(1+R^2\right)\right)^2} \left(1 + \left(1/\sqrt{q} + R\sqrt{D}\right)^2\right) \tag{C301}$$

$$1-k = \alpha \frac{ck}{1+ck\left(1+R^2\right)} \left(R\sqrt{D}/\sqrt{q} + R^2 D + 1\right) \tag{C302}$$

   so that the resulting order parameters k and q (for α_C given by equation 42):

$$k \approx \left(1 - \sqrt{\alpha/\alpha_C}\right)/(\alpha c + 1) \tag{C303}$$

$$\sqrt{q} \approx ck \frac{1+R^2}{R\sqrt{D}} \tag{C304}$$

11. Capacity in classification of spheres

We first note that equations C277 , C279 can be integrated over t_0 to yield the following self-consistent equations:

$$1=\alpha\int\chi_D\left(t\right)\left(t^2+\frac{\left(ck\right)^2}{\left(1+ck\right)^2}\left(1+1/q\right)\right)H(-1/\sqrt{q}+\frac{1+ck}{ck}t/R) \tag{C305}$$

$$+\alpha\int\chi_D\left(t\right)\frac{ck}{1+ck}\left(\frac{ck}{1+ck}1/\sqrt{q}-\frac{R^2}{1+ck\left(1+R^2\right)}t\right)\frac{1}{\sqrt{2\pi}}e^{-\left(1/\sqrt{q}-\frac{1+ck}{ck}t/R\right)^2/2} \tag{C306}$$

$$+\frac{\alpha\left(ck\right)^2\left(1+R^2\right)}{\left(1+ck\left(1+R^2\right)\right)^2}\int\chi_D\left(t\right)\left(1+\left(1/\sqrt{q}+Rt\right)^2\right)\left[H(-1/\sqrt{q}-Rt)-H(-1/\sqrt{q}+\frac{1+ck}{ck}t/R)\right] \tag{C307}$$

$$+\frac{\alpha\left(ck\right)^2\left(1+R^2\right)}{\left(1+ck\left(1+R^2\right)\right)^2}\int\chi_D\left(t\right)\left(1/\sqrt{q}+Rt\right)\left[\frac{1}{\sqrt{2\pi}}e^{-\left(1/\sqrt{q}+Rt\right)^2/2}-\frac{1}{\sqrt{2\pi}}e^{-\left(1/\sqrt{q}-\frac{1+ck}{ck}t/R\right)^2/2}\right] \tag{C308}$$

$$1-k=\alpha\int\chi_D\left(t\right)\left[t^2+\frac{ck}{1+ck}\right]H(-1/\sqrt{q}+\frac{1+ck}{ck}t/R) \tag{C309}$$

$$+\alpha\frac{ck}{1+ck\left(1+R^2\right)}\int\chi_D\left(t\right)Rt\left[\frac{1}{\sqrt{2\pi}}e^{-\left(1/\sqrt{q}+Rt\right)^2/2}-\frac{1}{\sqrt{2\pi}}e^{-\left(1/\sqrt{q}-\frac{1+ck}{ck}t/R\right)^2/2}\right] \tag{C310}$$

$$+\alpha\frac{ck}{1+ck\left(1+R^2\right)}\int\chi_D\left(t\right)\left(Rt/\sqrt{q}+R^2t^2+1\right)\left[H(-1/\sqrt{q}-Rt)-H(-1/\sqrt{q}+\frac{1+ck}{ck}t/R)\right] \tag{C311}$$

Now let us assume both $k,\sqrt{q}\ll1$ and further that $k=x\sqrt{q}$. For the first equation we have contributions only from the first term $\int_0^{xcR}\chi_D\left(t\right)\left(t^2+c^2x^2\right)$, and the third term $c^2x^2\left(1+R^2\right)\int_{xcR}^{\infty}\chi_D\left(t\right)$, leading to:

$$1=\alpha\int_0^{xcR}\chi_D\left(t\right)\left(t^2+c^2x^2\right)+\alpha c^2x^2\left(1+R^2\right)\int_{xcR}^{\infty}\chi_D\left(t\right) \tag{C312}$$

For the second equation we have contributions from the first term $\int_0^{xcR}\chi_D\left(t\right)t^2$ and the third term $xcR\int_{xcR}^{\infty}\chi_D\left(t\right)t$, leading to:

$$1=\alpha\int_0^{xcR}\chi_D\left(t\right)t^2+\alpha xcR\int_{xcR}^{\infty}\chi_D\left(t\right)t \tag{C313}$$

Combining those equations and replacing $xc\to x$ we have that $x=kc/\sqrt{q}$ and we get two equations which are independent of c, one for x and another for $\alpha=\alpha_C$:

$$x=\frac{R\int_{xR}^{\infty}\chi_D\left(t\right)t}{\left(1+R^2\int_{xR}^{\infty}\chi_D\left(t\right)\right)} \tag{C314}$$

$$\alpha_C^{-1}=\int_0^{xR}\chi_D\left(t\right)t^2+xR\int_{xR}^{\infty}\chi_D\left(t\right)t \tag{C315}$$

Now note that for $R\to0$ we have that $x=R\int_{xR}^{\infty}\chi_D\left(t\right)t=R\sqrt{2}\Gamma\left(\frac{D}{2}+\frac{1}{2}\right)/\Gamma\left(\frac{D}{2}\right)$ and $\alpha_C^{-1}=x^2$ (which converges to R^2D for large D), whereas for $R\to\infty$ we have $x\approx0$ and $\alpha_C^{-1}=D$.

When $D\gg1$ the distribution of χ_D is narrow around $\sqrt{D}$. If $\int_0^{xR}\chi_D\ll1$ we have a much simpler result; in this case $x\approx\frac{R\sqrt{D}}{1+R^2}$ and thus:

$$\alpha_C^{-1}=xR\sqrt{D}=\frac{R^2D}{1+R^2} \tag{C316}$$

and from the above limits on R we obtain that for large D this approximation is valid for any R.

12. Field and slack distribution for spheres

To derive the slack and field distribution we do not integrate away the slack variable in equation C215, and instead use the notation $k = 2l_0 = 2\hat{l}\,(q_0 - q)$:

$$G_1 = \frac{\alpha\,(D+1)}{2}\log(q_0-q) + \frac{\alpha\,(D+1)}{2}\frac{q}{q_0-q} - \alpha\int D^D\vec{t}\int Dt_0\log I \tag{C317}$$

$$I \doteq \int\frac{d^D\vec{v}_l}{\sqrt{2\pi}}e^{-\frac{1}{2}\frac{1}{q_0-q}\sum_l^D v_l^2 + t_l\frac{\sqrt{q}}{q_0-q}v_l}\int\frac{ds}{\sqrt{2\pi}}\int_{1-s+R\|\vec{v}\|}^{\infty}\frac{dv_0}{\sqrt{2\pi}}e^{-\frac{1}{2}\frac{1}{q_0-q}v_0^2 + t_0\frac{\sqrt{q}}{q_0-q}v_0 - Cs^2\hat{l}} \tag{C318}$$

$$= \int\frac{d^D\vec{v}_l}{\sqrt{2\pi}}e^{-\frac{1}{2}\frac{1}{q_0-q}\left(\vec{v}-\sqrt{q}\vec{t}\right)^2 + \frac{1}{2}\frac{q\|\vec{t}\|^2}{q_0-q}}\int\frac{ds}{\sqrt{2\pi}}\int_{1-s+R\|\vec{v}\|}^{\infty}\frac{dv_0}{\sqrt{2\pi}}e^{-\frac{1}{2}\frac{1}{q_0-q}\left(v_0-\sqrt{q}t_0\right)^2 + \frac{1}{2}\frac{qt_0^2}{q_0-q} - \frac{1}{2}\frac{1}{q_0-q}cks^2} \tag{C319}$$

So that we can write:

$$G_1 = \frac{\alpha\,(D+1)}{2}\frac{q}{q_0-q} + \frac{\alpha\,(D+1)}{2}\log(q_0-q) \tag{C320}$$

$$\cdots - \alpha\int D^D\vec{t}\int Dt_0\log\int\frac{d^D\vec{v}_l}{\sqrt{2\pi}}e^{-\frac{1}{2}\frac{1}{q_0-q}\left(\vec{v}-\sqrt{q}\vec{t}\right)^2 + \frac{1}{2}\frac{q\|\vec{t}\|^2}{q_0-q}}\int\frac{ds}{\sqrt{2\pi}}\int_{1-s+R\|\vec{v}\|}^{\infty}\frac{dv_0}{\sqrt{2\pi}}e^{-\frac{1}{2}\frac{1}{q_0-q}\left(v_0-\sqrt{q}t_0\right)^2 + \frac{1}{2}\frac{qt_0^2}{q_0-q} - \frac{1}{2}\frac{1}{q_0-q}cks^2} \tag{C321}$$

and denoting for brevity:

$$F \doteq -\frac{D}{2}\log(q_0-q) - \frac{1}{2}\frac{1}{q_0-q}\left(\vec{v}-\sqrt{q}\vec{t}\right)^2 - \frac{1}{2}\frac{1}{q_0-q}\left(v_0-\sqrt{q}t_0\right)^2 - \frac{1}{2}\log(q_0-q) - \frac{1}{2}\frac{1}{q_0-q}cks^2$$

$$G_1 = -\alpha\int D^D\vec{t}\int Dt_0\log\int\frac{d^D\vec{v}_l}{\sqrt{2\pi}}\int\frac{ds}{\sqrt{2\pi}}\int_{1-s+R\|\vec{v}\|}^{\infty}\frac{dv_0}{\sqrt{2\pi}}e^F$$

we have the limit:

$$\lim_{q_0\to q}(q_0-q)\,G_1 = -\alpha\lim_{q_0\to q}(q_0-q)\int D^D\vec{t}\int Dt_0\log\int\frac{d^D\vec{v}_l}{\sqrt{2\pi}}\int\frac{ds}{\sqrt{2\pi}}\int_{1-s+R\|\vec{v}\|}^{\infty}\frac{dv_0}{\sqrt{2\pi}}e^F \tag{C322}$$

$$= -\alpha\int D^D\vec{t}\int Dt_0\lim_{q_0\to q}(q_0-q)\log\max_{v_0\geq 1-s+R\|\vec{v}\|}e^F \tag{C323}$$

$$= -\alpha\int D^D\vec{t}\int Dt_0\lim_{q_0\to q}(q_0-q)\max_{v_0\geq 1-s+R\|\vec{v}\|}F \tag{C324}$$

$$= \alpha\int D^D\vec{t}\int Dt_0\min_{v_0\geq 1-s+R\|\vec{v}\|}\left\{\frac{1}{2}\left(\vec{v}-\sqrt{q}\vec{t}\right)^2 + \frac{1}{2}\left(v_0-\sqrt{q}t_0\right)^2 + \frac{1}{2}cks^2\right\} \tag{C325}$$

To solve the inner minimization problem we denote a Lagrangian:

$$\mathcal{L} = \frac{1}{2}\left(\vec{v}-\sqrt{q}\vec{t}\right)^2 + \frac{1}{2}\left(v_0-\sqrt{q}t_0\right)^2 + \frac{1}{2}cks^2 + \lambda\left(1-s+R\|\vec{v}\|-v_0\right) \tag{C326}$$

with derivative:

$$\frac{\partial\mathcal{L}}{\partial v_0} = v_0 - \sqrt{q}t_0 - \lambda = 0 \tag{C327}$$

$$\frac{\partial\mathcal{L}}{\partial v_l} = (v_l - \sqrt{q}t_l) + \frac{1}{2}\lambda R\frac{2v_l}{\|\vec{v}\|} = 0 \tag{C328}$$

$$\frac{\partial\mathcal{L}}{\partial s} = cks - \lambda = 0 \tag{C329}$$

so from KKT conditions:

$$0 = \lambda \left(1 - s + R\|\vec{v}\| - v_0\right) \tag{C330}$$
$$\lambda = v_0 - \sqrt{q}t_0 \tag{C331}$$
$$\sqrt{q}t_l = \frac{\|\vec{v}\| + \lambda R}{\|\vec{v}\|} v_l \tag{C332}$$
$$\lambda = cks \tag{C333}$$

and denoting $v = \|\vec{v}\|$ and $t = \|\vec{t}\|$ we have three solution regimes:

1. "Interior" regime: assuming $\lambda = 0$

$$v_0 \geq 1 - s + Rv \tag{C334}$$
$$v_0 = \sqrt{q}t_0 \tag{C335}$$
$$v_l = \sqrt{q}t_l \tag{C336}$$
$$s = 0 \tag{C337}$$
$$F = 0 \tag{C338}$$

   which is valid for $t_0 \geq 1/\sqrt{q} + Rt$.

2. "Touching" regime: assuming $\lambda > 0$, $v > 0$

$$v_0 = 1 - s + Rv \tag{C339}$$
$$v_l = \frac{v}{v + \lambda R}\sqrt{q}t_l \tag{C340}$$
$$v = \sqrt{q}t - \lambda R \tag{C341}$$
$$\|\vec{v} - \sqrt{q}\vec{t}\|^2 = \lambda^2 R^2 \tag{C342}$$
$$s = \frac{1 - \sqrt{q}t_0 + R\sqrt{q}t}{1 + ck\left(1 + R^2\right)} \tag{C343}$$
$$v_0 = \frac{\left(ckR^2 + 1\right)\sqrt{q}t_0 + \left(1 + R\sqrt{q}t\right)ck}{1 + \left(1 + R^2\right)ck} \tag{C344}$$
$$0 < v = \frac{\left(1 + ck\right)\sqrt{q}t - ckR + \sqrt{q}ckRt_0}{1 + \left(1 + R^2\right)ck} \tag{C345}$$
$$v_0 - \sqrt{q}t_0 = ck\frac{1 + R\sqrt{q}t - \sqrt{q}t_0}{1 + \left(1 + R^2\right)ck} \tag{C346}$$
$$F = \frac{ck}{1 + \left(1 + R^2\right)ck}\left(1 + R\sqrt{q}t - \sqrt{q}t_0\right)^2 \tag{C347}$$

   which is valid for $t_0 \geq 1/\sqrt{q} - \frac{1+ck}{ck}tR^{-1}$.

3. "Embedded" regime: assuming $\lambda > 0$, $v = 0$

$$v_0 = 1 - s \tag{C348}$$
$$cks = \lambda = v_0 - \sqrt{q}t_0 \tag{C349}$$
$$0 < s = \frac{1}{1 + ck} - \frac{\sqrt{q}}{1 + ck}t_0 \tag{C350}$$
$$v_0 = \frac{ck}{1 + ck} + \frac{\sqrt{q}}{1 + ck}t_0 \tag{C351}$$
$$v_0 - \sqrt{q}t_0 = \frac{ck - ck\sqrt{q}t_0}{1 + ck} \tag{C352}$$
$$F = qt^2 + \frac{ck}{1 + ck}\left(1 - \sqrt{q}t_0\right)^2 \tag{C353}$$

   which is valid for $t_0 < 1/\sqrt{q}$.

Using the conditions on t_0, t from each regime the following table summarizes the results:

Regime	Embedded	Touch	Interior
Range	$t_0 \leq 1/\sqrt{q} - \frac{1+ck}{ck} t/R$	$1/\sqrt{q} - \frac{1+ck}{ck} t/R \leq t_0 \leq 1/\sqrt{q} + Rt/$	$1/\sqrt{q} + Rt \leq t_0$
v_0	$\frac{ck}{1+ck} + \frac{\sqrt{q}}{1+ck} t_0$	$\frac{\left(ckR^2+1\right)\sqrt{q}}{1+(1+R^2)ck} t_0 + \frac{\left(1+R\sqrt{q}t\right)ck}{1+(1+R^2)ck}$	$\sqrt{q} t_0$
v	0	$\frac{(1+ck)\sqrt{q}t - ckR + \sqrt{q}ckRt_0}{1+(1+R^2)ck}$	$\sqrt{q}t$
s	$\frac{1}{1+ck} - \frac{\sqrt{q}}{1+ck} t_0$	$\frac{1+R\sqrt{q}t}{1+(1+R^2)ck} - \frac{\sqrt{q}}{1+(1+R^2)ck} t_0$	0
F	$qt^2 + \frac{ck}{1+ck}\left(1 - \sqrt{q}t_0\right)^2$	$\frac{ck}{1+(1+R^2)ck}\left(1 + R\sqrt{q}t - \sqrt{q}t_0\right)^2$	0

(C354)

or written explicitly, the field and slack distribution conditioned on t, t_0:

$$v_0 = \begin{cases} \frac{ck}{1+ck} + \frac{1}{1+ck}\sqrt{q}t_0 & t_0 \leq 1/\sqrt{q} - \frac{1+ck}{ck} t/R \\ \frac{\left(1+R\sqrt{q}t\right)ck}{1+(1+R^2)ck} + \frac{\left(ckR^2+1\right)\sqrt{q}}{1+(1+R^2)ck} t_0 & 1/\sqrt{q} - \frac{1+ck}{ck} t/R \leq t_0 \leq 1/\sqrt{q} + Rt \\ \sqrt{q}t_0 & 1/\sqrt{q} + Rt \leq t_0 \end{cases} \tag{C355}$$

$$v = \begin{cases} 0 & t_0 \leq 1/\sqrt{q} - \frac{1+ck}{ck} t/R \\ \frac{(1+ck)\sqrt{q}t - ckR}{1+(1+R^2)ck} + \frac{\sqrt{q}ckR}{1+(1+R^2)ck} t_0 & 1/\sqrt{q} - \frac{1+ck}{ck} t/R \leq t_0 \leq 1/\sqrt{q} + Rt \\ \sqrt{q}t & 1/\sqrt{q} + Rt \leq t_0 \end{cases} \tag{C356}$$

$$s = \begin{cases} \frac{1}{1+ck} - \frac{1}{1+ck}\sqrt{q}t_0 & t_0 \leq 1/\sqrt{q} - \frac{1+ck}{ck} t/R \\ \frac{1+R\sqrt{q}t}{1+(1+R^2)ck} - \frac{\sqrt{q}}{1+(1+R^2)ck} t_0 & 1/\sqrt{q} - \frac{1+ck}{ck} t/R \leq t_0 \leq 1/\sqrt{q} + Rt \\ 0 & 1/\sqrt{q} + Rt \leq t_0 \end{cases} \tag{C357}$$

and the slack variable moments, used above for the self-consistent equations, are given by:

$$\left\langle s^2 \right\rangle = \frac{q}{\left(1+ck\right)^2} \int \chi_D(t) \int_{-\infty}^{1/\sqrt{q} - \frac{1+ck}{ck} t/R} Dt_0 \left(1/\sqrt{q} - t_0\right)^2 \tag{C358}$$

$$+ \frac{q}{\left(1+\left(1+R^2\right)ck\right)^2} \int \chi_D(t) \int_{1/\sqrt{q} - \frac{1+ck}{ck} t/R}^{1/\sqrt{q}+Rt} Dt_0 \left(1/\sqrt{q} + Rt - t_0\right)^2 \tag{C359}$$

$$\langle s \rangle = \frac{\sqrt{q}}{1+ck} \int \chi_D(t) \int_{-\infty}^{1/\sqrt{q} - \frac{1+ck}{ck} t/R} Dt_0 \left(1/\sqrt{q} - t_0\right) \tag{C360}$$

$$+ \frac{\sqrt{q}}{1+\left(1+R^2\right)ck} \int \chi_D(t) \int_{1/\sqrt{q} - \frac{1+ck}{ck} t/R}^{1/\sqrt{q}+Rt} Dt_0 \left(1/\sqrt{q} + Rt - t_0\right) \tag{C361}$$

13. Classification error for spheres

Assuming $D \gg 1$, $t \sim \chi_D$ is concentrated around $\sqrt{D}$ and the distribution of v_0, v, s is a concatenation of truncated Gaussian (or δ) distributions which correspond to the different regimes. The slack distribution is then:

$$s \sim \begin{cases} \mathcal{N}\left(\frac{1}{1+ck}, \frac{q}{(1+ck)^2}\right) & \frac{\sqrt{q}}{ck}\sqrt{D}/R < s \\ \mathcal{N}\left(\frac{1+R\sqrt{q}\sqrt{D}}{1+(1+R^2)ck}, \frac{q}{(1+(1+R^2)ck)^2}\right) & 0 < s \leq \frac{\sqrt{q}}{ck}\sqrt{D}/R \\ \delta(0)\, H\left(1/\sqrt{q} + R\sqrt{D}\right) & s = 0 \end{cases} \tag{C362}$$

From this distribution the probability of error anywhere on the manifold is $\varepsilon_{tr}^{manifold} = P(s > 1) = H(\mathcal{S})$ for:

$$\mathcal{S} = \begin{cases} ck/\sqrt{q} & \frac{\sqrt{q}}{ck}\sqrt{D}/R < 1 \\ \left(1+R^2\right)ck/\sqrt{q} - R\sqrt{D} & \frac{\sqrt{q}}{ck}\sqrt{D}/R \geq 1 \end{cases} \tag{C363}$$

Given any classifier $\boldsymbol{w}$, we assume the test error is calculated by sampling uniformly from the sphere, then adding noise. When i.i.d Gaussian noise $\mathcal{N}\left(0,\sigma^2/N\right)$ is applied to each input component, as the weights are independent of this noise, the fields are affected by Gaussian noise $\mathcal{N}\left(0,\sigma^2 q\right)$. That is, the error is given by:

$$\varepsilon = P\left(h + \sigma\sqrt{q}\eta < 0\right) = \left\langle H\left(\frac{h}{\sigma\sqrt{q}}\right)\right\rangle_h \tag{C364}$$

where η is a standard Gaussian variable.

For a D-dimensional spheres of radius R, denote the fields $h(\vec{S}) = y\boldsymbol{w}\cdot\boldsymbol{x}(\vec{S}) = v_0 + \vec{S}\cdot\vec{v}$. For a given $\boldsymbol{w}$, we can always choose the coordinate system such as $u_1 \propto w$ so that $v_1 = w\cdot u_1$ and $v_i = 0$ for $i > 1$, so that $v = \|\vec{v}\| = v_1$. Denote $S_1 = z$ we note that $\vec{S}\cdot\vec{v} = zv$ and thus $h = v_0 + zv$. As the joint distribution of v_0, v is given by theory (equations C355,C356) we shall now derive the distribution of z under uniform sampling from the sphere. As $z \in [-R, R]$, we can denote $\boldsymbol{x} \in \mathcal{S}_{D-2}\left(\sqrt{R^2 - z^2}\right)$ a sphere of all choices for the values of $S_{2..D}$, and thus wish to calculate the following integral:

$$\varepsilon\left(v, v_0\right) = \int_{-R}^{R} \mu z \int \mu^{D-1}\boldsymbol{x}\delta\left(\|x\|^2 + z^2 - R^2\right) H\left(\frac{v_0 + zv}{\sigma\sqrt{q}}\right) \tag{C365}$$

where μz and $\mu^{D-1}\boldsymbol{x}$ denote the corresponding measures on z and $\boldsymbol{x}$.

Using the n-ball surface formula, $S_{n-1}\left(r\right) = \frac{2\pi^{\frac{n}{2}}}{\Gamma\left(\frac{n}{2}\right)}r^{n-1}$, the surface of the $D-1$ sphere with a radius $\|x\|$ is $S_{D-2}\left(\sqrt{R^2 - z^2}\right)$, which needs to be normalized by the total surface, given by $S_{D-1}\left(R\right)$. Furthermore, using polar coordinates the measure on z is given by $\frac{R}{\sqrt{R^2 - z^2}}$, yielding:

$$\begin{aligned}
\varepsilon\left(\vec{v}, v_0\right) &= \frac{1}{S_{D-1}\left(R\right)}\int_{-R}^{R}\frac{Rdz}{\sqrt{R^2 - z^2}}S_{D-2}\left(\sqrt{R^2 - z^2}\right)H\left(\frac{v_0 + z\|v\|}{\sigma\sqrt{q}}\right) && \text{(C366)}\\
&= \frac{\Gamma\left(\frac{D}{2}\right)}{2\pi^{\frac{D}{2}}R^{D-1}}\int_{-R}^{R}\frac{Rdz}{\sqrt{R^2 - z^2}}\frac{2\pi^{\frac{D-1}{2}}}{\Gamma\left(\frac{D-1}{2}\right)}\left(\sqrt{R^2 - z^2}\right)^{(D-2)}H\left(\frac{v_0 + z\|v\|}{\sigma\sqrt{q}}\right) && \text{(C367)}\\
&= \frac{\Gamma\left(\frac{D}{2}\right)}{\Gamma\left(\frac{D-1}{2}\right)\sqrt{\pi}}\int_{-1}^{1}d\hat{z}\left(1^2 - z^2\right)^{(D-3)/2}H\left(\frac{v_0 + Rz\|v\|}{\sigma\sqrt{q}}\right) && \text{(C368)}
\end{aligned}$$

by a change of variable $\hat{z} = z/R$. Thus we can write an expression for the full test error averaged on v, v_0:

$$\varepsilon = \frac{\Gamma\left(\frac{D}{2}\right)}{\Gamma\left(\frac{D-1}{2}\right)\sqrt{\pi}}\left\langle\int_{-1}^{1}d\hat{z}\left(1 - \hat{z}^2\right)^{(D-3)/2}H\left(\frac{v_0 + R\hat{z}v}{\sigma\sqrt{q}}\right)\right\rangle_{v_0,v} \tag{C369}$$

Using a change of variable $\hat{z} = \sqrt{t}$ and $d\hat{z} = \frac{1}{2}t^{-1/2}dt$ and using the Beta function:

$$\begin{aligned}
\int_{-1}^{1}d\hat{z}\left(1 - \hat{z}^2\right)^{(D-3)/2} &= \int_0^1 dtt^{-1/2}\left(1 - t\right)^{(D-3)/2} && \text{(C370)}\\
&= B\left(x = 1/2, y = \left(D - 3\right)/2 + 1\right) && \text{(C371)}\\
&= \sqrt{\pi}\Gamma\left(\frac{D-1}{2}\right)/\Gamma\left(\frac{D}{2}\right) && \text{(C372)}
\end{aligned}$$

Thus we define a bell-shaped distribution supported at $\hat{z} \in [-1, 1]$:

$$P\left(\hat{z}\right) = \frac{\Gamma\left(\frac{D}{2}\right)}{\sqrt{\pi}\Gamma\left(\frac{D-1}{2}\right)}\left(1 - \hat{z}^2\right)^{(D-3)/2} \tag{C373}$$

with moments: $\left\langle\hat{z}\right\rangle_{P(\hat{z})} = 0$ and $\left\langle\hat{z}^2\right\rangle_{P(\hat{z})} = 1/D$, and now write the error as an average with respect to $P\left(\hat{z}\right)$:

$$\varepsilon = \left\langle H\left(\frac{v_0 + R\hat{z}v}{\sigma\sqrt{q}}\right)\right\rangle_{\hat{z},v_0,v} \tag{C374}$$

For $D \gg 1$, by assuming that only the "touching" regime contributes to the error, we may evaluate the leading orders of $v_0 + R\hat{z}v$ in order to write a simpler expression for the error. In the "touching" regime:

$$v_0 = \frac{\left(1 + R\sqrt{q}t\right) ck + \left(ckR^2 + 1\right)\sqrt{q}t_0}{1 + \left(1 + R^2\right) ck} \tag{C375}$$

$$v = ckR\frac{\frac{1+ck}{ck}\sqrt{q}t/R + \sqrt{q}t_0 - 1}{1 + \left(1 + R^2\right) ck} \tag{C376}$$

where $t_0 \sim \mathcal{N}(0,1)$ and $t \sim \chi_D$. Noting that $\hat{z}, t, t_0$ are pairwise independent and also that $\hat{z}v$ is independent from v_0, the first two moments are:

$$\left\langle v_0 + R\hat{z}v \right\rangle_{\hat{z},t_0} = \frac{\left(1 + R\sqrt{q}t\right) ck}{1 + \left(1 + R^2\right) ck} \tag{C377}$$

$$\left\langle \delta\left(v_0 + R\hat{z}v\right)^2 \right\rangle_{\hat{z},t_0} = q\frac{\left(ckR^2 + 1\right)^2 + \frac{R^2}{D+1}\left(ck\right)^2 R^2\left[\left(\frac{1+ck}{ck}t/R - 1/\sqrt{q}\right)^2 + 1\right]}{\left(1 + \left(1 + R^2\right) ck\right)^2} \tag{C378}$$

and approximating $v_0 + R\hat{z}v$ as Gaussian, we have using $\left\langle H\left(x/a\right)\right\rangle_{x\sim\mathcal{N}(\mu,s^2)} = H\left(\mu/\sqrt{s^2+a^2}\right)$ that:

$$\varepsilon \approx \left\langle H\left(\frac{\left(1 + R\sqrt{q}t\right) ck}{1 + \left(1 + R^2\right) ck} \Big/ \sqrt{\sigma^2 q + q\frac{\left(ckR^2 + 1\right)^2 + \frac{R^2}{D}\left(ck\right)^2 R^2\left[\left(\frac{1+ck}{ck}t/R - 1/\sqrt{q}\right)^2 + 1\right]}{\left(1 + \left(1 + R^2\right) ck\right)^2}}\right)\right\rangle_t \tag{C379}$$

so that denoting σ_0^2 the contribution of those terms to the variance we have the approximation:

$$\sigma_0^2\left(t\right) = \left(ckR^2 + 1\right)^2 + \frac{R^4}{D}\left(ck\right)^2\left[\left(\frac{1+ck}{ck}t/R - 1/\sqrt{q}\right)^2 + 1\right] \tag{C380}$$

$$\varepsilon \approx \left\langle H\left(\left(1/\sqrt{q} + Rt\right) ck \Big/ \sqrt{\sigma_0^2 + \left(1 + \left(1 + R^2\right) ck\right)^2 \sigma^2}\right)\right\rangle_{t\sim\chi_D} \tag{C381}$$

and the training error is given by setting $\sigma = 0$. Near α_C we have $k \to 0$ such that $\sigma_0^2 = 1 + 1/\left(R^{-1} + R\right)^2 \approx 1$ and using equation C304:

$$\varepsilon \approx H\left(\frac{R\sqrt{D}}{1 + R^2}\frac{1}{\sqrt{1 + \sigma^2}}\right) \tag{C382}$$

14. Iterative algorithm for point-cloud manifolds

From the mean-field equations of spheres we get that a theory of general-manifolds would imply:

$$1 = \left(1 - L/q\right) k + \alpha \int D^D\vec{t} \int Dt_0 F\left(\vec{t}, t_0\right) \tag{C383}$$

$$F\left(\vec{t}, t_0\right) = \min_{\min_{\vec{S}\in M}\left\{v_0 + \vec{v}\cdot\vec{S}\right\} \geq 1/\sqrt{q}} \left\{\left\|\vec{v} - \vec{t}\right\|^2 + \frac{ck}{1 + ck}\left(v_0 - t_0\right)^2\right\} \tag{C384}$$

Denote a scalar function $g\left(\vec{v}\right) = \min_{\vec{S}\in M} \vec{v}\cdot\vec{S}$ and its subgradient:

$$\tilde{S}\left(\vec{v}\right) = \frac{\partial}{\partial v} g\left(\vec{v}\right) \tag{C385}$$

Denote a Lagrangian:

$$\mathcal{L} = \frac{1}{2}\left(\vec{v} - \vec{t}\right)^2 + \frac{1}{2}\frac{ck}{1+ck}\left(v_0 - t_0\right)^2 + \lambda\left(1/\sqrt{q} - v_0 - g\left(\vec{v}\right)\right) \tag{C386}$$

its derivations are

$$\frac{\partial \mathcal{L}}{\partial v_0} = \frac{ck}{1+ck}\left(v_0 - t_0\right) - \lambda = 0 \tag{C387}$$

$$\frac{\partial \mathcal{L}}{\partial v_l} = \left(v_l - t_l\right) - \lambda \tilde{S}\left(\vec{v}\right) = 0 \tag{C388}$$

so from KKT conditions:

$$0 = \lambda\left(1/\sqrt{q} - v_0 - g\left(\vec{v}\right)\right) \tag{C389}$$

$$\lambda = \frac{ck}{1+ck}\left(v_0 - t_0\right) \tag{C390}$$

$$\vec{v} = \vec{t} + \lambda \tilde{S}\left(\vec{v}\right) \tag{C391}$$

so that we got equation 55 when $v_0 \neq t_0$:

$$\tilde{S}\left(\vec{v}\right) = \frac{\vec{v} - \vec{t}}{\frac{ck}{1+ck}\left(v_0 - t_0\right)} \tag{C392}$$

Denoting $v = \|\vec{v}\|$ and $t = \|\vec{t}\|$ we have regimes:

1. "Interior" regime: assuming $v > 0$ and $\lambda = 0$ we have:

$$v_0 \geq 1/\sqrt{q} - g\left(\vec{v}\right) \tag{C393}$$

$$v_0 = t_0 \tag{C394}$$

$$v_l = t_l \tag{C395}$$

$$F = 0 \tag{C396}$$

2. "Embedded" regime: assuming $v = 0$ and $\lambda > 0$ we have:

$$v_0 = 1/\sqrt{q} - g\left(\vec{v}\right) = 1/\sqrt{q} \tag{C397}$$

$$\lambda = \frac{ck}{1+ck}\left(1/\sqrt{q} - t_0\right) \tag{C398}$$

$$\tilde{S}\left(\vec{v}\right) = -\frac{\vec{t}}{\frac{ck}{1+ck}\left(1/\sqrt{q} - t_0\right)} \tag{C399}$$

$$F = t^2 + \frac{ck}{1+ck}\left(1/\sqrt{q} - t_0\right)^2 \tag{C400}$$

3. "Touching" regime: assuming $v > 0$ and $\lambda > 0$ we have:

$$v_0 = 1/\sqrt{q} - g\left(\vec{v}\right) \tag{C401}$$

$$\lambda = \frac{ck}{1+ck}\left(1/\sqrt{q} - g\left(\vec{v}\right) - t_0\right) \tag{C402}$$

$$\vec{v} = \vec{t} + \frac{ck}{1+ck}\left(1/\sqrt{q} - \vec{v}\cdot\tilde{S}\left(\vec{v}\right) - t_0\right)\tilde{S}\left(\vec{v}\right) \tag{C403}$$

$$\vec{v}\cdot\tilde{S} = \frac{\left(1+ck\right)\vec{t}\cdot\tilde{S}\left(\vec{v}\right) + ck\left(1/\sqrt{q} - t_0\right)\tilde{S}^2}{1 + ck\left(1+\tilde{S}^2\right)} \tag{C404}$$

$$F = \frac{ck}{1+ck\left(1+\tilde{S}^2\right)}\left(1/\sqrt{q} - t_0 - \vec{t}\cdot\tilde{S}\right)^2 \tag{C405}$$

so that for the "touching" regime we have equation 58.